UNIVERSIDAD POLITÉCNICA DE MADRID
ESCUELA TÉCNICA SUPERIOR INGENIERÍA
AGRONÓMICA, ALIMENTARIA Y DE BIOSISTEMAS

A CONTROL APPROACH TO COMPLEXITY: FROM MOLECULAR VIBRATIONAL DYNAMICS TO COMPETITION GAMES ON NETWORKS

Amador López Pina
Ingeniero de Telecomunicación
Máster en Ingeniería Aeroespacial
Máster en Automática y Robótica

TESIS DOCTORAL

Enero 2019

UNIVERSIDAD POLITÉCNICA DE MADRID
ESCUELA TÉCNICA SUPERIOR INGENIERÍA
AGRONÓMICA, ALIMENTARIA Y DE BIOSISTEMAS

A CONTROL APPROACH TO COMPLEXITY: FROM MOLECULAR VIBRATIONAL DYNAMICS TO COMPETITION GAMES ON NETWORKS

Amador López Pina
Ingeniero de Telecomunicación
Máster en Ingeniería Aeroespacial
Máster en Automática y Robótica

Director:
Juan Carlos Losada González
Doctor en Ciencias Físicas

Enero 2019

To Melanie, Laura and Gabriel, with love

Aknowledgements

During the past few years I have had the opportunity to work in the exciting realm of complexity, which I associate with the last frontier of knowledge in many disciplines. I have always enjoyed the blend of beauty, challenge and comprehension of reality that science brings to us. The topic of complex systems nicely synthesizes this combination, and its strong relation with mathematics ultimately led me to pursue my PhD degree in this field.

I would like to thank Rosa María Benito for accepting me in the Grupo de Sistemas Complejos at the Polytechnical University of Madrid, for her reviews, proximity and wise surveillance all this time. It has been a pleasure to be part of this group, which has provided such a good atmosphere for research. In particular, I would like to recognize Tino Borondo for his sharp corrections and comments on my work related with Hamiltonian systems. Certainly, I also want to express my gratitude to my thesis director, Juan Carlos Losada, for his support, guidance, and smart discussions during the elaboration of this thesis. He has been very flexible with my multiple interests, and his know-how and continuous accessibility at all levels have been key for achieving the work presented in these pages. ¡Gracias Juancar!

I fondly appreciate the support and affection of my close family and friends as approaching this milestone. Similarly, my parents-in-law have been very supportive during all this years. My deepest gratefulness goes to them all.

También me gustaría agradecer el interés por aprender que me transmitieron mis padres, así como el cariño que me han dado siempre. Una parte muy importante de lo que soy se lo debo a ellos. ¡Muchas gracias a los dos!

Finally, I would like to thank my wife and children for the patience they had with me during the work conducting to this thesis. Their support, understanding and cheerful attitude have accompanied me over these years. This doctorate is dedicated to them.

Abstract

The ever-increasing understanding of the inherent laws underpinning the reality around us is a continuous quest that goes back to centuries of scientific advances. The foundational physical principles associated to many real systems have been discovered more than a century ago, and at this point our comprehension of a wide range of phenomena around us has reached a high level of maturity. This evolution in knowledge has eventually allowed mankind to design mechanisms, strategies, devices and algorithms aiming to dominate the associated dynamics in numerous applications and technologies. Many of these accomplishments are related to control theory, which is used in a wide range of scenarios in industry, automation, aerospace, robotics, etc. It should be remarked that these fields have a heavy reliance on the knowledge of physics such as fluid dynamics, classical and quantum mechanics, electromagnetism, etc, all these disciplines being by now strongly developed and understood by the scientific community.

In recent decades, however, a step beyond has been achieved on many areas whose complexity prevented until recently from a proper explanation of their inherent behaviour. This is the case of many fields which are now being tackled from a different point of view, such as stock markets, public opinion trends, gene networks, illness propagation, neuroscience, etc. Reality is complex by definition, and in fact ours is meant to be the century of complexity, according to distinguished minds such as S. Hawking, H. Pagels or E. Wilson [Wil98]. The comprehension of complex systems will be one of the subjects of study and research addressed from many different institutions, academia, private companies, etc.

The so called complexity theory encompasses many different disciplines such as complex networks, emergency, chaos theory, etc. The structural and dynamical phenomena observed in many circumstances are better understood with the introduction of these new tools of analysis. As in the case of more classical phenomena listed above, in the case of complex systems it is natural that science will make every effort to acquire tools for the control of such

complexity in the benefit of particular entities or for the common wealth in modern societies. Control of complex systems is therefore an area already subject to an intensive research activity.

Following this rationale, this thesis addresses the topic of complex systems from the perspective of control theory. One of the studied problems is the subject of control of molecular vibrational dynamics, which is very relevant in chemistry due to the applications in chemical processes, etc. The research conducted here provides an important insight in terms of control of those dynamics by means of an external time-varying magnetic field. In particular, a laser-perturbed HCN molecular system is studied, in terms of transitions between chaotic and regular dynamics, molecular dissociation, and the relation of both of them with the frequency of excitation laser. It has been observed that if the laser frequency is in resonance with the intrinsic vibrational frequencies of the system, the ratio of chaos trajectories increases, with a higher probability of molecular dissociation. On the other hand, if the ratio between the laser and the system frequencies is very irrational, regular trajectories survive.

The topic of consensus on complex networks is also very important with many practical applications (social networks, gene dynamics, capital markets, etc). Games between competing teams are established aiming to influence the collective behaviour of the components of the network according to the interest of each team, which in many cases will be conflicting with those of the opponent. In the research conducted in this thesis, several important conclusions have been reached on this regard. An optimal solution has been obtained in the selection of actions to be conducted by one of the teams in order to maximize the retrieved benefit associated to the state of the members of a target network of resources which are subject to consensus dynamics. Such network constitutes a population on which two teams compete, as for example the case of political parties competing for the popular vote on a given election. An alternative example is the competition between two companies on the fidelity of clients within a certain market. Furthermore, this thesis has obtained the best design of the connecting network to the population that one team should deploy in order to maximize achievable benefits. Moreover, it has studied the case where each team targets only part of the general population, for which game dynamics lead to a Nash equilibrium that depends on generic parameters present in the setup of the game. Therefore, the optimal control of the state of the population against the interest of the opponent team is presented in this thesis, allowing its application of such strategy to numerous scenarios.

Resumen

La creciente comprensión de las leyes que rigen la realidad a nuestro alrededor conlleva una búsqueda continua que data de siglos de avances científicos. Actualmente conocemos los principios físicos asociados a muchos sistemas reales, y nuestro entendimiento de un extenso abanico de fenómenos de la realidad ha alcanzado un alto nivel de madurez. Esta evolución del conocimiento ha permitido a la humanidad el diseño de mecanismos, estrategias, aparatos y algoritmos destinados a dominar la dinámica asociada en innumerables aplicaciones y tecnologías. Muchos de estos logros están relacionados con la teoría de control, que es usada en una amplia variedad de escenarios en la industria, la automoción, el sector aeroespacial, la robótica, etc. Todos ellos tienen una fuerte dependencia en el conocimiento de áreas de la física como la mecánica de fluidos, mecánica clásica y cuántica, electromagnetismo, etc. siendo todas ellas disciplinas que actualmente han sido ya ampliamente desarrolladas y comprendidas por la comunidad científica.

Por otro lado, en los últimos años se ha alcanzado un conocimiento más avanzado en muchas áreas cuya complejidad impedía hasta ahora una comprensión apropiada de su comportamiento. Éste es el caso de muchos campos que actualmente están siendo estudiados desde un nuevo punto de vista, como los mercados bursátiles, las tendencias en la opinión pública, las redes genéticas, la propagación de enfermedades, la neurociencia, etc. La realidad es inherentemente compleja, y el siglo XXI está llamado a ser el de la complejidad, según la opinión de S. Hawking, H. Pagels o E. Wilson [Wil98]. Los sistemas complejos son aquéllos cuyo comportamiento es difícil de modelar debido a la naturaleza de las dependencias e interacciones entre sus partes, y la comprensión de dichos sistemas es actualmente una tarea de intensa actividad. La llamada teoría de la complejidad agrupa muchas disciplinas tan diversas como las redes complejas, los fenómenos de emergencia, la teoría del caos, etc. Los fenómenos estructurales y dinámicos que se observan en muchas circunstancias son ahora comprendidos a un mejor nivel gracias a la introducción de nuevas herramientas de análisis (e.g. teoría de redes comple-

jas).

Como en el caso de fenómenos más clásicos referidos más arriba, en el caso de sistemas complejos cabe esperar que la ciencia busque métodos y herramientas para el control de dicha complejidad en el beneficio de entidades particulares y de la comunidad general en las sociedades modernas. Por eso el control de sistemas complejos es ya un área de intensa investigación. Esta tesis sigue esta línea de trabajo y se centra en el estudio de los sistemas complejos desde el punto de vista de la teoría de control. El primer problema que hemos estudiado es el control de la dinámica vibracional de sistemas moleculares, de una gran relevancia debido a las aplicaciones en el control de reacciones químicas. El estudio que se ha realizado aquí aporta importantes conclusiones relacionadas con el control de dicha dinámica mediante un campo electromagnético externo variable en el tiempo. En particular se estudia el sistema molecular HCN perturbado mediante un láser de frecuencia variable, en términos del análisis transiciones entre régimen regular y caótico, la disocación molecular y la relación entre ambos con la frecuencia de control del laser usado para excitar las moléculas. Hemos observado que si la frecuencia del láser está en resonancia con las frecuencias del sistema, la proporción de caos es mayor y aumenta la probabilidad de disociación de la molécula. Por otro lado si las relaciones de frecuencia son muy irracionales (multiplos de la razón áurea) más trayectorias regulares sobreviven.

Un problema en principio muy diferente, pero que también es estudiado desde la perspectiva del control de sistemas complejos es de juegos en redes. Cuando el control se realiza por parte de dos equipos con finalidades contrarias emergen determinadas dinámicas de juegos. En esta tesis se analizan los escenarios con una red compleja cuyos elementos presentan una dinámica de consenso, y que se pretende controlar mediante una acción externa. El consenso en redes complejas es muy importante debido a sus numerosas aplicaciones (redes sociales, dinámica de genes, mercados de capital, etc.) Frecuentemente se establecen juegos entre equipos que compiten por influir en el comportamiento de los componentes de una red, cada uno de acuerdo a sus intereses. En esta tesis se presentan resultados analíticos y numéricos importantes sobre juegos y consensos en redes complejas, como la solución óptima para la selección de las acciones que han de realizar los miembros de un equipo para maximizar el beneficio debido al estado de los elementos de la red objetivo. El estado de dicha red se considera como un recurso por el que se compite, como en el caso de partidos políticos que se disputan el voto popular en una elección, o el de la competencia entre dos empresas por la fidelidad de los clientes en un determinado mercado. Adi-

cionalmente, se ha obtenido el diseño óptimo para la red de conexión a la población objetivo que un equipo debería implementar para maximizar los beneficios disponibles. Además, se ha estudiado el caso donde cada equipo lucha por solo una parte de la población, y la dinámica del juego lleva entonces a un equilibrio de Nash que depende de los parámetros que definen el juego. Esta tesis presenta los fundamentos teóricos así como resultados numéricos asociados. La metodología presentada permite su aplicación en numerosos escenarios de competición entre equipos.

Contents

Notation

The following list defines the mathematical notation used in the text:

$\mathbb{R}$	Real numbers field
$\mathbb{C}$	Complex numbers field
$\mathbb{R}^n$	Set of real vectors of size n
$\mathbb{R}^{m \times n}$	Set of real matrices of size $m \times n$
A	Matrix
A_{ij}	Matrix indexed for some purpose
A^T	The transpose matrix of the matrix A
A^*	The Hermitian conjugate of the matrix A
A^{-1}	The inverse matrix of the matrix A
$\lambda(A)$	An eigenvalue of the matrix A
$\sigma(A)$	A singular vector of the matrix A
$tr(A)$	Trace of the matrix A
$\|A\|_p$	induced p-norm of the matrix A
$\|A\|_F$	Frobenius norm of the matrix A
$\mathbf{a}$	Vector (column-vector)
$\mathbf{a}^T$	Vector (row-vector) transpose of vector $\mathbf{a}$
a_i	The i^th element of the vector $\mathbf{a}$
$\mathbf{1}$	Column vector with all its entries = 1
$diag(\mathbf{a})$	Diagonal matrix with diagonal entries equal to the elements of the $\mathbf{a}$ vector
$\dot{\mathbf{a}}$	Time derivative of vector $\mathbf{a}$ $(= d\mathbf{a}/dt)$
$D\mathbf{f}(\mathbf{x})$	Jacobian matrix of vector $\mathbf{f}$
$\nabla_{\mathbf{p}} H$	Gradient of the H scalar along vector $\mathbf{p}$
$\nabla^2 H$	Hessian matrix of the H scalar
$span(\mathbf{a})$	Subspace generated by the vector $\mathbf{a}$

Chapter 1

Introduction

"The complexity of things - the things within things - just seems to be endless. I mean nothing is easy, nothing is simple."

– Alice Munro

"... No me atrevo a afirmar que son sencillos; no hay en la tierra una sola página que lo sea, ya que todas postulan el universo, cuyo más notorio atributo es la complejidad."

– Jorge Luis Borges, *Cuentos completos*

The concept of complexity of a system can be addressed from different perspectives. As a quality of the system it refers to what makes the system complex, such as the presence of emergent properties as a consequence of the interactions within the different parts of the system. In its second meaning, complexity refers to the amount of information needed to describe the system. For both points of view, complexity theory is a scientific discipline encompassing a wide range of concepts and phenomena which cannot be fully explained and analysed by traditional sciences and methodologies. Complex systems can display special properties such as spontaneous emergence, unpredictability and strong non-linearities, which yield distinctive effects on their behaviour. Complex systems theory includes ideas derived from a number of other disciplines such as physics, mathematics, computer science, information theory among others, and it covers such a wide spectrum of concepts as chaos theory, complex networks or nonlinear systems. The range of applications is very large: climatology, celestial mechanics, opinion trends on social networks, molecular dynamics, emergent phenomena and stock markets, to name a few. The modelling and analysis of the complex systems behavior has experienced an improvement in the last decades due to the development of several mathematical disciplines. In particular, two of the most commonly used are chaos theory and complex networks.

The concept of chaos is generally associated with randomness, but its mathematical definition rather refers to deterministic (not random) systems whose behavior is only predictable for a certain period of time. Said period depends on the nature of the problem under study, the available measurement accuracy and the uncertainty that is acceptable for practical purposes: it ranges in the order of miliseconds (electric chaotic circuits) to millions of years (solar system). Indeed, the study of chaotic behavior started with the classical mechanics description of the three-body problem, whose intricacies were addressed by several scientists since Newton, with important contributions from Lagrange, Laplace, Hamilton, Jacobi, Weierstrass, etc., but it was only the French mathematician Henri Poincaré who properly analyzed the integrability of such systems in the XIX century [Poi1890]. Perturbation theory of Hamiltonian systems is core for the understanding of chaotic behavior. This topics was nicely addressed in the seminal work of Kolmogorov, Arnold, and Moser, in the middle of the XX century [Kol54b] that provided an adequate setup for the analysis of chaos and the characterization of the transition from orderly trajectories to chaotic ones as the amplitude of the perturbation of a Hamiltonian system is increased. As an output of such research they produced the celebrated KAM theorem [Kol54a, Arn61, Mos68]. The study of dynamical chaos theory has substantially flourished thereupon, becoming an area of active research within the scientific community of dynamical systems [Ber78, Chi79, Gru00, Rad88, Lich92]. Furthermore, the interest in the field of chaos theory received an enormous boost since the 1960s after the advent of computers for analysis of practical scientific matters. Edward Lorenz was the pioneer in this line of research [Lor93] while working on the study of weather prediction, he came across with chaotic behavior when he decided to divide a simulation span in two parts, the second one starting with initial conditions based on the final output of the first one. The numerical accuracy in the definition of those conditions for the second simulation showed a completely different behavior than the one observed without dividing the simulation in two. Such sensitivity to initial conditions is the trademark of chaotic systems, and its relevance in disciplines such as climatology, physical chemistry, physiology or fluid turbulence has been extensively studied ever since.

On the other hand, the study of complex networks has been mostly conducted in this century, with mathematical origins rooted in the older branch of mathematics named graph theory. Nowadays, the relevance of networks in many fields (economics, communications, biology) and their applicability to describe complex phenomenon associated to the interconnections between a high number of agents make them very suitable for the analysis of

a high number of applications [New03]. Their presence spans such different topics as biological systems (gene regulatory networks, infection dynamics, species interaction), economics (bank lending mechanisms, market competitions, supply chains), telecommunications and electrical engineering (World Wide Web, power distribution grids) or sociology (professional associations, political parties, clubs, and the like). Research has proven that most social, biological, and technological networks are characterized by non-trivial topological features, with patterns of connection between their elements that are neither purely regular nor random. Besides the structural properties of complex networks, dynamical processes taking place on networks are also extremely important, such as the way traffic flows over the Internet or a disease spreads through a community. Scientific research on complex networks has been mostly focused on topological properties of networks and on the associated dynamics, while study of control techniques of such dynamics has basically started only in recent years.

As opposed to new developments on complex systems theory, the number of applications based on traditional physics had many years to develop and it is nowadays very extensively observed in all sort of daily technologies: internet, cell phones, air conditioning, terrestrial transportation, airplanes, television, etc. Numerous engineering applications have made use of the physics developed mostly during the XIX and XX centuries for their routine use in modern life. Additionally, mathematics has experienced also an extraordinary development in parallel to physics during those decades, mutually impacting each other. One of the subjects strongly related to mathematics and physics is control theory. As described in the following lines, the purpose of this thesis is to contribute to the application of control (extensively used in technologies such as those listed in this paragraph) to complex systems, by providing relevant insights and conclusions on two problems studied here in depth.

Although practically applied since ancient times, the theory of control as an independent discipline started up based on ideas developed from the XIX century on, like the principles of the governors used on rotative steam engines ([Kang16] and figure 1.1). Since the beginning, industry was one of the realms with more control applications: for instance, Jacquard's loom was a remarkable invention that allowed the automatic manufacturing of a variety of weaving patterns, and it was controlled by a chain of punched cards. Such idea was extensively used in the XX century for computer programming during several decades, and thus Jacquard's loom can be considered as an early application of programmable automatic control ([Ess04], figure 1.1).

Figure 1.1: Examples of centrifugal governor (left, [Por18]) and Jacquard's loom (right [Ver17]).

Thus, at that time the practical implementation of the control design was carried out by means of dedicated hardware as with the punch cards, but in the last decades the trend has been towards the use of software embedded in different sorts of central computing devices.

Two concepts are key in control theory: feedback and stability. The concept of feedback was present from the beginning as in the centrifugal governor's principle: two balls are connected to the rotary mechanism that is fed by a fuel valve. When the governor is at rest, the valve is open, while when it is rotating the balls rise due to the centrifugal force. This forces the central valve stem downward so that the valve gets closed, thus decreasing the rotation rate. This way, the engine is controlled to a constant speed by regulating the amount of fuel admitted, providing feedback to the system to compensate for variations in the load, external disturbances, etc.

The concept of stability is also of utmost importance in control. The design of a control mechanism must ensure the stability of the complete system in order to guarantee its behaviour within the expected range of conditions. The Nyquist stability criterion, developed by Harry Nyquist at the Bell Telephone Laboratories, sets the principles for analysing and designing the stability of a feedback system [Oga10]. At that time there was a strong motivation to analyse the stability of electronics designs in many applications (amplifiers, oscillators, etc). The stability theory for linear dynamical systems is extensively developed with many mathematical tools: Bode and Nichols plots, root locus, Routh criterion, etc (ibid.). The equivalent for nonlinear systems is the Lyapunov stability theory, which is applied in nonlinear control [Kha01]. However, the problem of finding an adequate Lyapunov

function to demonstrate and analyse the stability of nonlinear systems limits the range of applicability of said theory.

After 1960, the methods and ideas used hitherto began to be considered as part of classical control theory. The new technology developments and applications showed that models considered up to that moment were not accurate enough to describe the complexity of the real world. This generated important new efforts in this field and new techniques were found (mostly based on the time domain), including such substantial contributions as those obtained by R. Kalman in the filtering and estimation techniques [Kal60], or R. Bellman in the context of dynamic programming [Bry75]. For example, the Kalman filter was implemented in the Apollo program as a key algorithm to be used by the spacecrafts onboard navigation system on its way to the Moon [Grew10].

Besides the aforementioned concepts, optimization is another key topic in mathematics, engineering design and control. It can be regarded as a branch of mathematics whose goal is to maximize a benefit (or minimize a cost) by setting a number of variables to their most adequate value for such purpose. The underlying ideas are present in mathematical relevant topics such as the calculus of variations (the brachistochrone curve being a classical problem in this matter). Regarding control, one of the cornerstones of optimal control theory is the Pontryagin's maximum principle [Bry75], which allows finding the best possible control for taking a dynamical system from one state to another in the presence of constraints. Its rationale is based on the maximization of a Hamiltonian function (this function being also found in chaos theory as explained later on). Optimization theory is applicable to many practical situations (power consumption minimization, shortest or quickest path, transportation routes design, etc.).

Control and estimation theory are currently areas of very intensive research in many subdisciplines: robust control, artificial intelligence, machine learning, etc. Their applications are ubiquitous in the automotive and aeronautical fields, cell phones, industrial automation, robotics, telecommunications, space engineering, etc.

There is a discipline closely related to control theory which has reached an extraordinary development since the middle of the XX century: game theory. This can be defined as the study of mathematical models of conflict and cooperation between intelligent rational decision-makers [Mye91]. It has numerous applications in economics and business, international politics, computer science, biology, psychology, etc. Classical examples are zero-sum

games, prisoner dilemma, auctions, pricing strategy, or war bargaining. The basic elements which are always present in the setup of the problem are the players of the game, the set information and actions available to each of them (and the strategies chosen based on those options), and the payoff for each player of the combined actions taken by him and his opponents.

From a control theory perspective, one can interpret a control law as a type of intelligent rational decision-maker designed to produce a desired effect. Accordingly, game theory can be viewed as the study of conflict and cooperation between interacting controllers, where the identities and goals depend on the specific problem [Mar18]. For instance, the case of competition games considers two players where the benefit of one of them is obtained against the interests of the other. From a control point of view, the strategy followed by the opponent is considered by the other player as the environment and dynamics which the player is trying to control. Optimal control theory is also present in this setup, since the decision-making process followed by each player is defined to discern the best strategy against all possible decisions of the opponent. Furthermore, there is an important branch of control theory named robust control, in which the controller is designed based on a game theory setup using a minimax approach, where the external disturbance and noise are considered as opponent players against the robust controller, which chooses the optimal decision against all possible outcomes of disturbance and noise within a given range [Zho98].

A different game setting connected to control theory is that of cooperation games. Here, there can be many players and the defining feature is that all players follow decision dynamics ultimately leading to a given consensus. Generally, each player has access to different information, and thus it is not possible to follow a centralized controller implementation.

Therefore, game theory can be considered as a generalization of control theory. The second part of the thesis deals with both competition games and consensus dynamics.

As previously explained, the control theory is extensively developed in its application to linear systems [Oga10, Bay99]. Although to a lesser extent, stability and control theory for nonlinear systems has also the subject of deep research and application for many years. Important concepts in nonlinear control include perturbation theory and averaging, backstepping, sliding mode, etc. (see [Kha01] for a good review in the subject).

In terms of complexity, yet a step beyond standard linear and nonlinear control theory is the subject of chaotic systems control, which has also been

the topic of intensive investigation in recent decades. A key feature here is the fact that one can lead a given chaotic system to follow a certain desired dynamic behaviour by means of properly chosen small perturbations, as opposed to non-chaotic systems for which the effort to attain this goal is typically on the order of magnitude of the unperturbed evolution of the dynamical variables. A relevant technique based on this idea is the OGY method (Ott, Grebogi, and Yorke, [Ott90]). This procedure is based on determining some of the unstable low-period periodic orbits that are implicit in the chaotic system dynamics, and based on the location and the stability of these orbits the control designer selects one which yields the desired system performance. Another example of control of chaotic systems is the topic of chaos synchronization, which has also been the subject of detailed study [Hea94, Boc02], and it is related also to communication systems by means of chaos. An extensive review of chaotic systems control is presented in [Boc00].

The first part of this thesis deals with the subject of control of Hamiltonian systems, and in particular the dynamics of the HCN molecule. It should be noted that one topic of paramount relevance in chemical dynamics is the active control of molecular dynamical systems and chemical reactivity. In the present research, the goal of the control is to characterize and select the actions that entail transition between regular and chaotic regime (and also on the molecule dissociation) depending on the value of the control parameter (namely the frequency of the laser exciting the molecule). In this thesis we have characterized the associated behaviour both in phase space and frequency domain, providing evidence of the underlying rationale associated to KAM theory. The research reported here was published in [Lop16].

Another application of control theory carried out in this thesis to complex systems is the control of complex networks, which recently has been the subject of extensive research in the literature ([Liu11, Gao14, Liu16]). Here, the concepts of controllability and observability of linear systems are also applicable for the case of linear dynamics on complex networks, but in order to cope with large networks (that entail non-feasible tests on controllability and observability because of the scale of the problem) the concept of structural control is used to properly handle this issue, because it allows eliciting whether a network is controllable even when the weight of each edge on the network is not known (it is enough to know the existing links among the elements of the network). Taking this approach, the formulation allows deriving a dedicated algorithm identifying the minimum set of inputs that guarantee structural controllability. In this context, the second part

of this thesis also deals with control of complex networks but taken from a different perspective. As already explained above, game theory can be considered as an extension of control theory when more than one controller act on the dynamics of a certain system. The study of Games on Networks has been extensively explored in recent years from a number of perspectives [Nis07, Jack14, Bram14, Ell18, Kar11, Gal10, Ball06, Jack10]. The most commonly found framework features a number of agents linked by means of a complex network and following certain strategies, aiming to achieve a certain objective (i.e. maximizing an associated individual payoff). A typical example of this behaviour is given by the concepts of strategic complements and strategic substitutes, which constitute two canonical approaches for a variety of games [Jack14, Bram14, Gal10]. In many cases, the studied games deal with individuals' behaviour within a social structure, as in [Ell18], where the decisions of single agents towards improvement of their payoff is studied, analysing the features of the network that lead to better Pareto equilibria. Social activities can also imply the search of a key player [Ball06]. A generic review of social and economic networks and associated games is presented in [Jack10]. In other cases, dynamics between biological agents are investigated, as in [Kar11] which addresses the competition of two diseases within a human population, aiming to maximize their spreading over the network.

Additionally, consensus dynamics in networks are also addressed in numerous papers in the literature. This concept includes such important phenomena as synchronization of coupled oscillators, as in the celebrated Kuramoto model [Kur84] where several elements connected through a complex network follow oscillatory dynamics which can lead to phase synchronism (and therefore consensus) depending on the coupling gains. Another important consensus topic deals with flocks dynamics of mobile agents [Olf06] or robots cooperation [Ege02]. Other examples are related to consensus in small-world networks [Xia04] or information fusion algorithms for sensor networks [Xia05]. For a review of consensus dynamics, see [Olf07] and the references therein.

Both concepts of games on networks and consensus dynamics are taken into account in the study reported in [Zha14] and [Zha15], which consider the case of a competition between two agents, linked to a network of elements who are influenced by them. The goal of each player is to maximize its payoff, associated to the sum of the states of the elements of the population. A similar problem is addressed in reference [Far12], in which a number of disseminating agents must be located within a complex network, in order to maximize the distribution of correct information against a group of misin-

formers already localized in the network. This thesis generalizes the problem of games on a network where consensus dynamics are present, by broadening the associated scope. Instead of considering a competition between two single agents, games on networks between two competing teams are explored. A general population (GP) of elements is subject to certain consensus dynamics which depends on the nature of the real problem. Each competing team consists of a network of agents connected to GP, and each member of the team acts on the network with a certain intensity, influencing the consensus dynamics in order to maximize the team's payoff, while ensuring that the overall energy used by the team is bounded for the sake of competition fairness. The concept of energy is here associated to the effort exerted by each team on the game (e.g. money investment, resources dedication, etc.).

Moreover, this thesis considers several consensus dynamics among the members of GP to reach a steady state, obtaining a theoretical optimal set of actions of the team's members which takes into account such dynamics. Additionally, here we compare that result with numerical simulations obtained by genetic algorithms, verifying the optimal solution. The mathematical base relies on singular value decomposition aiming at maximum amplification in the desired singular vector. Furthermore, on this thesis we use the foundations set by this technique to establish the procedure for the optimal design of the connection between the elements of the team and the GP. As a result, one team is able to optimally connect with the general population so that its achievable performance is maximized against the other competing team which uses arbitrary connections.

The research presented here also analyses the possibility of each team aiming at some parts of the population, selecting its strategy and reacting to the action of the opponent team. The agents of each team are then divided in two or more subgroups, each of them specialized in targeting a certain subset of the general population. Thus, each team has the additional control variable of selecting how its action energy is distributed among those groups in order to maximize its payoff, taking into account the equivalent decision of the opponent team. In this case one singular value is associated to each target group, and the optimum action selection is still based on the solution described in the thesis for the whole GP. Finally, it is shown that this setup defines certain game dynamics. An application is considered at the end of the chapter including numerical simulation, where the associated strategies of both teams ultimately lead to a Nash equilibrium.

This thesis is organized as follows: Part I reviews important concepts on dynamical systems and control theory, including Hamiltonian systems,

chaos and also game theory as a generalization of control. Part II presents the study conducted on HCN molecule vibrational dynamics, its control by means of a laser and the results both in phase space and in frequency domain. Part III deals with dynamics on complex networks. In particular, consensus dynamics are described along with competition games between two teams over the state of the nodes of a network. Part IV list the conclusions reached during the research conducted in the framework of this thesis. Literature references and an appendix are available at the end of the document.

Part I

Dynamics and Control

Chapter 2

Dynamical Systems and Chaos Theory

2.1 Dynamical systems

A *dynamical system* changes its state over time, defined by a number of variables whose evolution is governed by a certain law, generally subject to external actions [Kat95, Hale91]. The rule for time evolution deterministically specifies how the state of the system, as given by a set of state variables, changes in time from a given initial condition (i.e. the initial state of the system). It is typically defined by a state vector (i.e. position, velocity, etc.) contained within the state space (for example $\mathbb{R}^n$, with n the number of parameters defining it). Therefore, the three main concepts present in a dynamical system are:

- A state (or phase) space M which is associated to those features of the system that change over time.
- A time variable (either continuous or discrete) which is directly related to the unfolding of events.
- A time-evolution law. This is a rule that determines the state of the system at a given time as a function of the state in previous times. This implies also dependency of the dynamics on external actions, if applicable.

A dynamical system can be formally defined ([Bro10]) as a structure consisting of a state space M and an evolution operator:

$$\begin{aligned} \phi : G \times M &\to M \\ (t, \mathbf{x}) &\mapsto \phi_t(\mathbf{x}) \end{aligned} \tag{2.1}$$

Here G is a semigroup (associated to the time) and $\mathbf{x}$ denotes the state vector of the dynamical system (each element in the vector representing one of the degrees of freedom of the system). The evolution operator satisfies the composition rule given by:

$$\phi_t \circ \phi_s = \phi_{t+s} \tag{2.2}$$

If G is a group, the dynamical system is invertible, resulting in the identity:

$$\phi_t \circ \phi_{t^{-1}} = \phi_e \tag{2.3}$$

where $\phi_{t^{-1}}$ denotes the inverse of ϕ_t and with ϕ_e being the identity element. We refer to the set of phase space points followed by the time evolution of the system ϕ_t as an *orbit* or *trajectory*, starting from the initial condition $x_0 \in M$.

There are two main types of dynamical systems depending on the nature of time:

- Continuous systems, with G = $\mathbb{R}$ (for reversible systems) or G = $\mathbb{R}^+$ (irreversible systems)
- Discrete systems, with G = $\mathbb{Z}$ (reversible systems) or G = $\mathbb{N}_0$ (irreversible systems)

The definition of reversibility is given at the end of this section, since it previously requires the concepts of vector field and map which are introduced in the following lines.

In this thesis both discrete and continuous dynamical systems are present. In particular, continuous Hamiltonian systems are studied in the first part of the thesis (vibrational dynamics of the HCN molecule). On the other hand, the second part deals with discrete dynamics over networks, in the form of consensus dynamics and games played over the network, both of which are described by a discrete time framework.

Let $\mathbf{f} \in C^\infty(M, \mathbb{R}^n)$ (with $M \subset \mathbb{R}^n$) be a function that implicitly defines the rule for the time evolution of an n-dimensional dynamical system by the *initial value problem* [Hale91]:

$$\dot{\mathbf{x}} = \mathbf{f}(\mathbf{x}) \text{ and } \mathbf{x}(0) = \mathbf{x}_0 \tag{2.4}$$

with $\mathbf{x}_0 \in M$ being a given initial condition. Geometrically, the *vector field* $\mathbf{f}$ is such that solutions to the initial value problem are curves on M that are tangent to $\mathbf{f}$ at each point. Indeed, a solution is nothing but the orbit associated to $\mathbf{x}_0$. The family of solutions of possible phase space points $\Phi : \mathbb{R}^n \text{ x } M \to M$ is called the *flow* of the dynamical system.

A set $U \subseteq M$ is said to be invariant if, for every $\mathbf{x} \in U$, $\phi_t(x) \subseteq U$ for all t. If a phase-space point is found such that $\phi_t(\mathbf{x}) = \mathbf{x}$ for all t, x is said to be a fixed point or *equilibrium point*. If, for a given $\mathbf{x} \in M$, there is some $T > 0$ such that $\phi_T(\mathbf{x}) = \mathbf{x}$, the minimum T for which this holds is called the *period* of the closed orbit passing through $\mathbf{x}$. An orbit is called *periodic* if one point of the orbit is periodic, and hence all points are, as it follows by the composition rule of the ow that $\phi_{t+T}(\mathbf{x}) = \phi_T(\mathbf{x})$. Clearly, a periodic orbit is also an invariant set of the dynamics.

A fixed point $\mathbf{x_e}$ is said to be *stable* if for any given neighbourhood $U(\mathbf{x_e})$ (i.e. any connected open set such that $\mathbf{x_e} \in U(\mathbf{x_e})$, there exists another neighbourhood $V(\mathbf{x_e})$ contained in it, $V(\mathbf{x_e}) \subseteq U(\mathbf{x_e})$, such that any solution starting in $V(\mathbf{x_e})$ remains in $U(\mathbf{x_e})$ for all $t \geq 0$. The set is said to be *asymptotically stable* if it is stable, and if there is a neighborhood of $\mathbf{x_e}$ such that for all $\mathbf{x_e}$ starting in it it holds that

$$\lim_{t \to \infty} \|\phi_t(\mathbf{x}) - \mathbf{x_e}\| = \mathbf{0} \tag{2.5}$$

Fixed points can be analyzed for both linear and non-linear systems. The dynamics of a linear system are given in general by means of the following equation:

$$\dot{\mathbf{x}} = A\mathbf{x} \tag{2.6}$$

where $\mathbf{x} \in \mathbb{R}^n$ is the state vector and $A \in \mathbb{R}^{n \times n}$ is the state or system matrix. A broader definition including control inputs and sensor outputs is considered later in this chapter when studying control systems, by means of equation 3.8. The stability of a linear system can be studied by means of the eigenvalues of the matrix A [Bay99].

In the case of a non-linear system, a well known technique to characterize stability of fixed points is given by means of the so called Lyapunov functions [Kha01]. Nevertheless, a first approach to grasp the stability behaviour in the neighbourhood of a fixed point can be achieved by linearization of the system around the equilibrium by means of the Jacobian matrix of first partial derivatives of the vector field $\mathbf{f}$:

$$\dot{\boldsymbol{\xi}} = D\mathbf{f}(\mathbf{x_e}) \cdot \boldsymbol{\xi} \tag{2.7}$$

with $\mathbf{x} = \mathbf{x_e} + \boldsymbol{\xi}$, and $\boldsymbol{\xi} \in M$ a vector with $\|\boldsymbol{\xi}\| << \|\mathbf{x_e}\|$.

When $D\mathbf{f}(\mathbf{x_e})$ has no eigenvalues with zero real part, $\mathbf{x_e}$ is called a *hyperbolic* equilibrium point. For this kind of points their stability type in the non-linear system is determined by the linearization process. This is not applicable for fixed points with zero real parts. In order to characterize the stability of a hyperbolic fixed point of the non-linear system, we first remind that a homeomorphism is an equivalence relation between points in two topological spaces that is continuous in both directions. Using this concept, an important theorem due to Hartman and Grobman [Guc83] states that for a hyperbolic fixed point $\mathbf{x_e}$ there is a homeomorphism h defined in some neighborhood U of $\mathbf{x_e}$ that locally associates orbits of the nonlinear flow $\phi_t(\mathbf{x}) \subseteq \mathbf{U}$ to those of the linear flow $e^{tD\mathbf{f}(\mathbf{x_e})}$.

We now define the local stable and unstable manifolds of $\mathbf{x_e}$ in the neighborhood U respectively as follows [Guc83]:

$$\begin{aligned} W^s_{loc}(\mathbf{x}) &= \{\mathbf{x_e} \in U, \phi_t(\mathbf{x}) \to \mathbf{x_e} \; as \; t \to \infty, \; and \; \phi_t(\mathbf{x_e}) \in U \; \forall t \geq 0\} \\ W^u_{loc}(\mathbf{x}) &= \{\mathbf{x_e} \in U, \phi_t(\mathbf{x}) \to \mathbf{x_e} \; as \; t \to -\infty, \; and \; \phi_t(\mathbf{x_e}) \in U \; \forall t \leq 0\} \end{aligned} \tag{2.8}$$

The global stable and unstable manifolds of $\mathbf{x_e}$ are given by propagating backwards in time the points in the local manifold W^s_{loc}, and forwards for those in the local manifold W^u_{loc}:

$$\begin{aligned} W^s_{loc}(\mathbf{x}) &= \bigcup_{t \leq 0} \phi_t(\mathbf{x})(W^s_{loc}(\mathbf{x})) \\ W^u_{loc}(\mathbf{x}) &= \bigcup_{t \geq 0} \phi_t(\mathbf{x})(W^u_{loc}(\mathbf{x})) \end{aligned} \tag{2.9}$$

An orbit connecting one fixed point to itself is referred as *homoclinic*. On the other hand, those trajectories that connect two distinct equilibrium

points are named *heteroclinic*. The closed path formed by heteroclinic orbits is called *heteroclinic cycles*.

The discrete-system counterpart of a vector field is a *map*. In physics and mathematics, a "map" is any mathematical transformation that is applied over and over again in sequence. Formally, it is a function that associates the state of the system at time $n+1$ with its state at time n.

$$\mathbf{x}(n+1) = \mathbf{f}(\mathbf{x}(n)) \tag{2.10}$$

where $\mathbf{f} : M \to M$ is a map of the state space M into itself and $(\mathbf{x}(n))$ denotes the state at the discrete time n. Each implementation of the mathematical equations is called an iteration of the map. Area preserving maps provide the simplest and most accurate means to visualize and quantify the behavior of conservative systems with two degrees of freedom. The logistic map is a classical scalar example (here M is given by $\mathbb{R}$), determined by a parameter $\lambda > 1$ and defined as:

$$x(n+1) = f(\lambda, x(n)) = \lambda x(n)(1 - x(n)) \tag{2.11}$$

The concepts of equilibrium points, stability and linearization described above for continuous systems are also applicable for discrete-time systems. The concepts of homoclinic and heteroclinic trajectories can also be applied for the Poincaré map defined by the Surface of Section in §2.4.1. This is of high relevance when studying the presence of elliptic and hyperbolic points in the PSOS of dynamical systems, in particular the HCN dynamics under study in part II.

Before finishing this section, let us now define the concept of *reversible dynamical system* [Wig03]. We provide the definition for either a continuous or a discrete time dynamical system, which are respectively given by equations 2.4 and 2.10. We consider a map:

$$F : \mathbb{R}^n \mapsto \mathbb{R}^n \tag{2.12}$$

such that:

$$F \circ F = \phi_e \tag{2.13}$$

where ϕ_e denotes the identity map. Then, a vector field $\mathbf{f}$ is said to be reversible if:

$$\frac{d(F(\mathbf{x}))}{dt} = -\mathbf{f}(F(\mathbf{x})) \tag{2.14}$$

This can be described as the dynamics in the phase space $F \cdot \mathbb{R}^n$ being given by the time reversed vector field.

Similarly, a map g is said to be reversible if

$$g(F(\mathbf{x}(n+1))) = F(\mathbf{x}(n)) \tag{2.15}$$

which implies that in the phase space $F \cdot \mathbb{R}^n$, the map g reverses the time direction of trajectories.

As a final remark, we should note that a dynamical system can be characterized by its behaviour in the time domain as described above (e.g. by means of differential equations in the continuous case or difference equations for discrete time systems) and also in the frequency domain (for example by means of transfer functions in the case of linear systems). This thesis mostly considers the time domain characterization, although frequency analysis is also used in some sections of part II, regarding dynamics of the HCN molecule.

2.2 Hamiltonian Systems

One of the most fundamental description of dynamical systems is the formulation of physical phenomena in terms of the Lagrangian and Hamiltonian mechanics. The derivation of the Lagrange's equation can be obtained based on the so called D'Alembert's principle [Gol80]. For this purpuse, we first define the virtual work of the i^{th} force in the system $\mathbf{F_i}$ along the virtual displacement $\delta\mathbf{r_i}$ by means of the dot product of these two vectors. Then, the dynamics of the system are included into D'Alembert's principle for systems where the virtual work of the forces of constraint vanishes. By introducing generalized coordinates q_j in the equations (which are independent of each other for holonomic constraints) the principle renders a preliminary form of Lagrange's equations, with $j = 1 \cdots N$ and N being the number of coordinates:

$$\frac{d}{dt}\left(\frac{\partial T}{\partial \dot{q}_j}\right) - \frac{\partial T}{\partial q_j} = Q_j \tag{2.16}$$

where T is the kinematic energy and Q_j denotes the generalized force defined by:

$$Q_j = \sum_{i=1}^{N} \mathbf{F}_i \cdot \frac{\partial \mathbf{r}_i}{\partial q_j} \tag{2.17}$$

when the external forces can be derived from the gradient of a scalar potential function V, equations 2.17 can be expressed in terms of the Lagrangian $\mathcal{L} = T - V$:

$$\frac{d}{dt}\left(\frac{\partial \mathcal{L}}{\partial \dot{q}_j}\right) - \frac{\partial \mathcal{L}}{\partial q_j} = 0 \tag{2.18}$$

which are the classical form of Lagrange's equations. It should be noted that this form of the equations can be used even if there is no potential function V which depends only on the generalized coordinates, but there is instead a generalized potential U which depends also on the generalized velocities $\dot{q}_j$, and the Lagrangian is then given by $\mathcal{L} = T - U$. A classical example of such systems is given by the Lorentz force which is applied when a charged particle moves in the presence of a magnetic field [Gol80].

Alternatively, the Lagrange's equations can also be derived from Hamilton's principle. If we define the line integral I of a system as the integral of the Lagrangian between two fixed times t_1 and t_2, this principle states that the motion of the system is such that the variation of the line integral is zero:

$$\delta I = \int_{t_1}^{t_2} \mathcal{L}(q_1, \cdots q_N, \dot{q}_1, \cdots \dot{q}_N, t) dt = 0 \tag{2.19}$$

An alternative description of the dynamics of a system is given in terms of Hamiltonian dynamics. According to Hamilton's formulation, mechanical dynamical systems are described in terms of position coordinates and its conjugate momenta, rather than of generalized velocities and positions as in the Lagrangian formulation. Hamilton's equations are given by [Gol80, Fet80]:

$$\begin{aligned} \dot{q}_i = \frac{\partial \mathcal{H}}{\partial p_i}, \qquad & \dot{p}_i = -\frac{\partial \mathcal{H}}{\partial q_i}, \\ \frac{\partial \mathcal{H}}{\partial t} = -\frac{\partial \mathcal{L}}{\partial t} \qquad & i = 1, \ldots, N \end{aligned} \tag{2.20}$$

where N is the number of degrees of freedom; and $\{q_i\}$ and $\{p_i\}$ are the generalized coordinates and their corresponding conjugate momenta, respectively. The vectorial form is expressed as follows:

$$\frac{d\mathbf{q}}{dt} = \frac{\partial \mathcal{H}}{\partial \mathbf{p}}, \qquad \frac{d\mathbf{p}}{dt} = -\frac{\partial \mathcal{H}}{\partial \mathbf{q}}, \tag{2.21}$$

with $(\mathbf{q}, \mathbf{p}) = (q_1, q_2, \ldots, q_N, p_1, p_2, \ldots, p_N)$ being the state vector formed by the coordinates and the corresponding conjugate momenta.

$\mathcal{H}$ and $\mathcal{L}$ respectively denote the Hamiltonian and Lagrangian functions describing the system, which are related by the Legendre transformation:

$$\mathcal{H}(q, p, t) = \sum_{i=1}^{N} (\dot{q}_i p_i) - \mathcal{L}(\mathbf{q}, \dot{\mathbf{q}}, t), \tag{2.22}$$

where $\dot{q}_i$ are the first derivatives of the generalized coordinates and $p_i = \dfrac{\partial L}{\partial \dot{q}_i}$ are defined as the i^{th} generalized or canonical momenta.

2.2.1 Phase Space

The $2N$ dimensional space formed by the coordinates of the system $\{q_i\}$ and their conjugate momenta $\{p_i\}$ is called the *phase space* of the system, as opposed to that formed only by the position coordinates, which is known as the *configuration space*. In phase space, each point represents a particular state of a dynamical system. The coordinates of the point are numerically equal to the values that the variables assume when the state occurs. Therefore, when these states of the system form a chain of points, this sequence represents the flow of the change of state of the dynamical system.

The motion of the system is obtained by integration of Eq. 2.20, starting from a suitable set of initial conditions, $\mathbf{p}(0)$, $\mathbf{q}(0)$. In this way, trajectories in phase space can be calculated as the evolution in time of this point ($\mathbf{p}(t)$, $\mathbf{q}(t)$), where the motion of the system is most clearly visualized, since all dynamical information is readily apparent.

The Hamiltonian phase space has very special properties. If the system has some translational symmetry then some momenta may be conserved quantities [Fet80]. This concept is generalized in the Noether's theorem [Noe1918].

Additionally, if the Hamiltonian $\mathcal{H}$ does not depend upon time in an explicit way, then the system is also conservative, and it is defined as:

$$\mathcal{H} = T + V(\mathbf{q}), \tag{2.23}$$

and represents the total energy of the system. For the general case, however, the Hamiltonian is not always conservative. For Hamiltonian systems there will be $2N$ dimensions for N degrees of freedom and chaos can occur only when $N > 1$, so that 2 degrees of freedom must be available to observe Hamiltonian chaos.

Phase Space Volume Conservation

A volume element at some initial time, t_0, can be written as

$$dV_{t_0}^N = dp_1(t_0)...dp_N(t_0)dq_1(t_0)...dq_N(t_0). \tag{2.24}$$

It is related to a volume element, dV_t, at time t by the *Jacobian*, $J_N(t_0, t)$ of the transformation between phase space coordinates at time t_0, $\{p_i(t_0)\}$, $\{q_i(t_0)\}$ and coordinates at time, t, $\{p_i(t)\}$, $\{q_i(t)\}$. Thus

$$dV_t^N = J_N(t, t_0)dV_{t_0}^N. \tag{2.25}$$

For systems obeying Hamilton's equations (even if they have a time dependent Hamiltonian), the *Jacobian* is a constant of the motion,

$$\frac{dJ_N(t, t_0)}{dt} = 0, \tag{2.26}$$

and therefore volume elements do not change in time. Thus the phase space behaves like an incompressible fluid.

On the other hand, *dissipative systems* are those for which phase-space volume contracts under the flow.

2.2.2 Conservative Systems

The physical system that conserve total energy have always raised a special interest in the world of physics and mathematics. Often, a complicated system problem can be simplified to a conservative system and enough insight obtained that the task of analyzing the real system is made far easier. A system is considered conservative if the work to displace a particle between two arbitrary points is independent of the path followed between those two points. It can be shown that a necessary and sufficient condition for such result is that the applied force can be derived from a scalar function of position. Thus, in a conservative system the potential energy, V, depends only on the position coordinates. For such systems the total energy E, remains constant with time and the classical mechanical *Hamiltonian function* turns out to be simply the total energy expressed in terms of position coordinates

and conjugate momenta. Conservation of energy in Hamiltonian mechanics requires that $\partial\mathcal{H}/\partial t = 0$. Then, the value of the Hamiltonian remains constant along any trajectory.

Conservative systems themselves are divided into two types, integrable and non–integrable systems. In the following we review some properties of integrable systems.

Integrable Systems

In general, integrable systems have as many independent integrals of motion as they have degrees of freedom (Integrals of motion are also called constants of motion), and the corresponding dynamics is regular.

The mathematical condition for the conservation of a physical magnitude can be expressed by means of Poisson brackets [1].

Let us consider a phase space function, $f(q_i,\, p_i,\, t)$

$$\frac{df}{dt} = \frac{\partial f}{\partial t} + \sum_{i=1}^{N}\left(\frac{\partial f}{\partial q_i}\dot{q}_i + \frac{\partial f}{\partial p_i}\dot{p}_i\right). \tag{2.27}$$

By using Hamilton equations, Eq. 2.27 can be rewritten as

$$\frac{df}{dt} = \frac{\partial f}{\partial t} + \{f, \mathcal{H}\}_{\text{Poisson}}, \tag{2.28}$$

where

$$\{f, \mathcal{H}\}_{\text{Poisson}} = \sum_{i=1}^{N}\left(\frac{\partial f}{\partial q_i}\frac{\partial \mathcal{H}}{\partial p_i} - \frac{\partial f}{\partial p_i}\frac{\partial \mathcal{H}}{\partial q_i}\right). \tag{2.29}$$

These relation can be used to express Hamilton's equations as follows [Gol80]:

$$\dot{q}_i = \{q_i, \mathcal{H}\}_{\text{Poisson}}, \qquad \dot{p}_i = \{p_i, \mathcal{H}\}_{\text{Poisson}} \tag{2.30}$$

It can be easily shown that the Poisson brackets fulfill

$$\{f, g\}_{\text{Poisson}} = -\{g, f\}_{\text{Poisson}}$$

[1] The Poisson bracket of two functions, $r(q,p)$ and $s(q,p)$, of the generalized coordinates and momenta, q_j,p_j, is defined as

$$\{r, s\}_{Poisson} = \sum_j \left[\frac{\partial r}{\partial q_j}\frac{\partial s}{\partial p_j} - \frac{\partial r}{\partial p_j}\frac{\partial s}{\partial q_j}\right]$$

and are invariant under canonical transformations[2].

The conservation condition for a function $f(q_i, p_i, t)$ can then be expressed in terms of Poisson brackets as:

$$\{\mathcal{H}, f\}_{\text{Poisson}} = \frac{\partial f}{\partial t} \tag{2.31}$$

Moreover, the integrability condition for a time independent conservative systems can be expressed as

$$\{f_i, f_j\} = 0 \qquad (i, j = 1, \ldots, N), \tag{2.32}$$

where one of the conserved function is the Hamiltonian.

Action–Angle Variable

Hamilton equations of motion can be written in terms of any convenient set of generalized coordinates. Therefore, one can transform between coordinate systems and leave the form of Hamilton's equations invariant via canonical transformations. There is, however, one set of canonical coordinates which plays a distinctive role in terms of the analysis of chaotic behavior in classical nonlinear systems. These are the action–angle variables [Fet80]. The systems in which motion is periodic are have a significant importance in physics. For the case of one degree of freedom, there are two types of periodic motion if we consider the evolution in the phase space.

1. In the first case, the orbit is closed and the system periodically revisits the same point in such space. This type of motion is referred as *libration* or also as a oscillatory motion.

2. The second type implies that the generalized momentum p periodically depends on the generalized coordinate q. This type of motion is generally defined as a *rotation*, and in this case q increases indefinitely (for a conservative system).

A classical example for one degree of freedom is the simple pendulum with mass m and longitude l. The Hamiltonian of the system is given by:

$$\mathcal{H}(p, \theta) = mgl(1 - cos(\theta)) + \frac{p^2}{2ml^2} \tag{2.33}$$

[2]Canonical transformation deal effectively with integrable systems. They corresponds to a transformation from one set of Hamiltonian coordinates ($\mathbf{q_A}$, $\mathbf{p_A}$) to another ($\mathbf{q_B}$, $\mathbf{p_B}$), and satisfying $\partial(\mathbf{q_B}, \mathbf{p_B})/\partial(\mathbf{q_A}, \mathbf{p_A}) = 1$

which is equal to the total energy E. Here, θ denotes the angle of the pendulum with respect to the vertical direction and g is the gravity acceleration. When the energy of the system is below the maximum potential energy $E < 2mgl$, the motion follows an oscillatory pattern. The orbits have a stable equilibrium point for $\theta = 0$, which is called an *elliptic point*. When $E > 2mgl$ the motion of the system is described by a rotation. The limit value $E = 2mgl$ is a bifurcation point between both types of motion. It is an unstable equilibrium point (*hyperbolic*) because all trajectories diverge from this point.

For either type of periodic motion we can define a new variable named action and defined in terms of the generalized coordinate and angular momentum:

$$I = \oint p dq \tag{2.34}$$

In this equation, the integration is conducted over a complete period of the motion. Let us now consider a generic case of an integrable system. A canonical transformation from the old variables ($\mathbf{p}$, $\mathbf{q}$) to a new set of angle action variables, ($\mathbf{I}$, $\boldsymbol{\theta}$), always exists, such that $\mathcal{H}$ only depends on the actions. Hamilton equations in these new coordinates present a specially simple form

$$\begin{aligned} \dot{\theta}_i &= \frac{\partial \mathcal{H}}{\partial I_i} = \omega_i(\mathbf{I}) \\ \dot{I}_i &= -\frac{\partial \mathcal{H}}{\partial \dot{\theta}_i} = 0 \end{aligned} \tag{2.35}$$

that can be easily integrated giving

$$\begin{aligned} \theta_i &= \omega_i(\mathbf{I})t + \delta_i \\ I_i &= I_{i0} \end{aligned} \tag{2.36}$$

where ω_i are the N frequencies characterizing the motion.

For an integrable classical mechanical system with N degrees of freedom, each isolating integral of motion constrains flow of trajectories to a $2N - 1$ dimensional surface in the $2N$ dimensional phase space. The actual flow of trajectories in phase space lies on the intersection of these N surfaces. Thus, for integrable systems a given trajectory lies on an N dimensional surface (the interaction of N surfaces) in the $2N$ dimensional phase space and every trajectory is either quasiperiodic or periodic stable.

2.3 Dynamical Chaos and KAM theory

2.3.1 Non–Integrable Classical Systems. Chaos

As commented in the introduction, Henri Poincaré was one of the first to discover the deterministic type of chaos. Edward Lorenz referred to chaos as physical processes that appear to proceed according to chance even though their behaviour is in fact determined by precise laws [Lor93].

Formally, chaos is defined in terms of the dynamical behavior of pairs of orbits which initially are close together in phase space. If the orbits move apart exponentially in any direction in the phase space, the flow is said to be chaotic, which means that the flow defined by the dynamical system shows a sensitive dependence on initial conditions. A flow $\phi_t : A \to A$ exhibits such dependence if there is some $\delta > 0$ such that for any $\mathbf{x} \in A$ and any neighborhood $U(\mathbf{x})$ there exists $\mathbf{y} \in A$ and $t \geq 0$ so that

$$\|\phi_t(\mathbf{x}) - \phi_t(\mathbf{y})\| > \delta \tag{2.37}$$

In order to determine the dependence of a dynamical system to initial conditions, the concept of Lyapunov exponents is commonly used. Lyapunov exponents are asymptotic measures of the average exponential rate of divergence of infinitesimally nearby initial conditions. Let us consider a dynamical system evolving on an n-dimensional phase-space manifold M and a connected region $U \to M$, such that any orbit starting within it, possibly after going through a transient, settles onto an attractor. Let us further assume the dynamics of the continuous-time system to be represented by a system of first-order ODEs (see equation 2.4) starting from a given initial condition $\mathbf{x_0} \in U$. Then, an infinitesimal displacement along the trajectory represented by $\mathbf{y}(t) \in T_{\mathbf{x}(t)}M$ where $T_{\mathbf{x}(t)}M$ is the tangent (linear) space at the orbit point $\mathbf{x}(t)$, evolves according to the following equation:

$$\dot{\mathbf{y}} = D\mathbf{f}(\mathbf{x}) \cdot \mathbf{y} \tag{2.38}$$

with $D\mathbf{f}(\mathbf{x})$ being the Jacobian matrix evaluated at $\mathbf{x}(t)$. The solution to 2.38 can be expressed by:

$$\mathbf{y}(t) = Y(t, \mathbf{x}) \cdot \mathbf{y}(0) \tag{2.39}$$

where $Y(t, \mathbf{x})$ is the fundamental matrix of solutions of equation 2.38. For ease of notation we will simply denote $Y(t, \mathbf{x}) \cdot \mathbf{y}$ as $Y_t \cdot \mathbf{y}$. Then, the Lyapunov Characteristic Exponent (LCE) of order 1 for an orbit starting at $\mathbf{x}$ and a tangent (deviation) vector $\mathbf{y}(t) \in T_{\mathbf{x}(t)}M$ is defined as

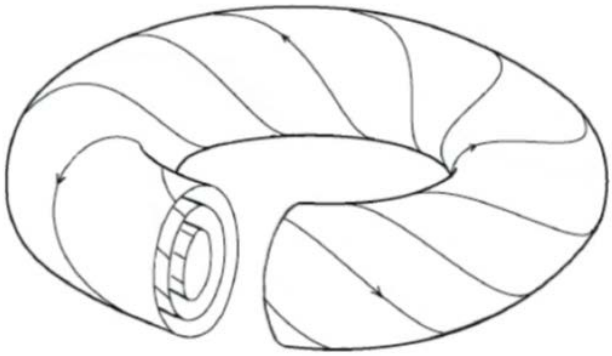

Figure 2.1: Graphical representation of phase space foliated by tori. (Adapted from [Sco14])

$$\chi(\mathbf{x}, \mathbf{y}) = \lim_{t \to \infty} sup \frac{1}{t} log \|Y_t \cdot \mathbf{y}\| \tag{2.40}$$

There will be one such exponent for each dimension phase space. If all the Lyapunov exponents are zero, the dynamical flow is regular. If just one exponent is positive, the flow will be chaotic.

As stated before, a system with N degrees of freedom is integrable if it has N independent isolating integrals. In the same way, the systems which do not fulfill this condition are said to be non–integrable or chaotic.

Non–integrable systems may themselves be divided into two classes. One class contains the completely chaotic systems such as the Sinai billiard and the non–circular stadium. Such systems generally have infinite hard convex surfaces or hard surfaces and irregular shape. The hard surface makes the Hamiltonian non–smooth. They contain an infinite number of periodic orbits but they are all unstable. Non–integrable systems with smooth Hamiltonians comprise the second class of non–integrable system.

The class of mechanical systems that we deal with belongs to the second class of chaos (smooth chaos). It generally contains a mixture of quasiperiodic orbits and chaotic orbits, and a mixture of stable and unstable periodic orbits. Although the motion of these systems is not restricted to tori, it can in general be very complicated. Chaotic regions occur when isolating integrals of motion are destroyed locally by nonlinear resonances.

2.3.2 KAM and Poincaré–Birkhoff Theorems

Between the two extreme cases of the behavior of the dynamical system, integrable and completely ergodic, there are many intermediate cases. Some of invariant tori, resonant tori, which affected by the perturbation will be destroyed, meanwhile the non–resonant ones resist to destroy and continue as invariant tori. The non–resonant tori which have not been destroyed by resonances are called KAM tori or KAM surfaces. The KAM theory applies to a generic Hamiltonian system whose motion is governed by a Hamiltonian of the form

$$\mathcal{H} = \mathcal{H}_0 + \varepsilon\mathcal{H}_1 \tag{2.41}$$

where ε is a small parameter controlling the degree of the perturbation. The zeroth–order Hamiltonian, $\mathcal{H}_0$, is an integrable approximation to $\mathcal{H}$, which has nonzero Hessian and $\mathcal{H}_1$ is the perturbation term which for oscillator systems can be written in terms of action–angle variable as

$$\mathcal{H}_1 = \sum_{n_1=-\infty}^{\infty} \sum_{n_2=-\infty}^{\infty} V_{n_1,n_2}(I_1, I_2) e^{i(n_1\theta_1 + n_2\theta_2)}, \tag{2.42}$$

The KAM theorem (due to Kolmogorov, Arnold and Moser) demonstrates the continued existence of certain invariant tori as the perturbation parameter ε increases from 0, at which the system is considered to be integrable. When $\varepsilon \neq 0$ the system moves to non–integrability, but in a way which is explained by this theorem. The tori which are characterized by a "sufficiently irrational" frequency ratio, $\alpha = \omega_1/\omega_2$, survive. Such ratio is also referred as *winding number*. For a two degrees of freedom system this irrationality condition is given by

$$\left| \frac{\omega_1}{\omega_2} - \frac{n}{m} \right| > \frac{K(\varepsilon)}{m^{5/2}} \tag{2.43}$$

for all integer numbers n and m. $K(\varepsilon)$ is a function of the perturbation which tends to zero as the perturbation disappears. These tori, which are only distorted by the perturbation, are called *KAM tori*. The rest of tori are destroyed, but according to two different mechanisms depending on the value of α (see figure 2.2).

If α is a rational number (resonant tori), the previous condition does not hold for any value of the perturbation. The fate of these tori is regulated by the Poincaré–Birkhoff theorem [Losk07, LeC10], which states that: *under small enough perturbations, an even number of fixed points of the original*

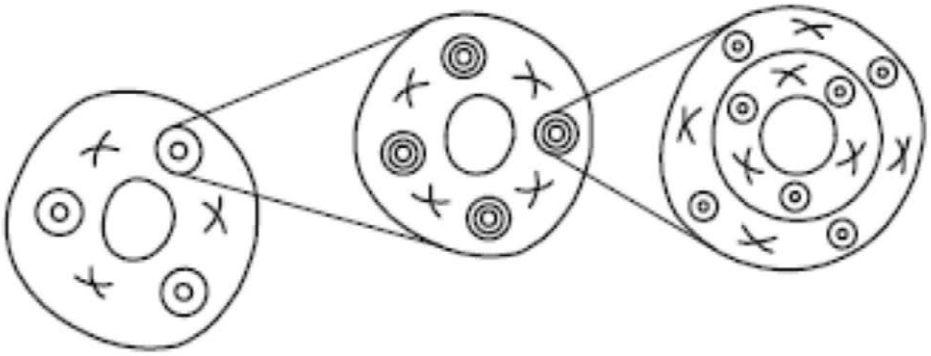

Figure 2.2: Destruction of tori. Source: [Losk07]

torus survive; half of them are elliptic, and the other half are hyperbolic. The elliptic points are surrounded by new tori (stability islands), some of them rational, and some of them irrational. Again the rationals and some of irrationals will be destroyed by the perturbation, according to the KAM theorem. Then, the previous structure is repeated again and again at a finer scale.

In the neighborhood of the hyperbolic points (related to the separatrix of $\mathcal{H}_0$) the motion becomes very complex, due to the homoclinic oscillations discovered by Poincaré. The incoming and outcoming manifolds cannot cross, and then they cross to themselves an infinite number of times. The points at which they cross are referred as homoclinic, and they form the so called homoclinic tangle (see figure 2.3). These tangles constitute bands of stochasticity or chaos, which are separated from each other by the intact KAM tori [Chi79].

Rational Approximates

Each KAM torus has an irrational winding number. For this reason it is impossible to locate a given KAM torus exactly numerically. Each irrational number can be approximated by a unique sequence of fractions which converge to the irrational number. Thus the winding number can be presented

in term of a continued function as follow:

$$w \equiv [a_0, a_1, a_2, ...] = a_0 + \frac{1}{a_1 + \frac{1}{a_2 + \frac{1}{a_3 + ...}}}, \tag{2.44}$$

with a_i integer and $a_i \geq 1$ for $i \geq 1$. Each rational and irrational number may be represented uniquely by a sequence [a_0, a_1, ...]. For irrational numbers the sequence will contain an infinite number of entries. The rational approximates to a given continued fraction are obtained by terminating the sequence by letting $a_i = \infty$. Thus, for a given sequence, $w = [a_0, a_1, a_2, ...]$, the rational approximates N_i/M_i, are given by

$$\frac{N_i}{M_i} = [a_0, a_1, ..., a_i, \infty] \tag{2.45}$$

The most "irrational number" is given by the sequence $a_i = 1$ for all i. That is

$$[1, 1, 1, ..., 1, ...] \equiv \gamma = \frac{1}{2}(1 + \sqrt{5}). \tag{2.46}$$

The number γ is called the golden mean is considered to be the most irrational number because it is hardest to approximate by rationals. Indeed the sequence ending in a series of 1's are the slowest converging sequence and represent those rational numbers which are the hardest to approximate by rationals. This has important sequence for dynamics.

It is well known that the KAM tori are destroyed by resonances between degrees of freedom whose periods are rationally related. Thus, each rational approximate will be associated to a resonance region in the phase space and a corresponding island chain. Furthermore, the last KAM torus that is destroyed has an winding number equal to the aforementioned golden mean.

Cantori

As it is mentioned before, a KAM tori is destroyed when the resonance zones associated with neighboring periodic orbits begin to squeeze holes in it. The tori which are not irrational enough according to Eq. 2.43, are also destroyed by the perturbation. But they turn into invariant ensembles called *cantori* [Rad88]. The nature of the cantori is well understood in terms of their Poincaré surface of section (PSOS, see section §2.4). They are quasiperiodic orbits, similar to the normal invariant tori, but they are fractal geometrical objects, with non-integer dimensions, which is a Cantor set, in the PSOS. Contrary to what happens with the invariant tori, the cantori only represent partial barriers for the flux of trajectories in phase space [Losk07]. In some

Figure 2.3: Graphical representation of the Poincaré Homoclinic tangles, adapted from [Losk07]

sense, they can be considered remnants of regularity, similar to the periodic orbits, which are embedded in the chaotic part of phase space, imposing some sort of structure in it.

Systems With More Than Two Degrees Of Freedom

For systems with two degree of freedom, the existence of invariant tori has a drastic effect in the structure of the phase space. Since two trajectories cannot cross in phase space, each cantorus divide it into two unconnected parts. However, for systems with $N > 2$ this is not true: a hypersurface of N dimensions (corresponding to an invariant torus of a N–dimensional system) do not define an inner and an outer regions in a space of $2N$ - 1 dimensions (energy shell).

Then, despite the existence of zones of regular motion, the chaotic areas are interconnected, constituting what is known as the Arnold web, and a single trajectory can explore the whole chaotic region, giving rise to which is known as Arnold diffusion.

2.4 Chaos indicators

There are several indicators that can be used for the characterization of the dynamics of Hamiltonian systems, The most popular one is the Poincaré

Surface of Section (PSOS) which has the limitation of being applicable only to 2D dynamical systems. This chapter describes this method along with the SALI coefficient and the Frequency Analysis indicator.

2.4.1 Poincaré Surface of Section (PSOS)

A very convenient way to distinguish between regular (non–chaotic) behavior and chaotic motion is by looking at a diagram called a *Poincaré surface of section* (PSOS), which is used to visualize the structure of phase space in 2D dynamical systems. The PSOS is a representation of the intersection of a given trajectory with a suitable plane in phase space, taking only those points for which the plane is crossed in a given direction.

The PSOS defined in this way consists of a sequence of points

$$\begin{aligned} (p_1(0), q_1(0)) &\xrightarrow{T} (p_1(1), q_1(1)) \\ (p_1(1), q_1(1)) &\xrightarrow{T} (p_1(2), q_1(2)) \\ &\cdots\cdots \end{aligned} \tag{2.47}$$

and the transformation T is a *map*. For Hamiltonian systems this Poincaré map is an area preserving map, due to the Liouville theorem.[1]

In order to visualize the PSOS, let us consider a conservative system. The Hamiltonian of a conservative system is the isolating integral of the motion and can be written as

$$\mathcal{H}(q_1, q_2, p_1, p_2) = E, \tag{2.48}$$

where the energy, E, is constant and restricts trajectories to lie on a three dimension surface embedded in the four dimension of phase space. So that, one can express one of the variables as a function of the others. For example, let us take p_2 as

$$p_2 = p_2(q_1, q_2, p_1, E) \tag{2.49}$$

It is evident from Eq. 2.49 that p_2 depends parametrically on the energy, E. If the system has more than one spatial dimension, one must take a slice through phase space (which has twice as many dimensions as the number of spatial dimensions: i.e. a 2D system has a 4–dimensional phase space) in order to create a 2D plot

$$[q_1, q_2, p_1, p_2] \rightarrow [q_1, q_2, p_1, p_2(q_1, q_2, p_1, E)] \rightarrow [q_1, q_2, p_1]E, \tag{2.50}$$

[1]The Liouville equation is a linear partial differential equation. In non–integrable classical systems, the evaluation of individual orbits in phase space can be examined using *PSOS*. At this level, the chaos can be seen in some regions of phase space. However, if we were to describe their evolution in terms of the probability distribution in phase space using the Liouville equation, we would see no chaos.

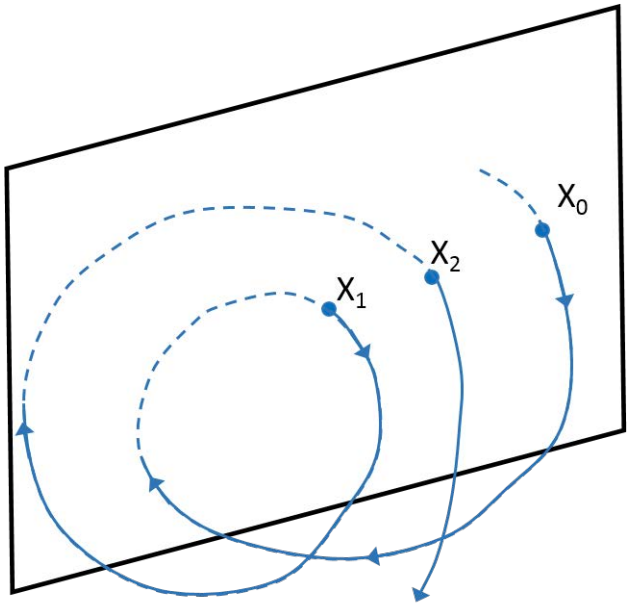

Figure 2.4: Graphical representation of the Poincaré Surface of Section.

$$[q_1, p_1]_E, q_2 = cte. \tag{2.51}$$

If the system has a second isolating integral,

$$I(q_1, q_2, p_1, E) = I_0(= cte.), \tag{2.52}$$

the Eq. 2.52 can be used for obtaining

$$I(q_1, q_2, p_1, p_2(q_1, q_2, p_1, E)) = I(q_1, q_2, p_1, E) = I_0(E), \tag{2.53}$$

The combination of Eq. 2.52 and Eq. 2.53 gives

$$p_1 = p_1(q_1, q_2, E, I_0) \tag{2.54}$$

If q_2=0, then the trajectory lies on a one dimensional curve. By the construction of the PSOS, it will be easy to distinguish between the motion in the regular regime and the motion in the ergodic regime. The motion in the regular regime takes place on the surface of a torus, which renders a line in the PSOS when it is cut by the sectioning plane. On the other hand, in the ergodic regime, the motion takes place in the 3D energy shell, and then the successive intersections of the trajectory with the PSOS will fill in an area.

Another important property of the PSOS is that it allows to observe the appearance of chains of islands. When chaos is present in Hamiltonian

systems, it is observed that regular motion and chaos regions coexist for any energy, and that the proportion of chaos increases with energy. This behaviour is general for any typical Hamiltonian system and can be explained with the aid of the (previously described) KAM and Poincaré – Birkhoff theorems.

The global structure of the phase space can be visualized by *composite* PSOS, which consists in the superposition, in the same figure, of the PSOS of a significant ensemble of trajectories calculated with different initial conditions, all of them calculated at the same energy.

2.4.2 The SALI coefficient

The Small Alignment Index (SALI) is a chaos indicator based on the analysis of the separation of nearby orbits, gauging the behavior of the associated vectors. It is calculated from the integration of Eqs. (2.20), and its applicability is essentially independent of the dimensionality of the system.

Let us consider a reference trajectory, defined by the system state (column) vector

$$\mathbf{z} = (\mathbf{q}, \mathbf{p})^*, \tag{2.55}$$

where the asterisk denotes the transpose operation. Hamilton equations of motion for this variable are written in symplectic form as

$$\frac{d\mathbf{z}}{dt} = J\,\frac{\partial \mathcal{H}(\mathbf{z})}{\partial \mathbf{z}} = J\,\nabla \mathcal{H}(\mathbf{z}) \tag{2.56}$$

with

$$J = \begin{bmatrix} 0_N & I_N \\ -I_N & 0_N \end{bmatrix} \tag{2.57}$$

Let us consider now two nearby trajectories, $\mathbf{z_1}$ and $\mathbf{z_2}$, as shown in Figure 2.5. The evolution of the deviation vectors $\mathbf{v_i} = \mathbf{z} - \mathbf{z_i}$ $(i = 1, 2)$ is given as

$$\frac{d(\mathbf{z} - \mathbf{v_i})}{dt} = J\,\nabla \mathcal{H}(\mathbf{z} - \mathbf{v_i}) \tag{2.58}$$

Now by Taylor expanding $\mathcal{H}$ for small $\mathbf{v_i}$ and taking Eq. (2.56) into account, one obtains

$$\frac{d(\mathbf{v_i})}{dt} = J\,\nabla^2 \mathcal{H}(\mathbf{z})\mathbf{v_i} \tag{2.59}$$

Let us point out that all derivatives involved in the above expression can be analytically evaluated for the HCN model that are used.

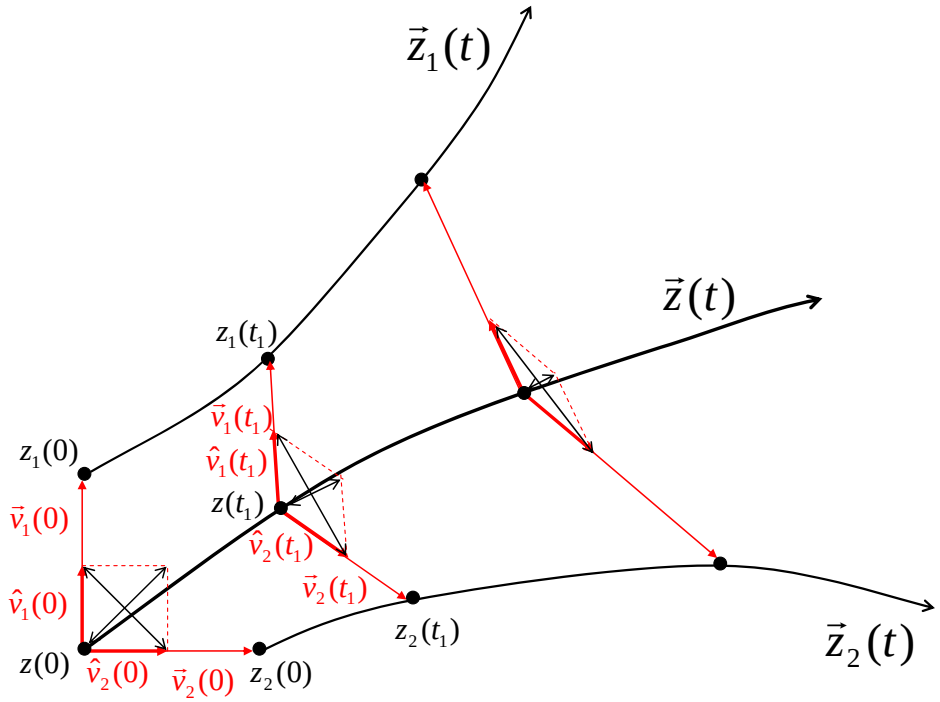

Figure 2.5: Graphical illustration of the calculation of the SALI indicator [Lop16].

Then, Eqs. (2.56) and (2.59) are simultaneously propagated for a given set of initial conditions, thus obtaining both the reference trajectory and the deviation vectors of the two nearby orbits.

When the dynamics are chaotic in the vicinity of the reference trajectory, the nearby orbits exponentially diverge, and one of the axes of the rhomboid formed by the two deviation vectors will quickly go to zero, as time progresses (see Figure 2.5). The SALI indicator is then defined as [Ege02]

$$SALI(t) = \min\left(\left|\hat{\mathbf{v}}_1 + \hat{\mathbf{v}}_2\right|, \left|\hat{\mathbf{v}}_1 - \hat{\mathbf{v}}_2\right|\right) \tag{2.60}$$

where $\hat{\mathbf{v}}_{1,2}$ are unit vectors in the directions of $\mathbf{v}_{1,2}$. It is common practice to take as the representative value of the $SALI(t)$ for a given trajectory its maximum in the tail of the orbit. In the case of a chaotic trajectory, this indicator exponentially decreases in time towards zero, while for regular orbits it remains close to a fixed value [Beni15].

2.4.3 Frequency analysis

An alternative approach to characterize the behavior of a dynamical system is the use of the so-called frequency map analysis introduced by Laskar [Xia04], which has been extensively used in different areas, such as celestial mechanics, [Bay99] highly excited atoms, [Ott90] and vibrational dynamics of small polyatomic molecules [Boc02, Boc00, Liu11]. This technique provides very straightforward pictures of the global dynamics of multi-dimensional systems in the frequency domain.

For each initial condition in phase space, the system frequencies are computed over a finite time span. From it, the fundamental frequency, i.e. that with the highest amplitude, is retained. In particular, it is first computed as

$$f_j(t) = q_j(t) + ip_j(t), \qquad j = 1, 2, \cdots, N \tag{2.61}$$

with $q_j(t)$ and $p_j(t)$ being the j^{th} generalized coordinates and momenta at time t, respectively.

The frequency decomposition of any of the above defined functions over a finite time interval $[-T, T]$ can be calculated by means of the Fourier Transform (FT)

$$f(t) = \sum_{n=-\infty}^{\infty} a_n \, e^{i\pi nt/T} \tag{2.62}$$

to obtain a set of frequencies with a precision of $\sim \pi/T$. To go beyond this limitation one must resort to a different basis set, using better suited exponents. For this purpose, the prescription proposed by Laskar [Gao14] is use herein. A first frequency, ν_1, is evaluated by maximizing the scalar product

$$\phi_1(\nu) = \langle e^{i\nu_1 t} | f(t) \rangle \tag{2.63}$$

where $\langle \ | \ \rangle$ denotes a complex symmetric inner product (not complex conjugation!). This procedure is started from an initial guess, obtained with a standard fast Fourier transform (FFT) method. The other frequencies are then obtained in a similar way by finding those values of ν_n maximizing

$$\phi_n(\nu) = \langle e^{i\nu_n t} | f_{n-1}(t) \rangle \tag{2.64}$$

where $f_{n-1}(t)$ are functions obtained by eliminating from $f(t)$ the contribution of the previously determined frequencies, $\{\nu_1, \nu_2, \ldots, \nu_{n-1}\}$. Since the basis set formed by the elements $e^{i\nu_n t}$ is not orthogonal, it is necessary to carry out a (Gram-Schmidt) orthonormalization procedure. After that, one finally obtains

$$f(t) = \sum_{n=-\infty}^{\infty} b_n \, e^{i\nu_n t} \tag{2.65}$$

It should also be mentioned that a Hamming window filter, $\chi(t) = 1 +$

$\cos(\pi t/T)$, is used in the computation of the previous scalar products, in order to accelerate the convergence. In this way, very accurate, i.e. $\sim T^{-3}$, values for the frequencies, four orders of magnitude more precise than those rendered by the standard FFT methods, are typically obtained. Afterwards, the fundamental frequencies in each coordinate, ω_1 and ω_2 for the case of two degrees of freedom, are obtained by examination of the results associated to the largest weights (which consists of the fundamental frequencies plus the different harmonics and combination bands among them).

When these two frequencies are in a $n_1 : n_2$ resonance, condition $\omega_1/\omega_2 = n_1/n_2$ is fulfilled. We will denote these resonant frequencies as $\omega_{1,2}^{[n_1:n_2]}$ with the subindex and superscript identifying, respectively, coordinate and order of the resonance.

2.4.4 Diffusion coefficient

In the analysis presented in following chapters, we also calculate the local diffusion strength coefficient, providing an estimation of the local (regular

or chaotic) behavior of the orbit, by computing along the trajectory the following expression

$$\mathcal{D}(t) = \max\left\{\frac{\partial\omega_1}{\partial t}, \frac{\partial\omega_2}{\partial t}\right\} \tag{2.66}$$

That is, for each trajectory, the derivatives of the fundamental frequencies on each coordinate are obtained numerically using a finite differences procedure, only retaining that corresponding to the maximum value, as expressed in the above equation. Here, large values of $\mathcal{D}$ correspond to big variations in the frequencies, and hence to a chaotic behavior, while the opposite happens in the areas of regular motion.

In this case, and similarly to what is done in the previous subsection with the SALI indicator, this magnitude is computed for a large number of trajectories with initial conditions chosen on a fine grid in the corresponding (q_1, p_1) PSOS, and plot the corresponding values of $\mathcal{D}(t)$ superimposed to the PSOS points rendered by the trajectory using a suitably defined scale of colors. In this way, a PSOS colored with $\mathcal{D}$ map is obtained, which allows to characterize the structure of phase space from the point of view of the local diffusion coefficient, simply analyzing the dynamical properties of single trajectories.

Chapter 3

Control theory: mathematical background

The theory of control is an extensive branch of knowledge that is subject to constant research and that encompasses many different concepts: linear control, frequency versus time domain analysis, robust control, estimation algorithms, optimal control, etc. The available literature in this field is vast, including innumerable and excellent general reviews (e.g. [Oga10, Bay99, Kha01]). This section describes some basic concepts which are applied to all sorts of control systems commonly found in engineering problems.

3.1 Control Concepts

The term control generally refers to the action of bringing a dynamical system from a certain point in the state space onto the one desired and specified in the problem. This can include achieving a fixed point in time, or tracking a particular reference trajectory. In a broader approach, it can also include the change of its dynamic regime into a desired one, as in the case of part I of this thesis.

The main elements of a control problem are (see figure 3.1):

- The *plant*, corresponding to the dynamical system subject to the control action, which the designer is trying to bring to a certain desired behaviour or state.
- The *sensors*, which measure the state of the system in a direct or indirect way (for example measuring a voltage directly linked to a physical property of the system).

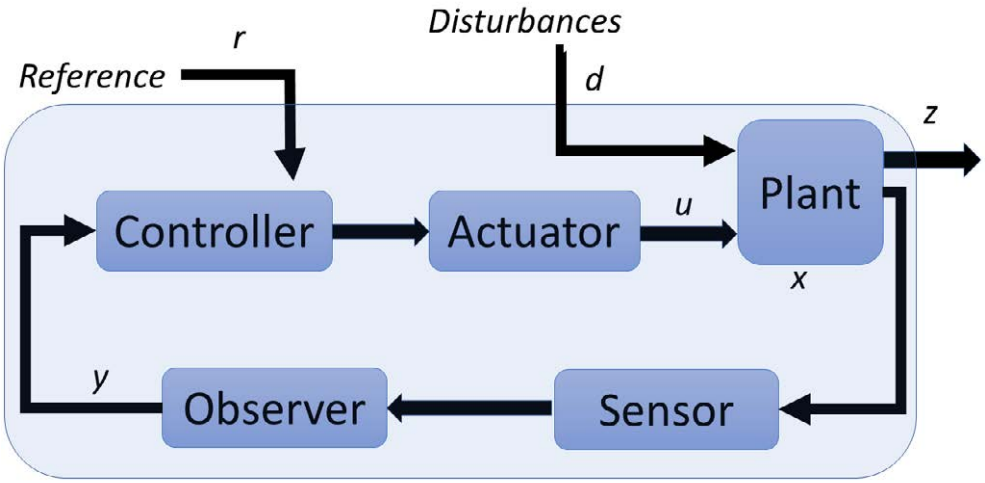

Figure 3.1: Typical control layout

- The *actuators*, which exert an action on the system (torque, force, heat, etc.) in order to bring it to the desired state.
- The *observer*, which estimates the state of the system (or part of it) based on the measurements provided by the sensors and potentially on a model of the system's dynamics.
- The *controller*, defined as a mathematical expression or algorithm that computes the action to be applied by the actuators as an input to the dynamical system in order to lead it to the desired behaviour. Control design can then be conducted and the available techniques for this task is very wide : root locus, state-space, Linear-Quadratic Regulator, robust control, etc.
- The *disturbances*, which are present in the environment and affect the dynamics of the system in an undesired but unavoidable way.
- The *reference signals* or commands, which indicate the desired behaviour or trajectory of the system in the state space.

Thus, the general control architecture involves six (possibly vector) signals of fundamental significance in any control problem. These are the system state x, the reference signal r, the exogenous disturbances d, the controlled input u, which is to be provided by the actuators to the plant, the performance z of the system which indicates how well the system behaves according

to a criterion established by the user or designer (and which depends directly or indirectly in the state of the system), the estimated output y based on measurements, which provides information of the system's state and it is used as an input to the feedback controller.

There are two main types of control systems:

Open loop control The control architecture is such that feedback sensors are not used, and the control is applied to the actuators by means of feedforward. This scheme is used for rejection of disturbance when this can be measured, and also for command following based on model of the plant. Also the scheme is applied when state of the system cannot be measured directly or indirectly.

Closed loop control This scheme is the most frequently used, and it is applied when there are relevant uncertainties in the dynamics or in the disturbances. In this case, feedback is used to include the estimation of the state as an input to the controller (as shown in figure 3.1). Stability issues have to be carefully considered.

For any control problem, it is always very important having a proper model of the dynamical system. Very often this implies issues in the control performance (model uncertainties, non-modelled dynamics, etc.). Typically the model is based on a set of differential equations, or in some cases by characterizing the frequency response. Often the model relies on linear equations, which allow a substantial set of tools if the system is also time-invariant (transfer function in the frequency domain, Nyquist plots, gain and frequency stability margins, etc). However, the nonlinear part of the dynamics is to be assessed in case it significantly alters the modelled linear dynamics. In that case, nonlinear control is meant to deal with those type of systems.

The generic description of linear systems by means of state space equations is as follows:

$$\begin{aligned} \dot{\mathbf{x}} &= A\mathbf{x} + B\mathbf{u}, \\ \mathbf{y} &= C\mathbf{x} + D\mathbf{u} \end{aligned} \tag{3.1}$$

where $\mathbf{x} \in \mathbb{R}^n$ is the state vector, $\mathbf{u} \in \mathbb{R}^m$ is the control vector that includes all control signals, and $\mathbf{y} \in \mathbb{R}^l$ is the output vector, denoting the signals observed by the sensors. On the other hand, $A \in \mathbb{R}^{n \times n}$ is the state

or system matrix, $B \in \mathbb{R}^{n \times n}$ is the input matrix, $C \in \mathbb{R}^{l \times n}$ and $D \in \mathbb{R}^{l \times m}$ is the feedthrough matrix is the output matrix. In general, those matrices depend on time, but in the case they are constant, the system is known as linear time-invariant (LTI).

In general, the setup described above is defined as Multiple-Input Multiple-Output (MIMO). In many applications there is only one stated being controlled (for example azimuth rotation) by means of a single control signal (e.g., applied motor torque). In such cases the system is referred as Single-Input Single-Output (SISO).

Two important elements are typically needed in control engineering: estimation of the dynamical system state and computation and application of a control action to bring the system to the desired reference value. They have associated two important definitions:

Observability A system is observable in an interval $[t_0, t_1]$ if, for an initial state $x(t_0)$, knowing the input u(t) and the output y(t) over the same interval allows to uniquely determine the initial state $x(t_0)$.

Controllability A system is controllable in an interval $[t_0, t_1]$ if there exists a control input u(t) such that when applied to the system from an initial state $x(t_0)$, brings the system to the desired state $x(t_1)$.

For linear systems, there is a standard test to determine whether a system is controllable and/or observable [Bay99]. The controllability is checked by verifying that the controllability matrix P has rank n (being n the size of the state vector). P is defined as follows:

$$P = [B \quad AB \quad A^2B \quad \cdots \quad A^{n-1}B] \tag{3.2}$$

Similarly, a linear system is observable if its observability matrix O is full rank (rank = n). Matrix O is given by:

$$O = [C \quad CA \quad CA^2 \quad \cdots \quad CA^{n-1}]^T \tag{3.3}$$

Here, the matrices A, B and C are as given in (3.8). As commented in the introduction, such tests becomes intractable for complex networks due to the size of the associated matrices, and other alternatives have been recently explored, based on structural control theory [Liu11, Liu16].

Other important concepts in control theory are the following:

Stability Another key concept in control theory is stability. A controller designed for a dynamical system must ensure that the dynamics of the overall system is stable. In linear control, this can be ensured for example by guaranteeing that the poles of the closed loop transfer function are in the left half of the complex plane. For nonlinear systems, stability is typically checked by means of the Lyapunov theory.

Robustness Besides stability, another key issue is robustness. This is related to the capability of the control system to ensure stability and performance despite uncertainty present in the system dynamics not covered in the model. In the case of linear systems, this is typically ensured by the gain and phase margins, and in the case of robust control by more advanced criteria [Zho98].

Optimality Optimal control is also a relevant part of control theory, still being an important area of research. It is closely related with the calculus of variations. The goal is to obtain a control action u(t) that reaches the target system behaviour in an optimal way (for example within a minimum time, or optimizing the energy expenditure). The concept of optimality is also extensively treated in game theory (for example by the search of best response to the opponent strategy) as it is described in part II of this thesis.

The study of *Optimal Control* has a formal setup [Bry75] which represents a generalization of the calculus of variations. If we consider the initial value problem given by (2.4), and extend it to include the control input, we have

$$\dot{\mathbf{x}} = \mathbf{f}(\mathbf{x}(t), \mathbf{u}(t), t) \text{ and } \mathbf{x}(t_0) = \mathbf{x}_0 \text{ with } t_0 \leq t \leq t_f \tag{3.4}$$

We consider a performance index of the form:

$$J = \phi[\mathbf{x}(t_f), t_f] + \int_{t_0}^{t_f} L[\mathbf{x}(t), \mathbf{u}(t), t]dt \tag{3.5}$$

being ϕ the terminal performance (cost or payoff, depending on the considered problem) and L is the running performance during the trajectory towards the final state. A *Hamiltonian* is then defined as:

$$H[\mathbf{x}(t_f), t_f] = L[\mathbf{x}(t), \mathbf{u}(t), t] + \lambda^T(t)\mathbf{f}(\mathbf{x}(t), \mathbf{u}(t), t) \tag{3.6}$$

The solution is obtained by solving the differential equations:

$$\begin{aligned} \dot{\mathbf{x}} &= \mathbf{f}(\mathbf{x}(t), \mathbf{u}(t), t), \\ \dot{\lambda} &= -(\frac{\partial \mathbf{f}}{\partial \mathbf{x}})^T \lambda - (\frac{\partial L}{\partial \mathbf{x}})^T \lambda \end{aligned} \tag{3.7}$$

where we also have:

$$\frac{\partial H}{\partial \mathbf{u}} = 0 \text{ and initial conditions } \mathbf{x}(t_0) = \mathbf{x}_0 \text{ and } \lambda(t_f) = (\frac{\partial \phi}{\partial \mathbf{x}})^T \tag{3.8}$$

The optimal control setup is naturally extended to optimal differential games [Bre11]. For two players, each controller i optimizes the index function:

$$J_i = \phi_i[\mathbf{x}(t_f), t_f] + \int_{t_0}^{t_f} L_i[\mathbf{x}(t), \mathbf{u_1}(t), \mathbf{u_2}(t), t]dt \tag{3.9}$$

with $\mathbf{u_1}(t)$ and $\mathbf{u_2}(t)$ being the control actions at time t of player 1 and 2, respectively, and i = 1 or 2 as applicable.

Robust Control is another branch of control theory that reaches a vast scope with the research conducted in the last decades [Zho98]. It includes very important areas such as H_∞ optimization theory, $\mu-$synthesis/analysis, Linear Matrix Inequalities (LMI) tools, Quantitative Feedback Theory (QFT), etc. Details on this issue are out of the scope addressed here, but some basic ideas are succinctly presented. As previously mentioned, models of real systems used for control design have inevitable uncertainties with respect to actual dynamics and parameter numerical values. The purpose of robust control is to guarantee stability and performance within a certain range of uncertainties present in the model. A standard approach followed to tackle this issue is to introduce the uncertainties as an additional part of the dynamics, considered as external disturbances that are cleverly incorporated in the overall setup. The problem definition searches for an optimal controller that minimizes the control error for a maximum value of the uncertainties, while ensuring also internal stability. This minimax scenario is then defined which can be interpreted in terms of game theory, the players being respectively the controller and the external disturbances, where the later can simultaneously capture model uncertainty, guidance commands and sensor noise. In the case of the H_∞ theory, the control design incorporates weighting functions that address the specifications in terms of performance, stability, etc. The analytical solution renders two Ricatti equations to be solved in parallel, and a suboptimal solution is numerically searched. Reduction techniques are typically followed in order to ensure reasonable controller filter order for practical implementation purposes.

Chapter 4

Game Theory

Game Theory is the study of optimal decision making under competition when the decisions of one individual affects the outcome of a situation for the rest of involved individuals. According to R. Myerson, it is the study of mathematical models of conflict and cooperation between intelligent rational decision-makers [Mye91]. The foundations of Game Theory were established in the first half of the XX century by Oskar Morgenstern, John von Neumann and John Nash among others. It is a broad discipline that entails tight interactions with Control Theory, Operation Research, Computer science, Economics, Biology, Psychology, etc. In this chapter we briefly review some basic concepts that are used in part III of the thesis. There are several areas that can be considered within this discipline:

1. Classical Game Theory. The individuals in the game are assumed intelligent, rational and selfish. Furthermore, probability is implicit in the process of the game (either by the players or by the setup of the game).

2. Combinatorial Game Theory. The difference with the previous one is that here chance is not a factor in the game (e.g. chess, go, etc.)

3. Modern Game Theory. The players are rational but they also assume in their behaviour that all players are rational in such a way that they can coordinate their strategy towards a Nash Equilibrium (NE, see later for its definition).

4. Dynamic Game Theory. It deals with the analysis of games in which players must make decisions over time and in which those decisions influence the result in the next moment in time.

5. Other topics. This includes for example Evolutionary Game Theory.

The games can be classified in different ways:

1. Zero-sum versus Non-zero-sum. In the first case, the total payoff added over the whole set of players equals zero, which implies that any player can only increase its benefit at the expense of others. In the second option, this is not the case and players can improve their benefit without necessarily reducing the benefit of others.

2. Strategic games (playing once simultaneously) versus Extensive games (playing several times sequentially).

3. Symmetric versus Asymmetric Games. In the first case, the payoff for a strategy is a function of the other available strategies, while in the second case it also depends on whom is choosing such strategy.

4. Discrete versus Continuous Games. In the first case, a finite number of players and strategies is considered, while in the second option the players have at their reach a continuum of strategies to be selected from.

5. Differential Games. In these games the evolution of the players' state variables is governed by differential equations. The problem of finding an optimal strategy in a differential game is closely related to the Optimal Control Theory. There are two types of strategies which are already present in Optimal Control: the open-loop strategies are found using the Pontryagin maximum principle while the closed-loop strategies are found using Bellman's Dynamic Programming method. Differential games are a generalization of optimal control problems where there is more than one controller or player.

As a formal definition, a game consists of a group of N *players* P = $p_1, p_2, ..., p_N$, where each player i has its own set of possible *strategies* $S_i \subset S$, S being the set of all available strategies. Each of the strategies available to player i is called a pure strategy, denoted by s_j with j=1,...,n_i. On the game, the player i selects a strategy $s_i \in S_i$. The vector of strategies selected by the N players is denoted by s=$(s_1, s_2, ..., s_N)$. This vector $s \in S$ determines the outcome for every player.

Another relevant concept in the game definition is the *payoff function*. In order to make a decision over the set of strategies, each player needs a set of preference ordering of the outcomes associated to each vector s. This ordering must be a complete, transitive and reflexive binary relation on S. The simplest way to set those preferences is by means of a payoff function

$\pi : S \to R^N$ which assigns to each player a value of the outcome associated to each vector s of strategies chosen by all the players in the game, including itself. Each player will chose its strategy s_i based on such function and the information (or expectation) of the strategies chosen by the rest of players. The triple G = (P, S, π) is the definition of a game in a strategic normal form.

The two-player games given in strategic form are also sometimes called matrix games, because the payoff function for each player is completely defined by a matrix. If the strategies in S_i (i=1,2) for each player are defined as $(s_i^1, s_i^2, ..., s_i^{n_i})$, there is a matrix $A_i \in R^{n_1 x n_2}$ so that element (r,c) of A_i is given by $\pi_i(s_1^r, s_2^c)$. The matrix formulation is used for many discrete two-players games. Typical examples of those games are prisoners dilemma, hawk-chicken, etc.

The player i can also choose a *mixed strategy vector* to which we can associate a vector $\mathbf{x_i} = [x_i^1, x_i^2, ..., x_i^{n_i}]$ satisfying the following properties:

1. $x_i^j \geq 0$ for j=1,..., n_i
2. $\sum_{j=1}^{n_i} x_i^j = 1$

For a game defined in normal form we have the simplex given as:

$$\Delta_{n_i} = \left\{ [x_i^1, x_i^2, ..., x_i^{n_i}]^T \in \mathbb{R}^{nx1} : \sum_{j=1}^{n_i} x_i^j = 1; x_i^j \geq 0, j = 1, ..., n_i \right\}$$

This set is the mixed strategy space in n_i dimensions por player i, and the mixed strategy space for the game is given by:

$\Delta = \Delta_{n_1}$ x Δ_{n_2} x ...x Δ_{n_N}

With these considerations, the mixed strategy payoff function for player i is given by:

$$\Phi_i(x^1, ..., x^N) = \sum_{i_1=1}^{n_1} \sum_{i_2=1}^{n_2} ... \sum_{i_N=1}^{n_N} \pi_i(s_{i_1}^1, s_{i_2}^2, ..., s_{i_N}^{n_N})$$

A Nash equilibrium [Gri10] is then defined as a tuple of mixed strategies $[x^{1*}, x^{2*}, ..., x^{N*}] \in \Delta$ such that for i=1,...,N:

$$\Phi_i(x^{1*}, ..., x^{i*}, ..., x^{N*}) \geq \Phi_i(x^{1*}, ..., x^i, ..., x^{N*}) \text{ for all } x^i \in \Delta_{n_i}$$

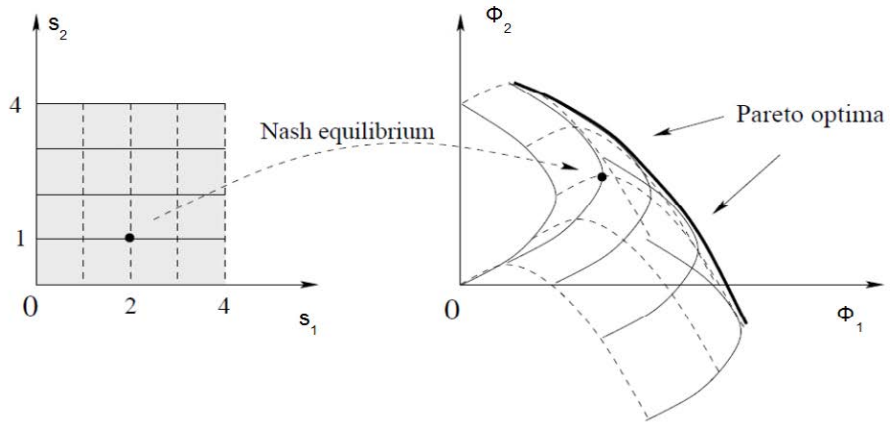

Figure 4.1: Nash equilibrium and Pareto optima. Adapted from [Bre10]

Another way to explain this concept is that the set of mixed strategies $[x^{1*}, x^{2*}, ..., x^{N*}]$ constitutes a Nash equilibrium if no player has any reason to deviate unilaterally from its mixed strategy.

The strategies of two competing players (s_1^*,s_2^*) are said to be *Pareto optimal* if there exist no other pair (s_1,s_2) such that:

$\Phi_1(s_1, s_2) > \Phi_1(s_1^*, s_2^*)$ and $\Phi_2(s_1, s_2) \geq \Phi_2(s_1^*, s_2^*)$ or

$\Phi_1(s_1, s_2) \geq \Phi_1(s_1^*, s_2^*)$ and $\Phi_2(s_1, s_2) > \Phi_2(s_1^*, s_2^*)$

This can be phrased as not being possible to strictly increase the payoff of one player without strictly decreasing the payoff of the other. In general, a game can have several Pareto optima. It should be noted also that a Nash equilibrium many not be a Pareto optimum (see figure 4.1). In that figure, level curves correspond to the payoff of each of the two player (dashed and solid lines, respectively). Nash equilibria correspond to points where the gradient of payoff i with respect to strategy i is zero for both i=1,2, while Pareto optima render a maximum in the payoff for both players. This is also observed in the game studied in section §10.4.2.

Although games dynamics often lead to an equilibrium as described above, it should be remarked that sometimes they rather imply chaotic behaviour [Sat02]. In the following chapters in Part II, chaos phenomena are extensively found within the study of the HCN molecule dynamics.

Part II

Control of HCN Molecule via Laser Excitation

Chapter 5

HCN molecule and laser dynamics

5.1 Introduction

One of the most important goals of chemistry is to control the rate and distribution of products in chemical reactions, minimizing undesirable side reactions and improving the efficiency of industrial processes [Atk06]. Since vibrational molecular dynamics play a relevant role in those reactions, they need to be properly described both at experimental and theoretical level. On the first point, several techniques have been developed over the last decades to characterize these phenomena, such as coherent vibrational spectroscopy, experimental probes of reactive collisions, spectroscopic observation of activated complexes, etc [Atk06, Silv08]. On the other hand, theoretical explanation of the processes undergoing molecular dynamics is of paramount importance for a complete comprehension of such phenomena. For this reason, since the last quarter of the 20th century classical mechanics has seen an unprecedented popularity among chemical physicists, for whom the main concern is the investigation of molecular motions and transformation. One of the main factors for the adoption of the classical mechanics approximation (which describes the motions of macroscopic bodies) in chemical dynamics is the ability to perform calculations for many body problems, and to obtain results in good agreement with the experiment. Vibrational spectrum is considered the fingerprint of the nuclear motions in the molecule. Classical mechanics offer important tools not only for qualitative answers, but also with a predictive power for the motions of the polyatomic molecules at high energies where nonlinear effects are strong.

The theoretical framework for this kind of studies is based both on classi-

cal and quantum mechanics, having profound roots in the characterization of chaos in Hamiltonian systems and KAM theory that have been described in chapter §2. The hierarchical organization of phase space described there entails a high relevance when considering intramolecular vibrational relaxation (IVR) in small molecules [Gru00, Gru04, Lei05], an issue of outmost importance to the potential development of a mode-specific chemistry [Blo84].

One topic of much interest in this branch of chemical dynamics is the active control of molecular nonlinear dynamical systems and chemical reactivity, typically using lasers. An extensive literature has been produced on this subject (see [Ric00, Ban02, Rab03, Sha03, Sha03] and the references therein). In relation to the work presented here with the HCN molecule, the laser control of bond excitation, bond dissociation (typically of the strong CN bond), and the isomerization of HCN has been extensively considered in the literature [Brez04, Set12, Che91, Che96, Bot95, Has02, Gong05a, Gong05b]. Also, other alternative methods of control in this molecule not making use of lasers has been recently explored [Gong05a, Gong05b]. The work in [Brez04] and [Set12] is most relevant for the present study.

In the first paper, Brezina and Liu[Brez04] considered the possibility of controlling the CH and CN excitation and and dissociation with laser pulses. For this purpose, they used a classical mechanics widespread vibrational model consisting of two kinetically coupled Morse bond functions freezing the bending at its equilibrium value [Jaf80, Sib82, Dav81]. Special attention was paid to the role played by IVR, considering different values of the laser frequency and amplitude. These authors found that simple linearly chirped pulses are effective in exciting and dissociating the CH, while this is more difficult for the stronger CN bond.

Subsequently, Sethi and Keshavamurthy [Set12] revisited the same problem, concentrating only in one of the laser frequencies considered by Brezina and Liu. This work was a start in the identification of the main aspects of the dissociation dynamics and mechanism in phase space, and the characterization of the system in terms of the classical dynamical resonances (Arnold) network. They found the importance of two regions of frequency space, which were called *dissociation hub* (DH) and *noble hub* (NH), respectively. The former constitutes a 'gateway' for those trajectories leading to dissociation, while the later, characterized by very irrational frequency ratios, constitutes a very sticky area where trajectories are trapped for a considerable time, being the most visited region in the web.

This thesis extends the analysis of Sethi and Keshavamurthy for the HCN

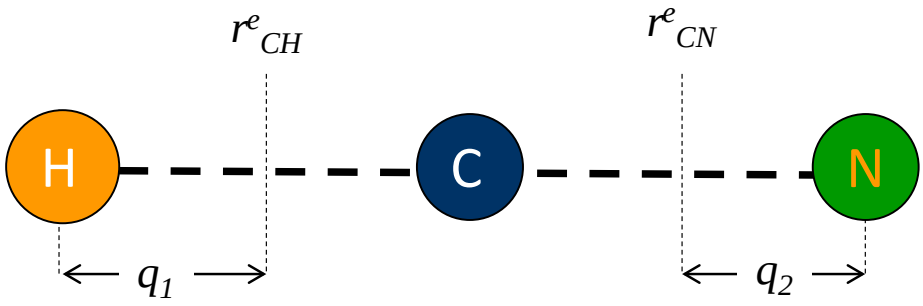

Figure 5.1: HCN molecule vibrational dynamics stretching degrees of freedom

molecule, by considering the influence of the laser frequency in the dynamics, in order to check the possibility of using it as a possible control parameter by varying the dynamical structure of the system. In this way, we can be more precise than previous works in predicting which laser frequencies are best in order to promote dissociation. Indeed, in Ref. [Brez04] it was inferred from the dissociation yield versus laser frequency plot that the important resonance was with the harmonic bond frequencies dissociation. Actually, Sethi and Keshavamurthy [Set12] chose to be out of this resonance to perform their study in order to avoid significant participation of the CN dynamics. While this resonance assumption is true at low energies, in this thesis it is found that the most important frequencies for the CH excitation and dissociation are those associated to regular motions, and that changes significantly with the excitation of the HCN. The detailed characterization has been carried out both in the phase and frequency spaces. Let us remark, that this is not an easy task from the theoretical point of view, since the dynamical problem consists in more than two degrees of freedom [Simo99].

5.2 The HCN vibrational model

The molecule under study is HCN. It is known to have two stable linear isomers, being H–C–N the most stable one [Var06, Arr10]. Taking this fact into account, and also that the bending motion has a much lower frequency than the stretching, the linear configuration is frozen here, using a minimal 2D linear model consisting only of the two stretching modes, r_{CH} and r_{CN}, respectively. Coordinates relative to their equilibrium values, $q_1 = r_{\mathrm{CH}} - r^e_{\mathrm{CH}}$ and $q_2 = r_{\mathrm{CN}} - r^e_{\mathrm{CN}}$, will be used instead (see figure 5.1). Also, and due to the relatively high energies that are going to be considered, quantum effects such as tunnelling are not expected to play a significant role in the present

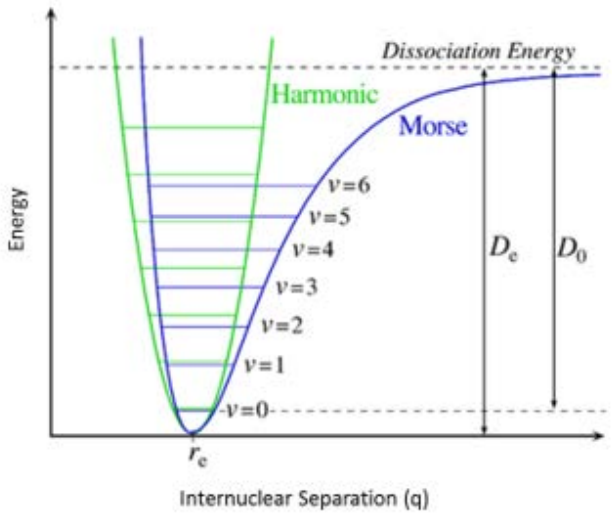

Figure 5.2: Morse potential energy versus separation between atoms, compared with harmonic potential for reference

study.

The resulting dynamics are described by a classical Hamiltonian, $\mathcal{H}_0$, which has been previously used in other studies of IVR [Jaf80, Sib82]. An additional term, $\mathcal{H}_I$, associated to the actuation of a monochromatic laser, is introduced, and thus, the description of the whole system is given by

$$\mathcal{H}(t) = \mathcal{H}_0 + \mathcal{H}_I = T + V + \mathcal{H}_I(t), \tag{5.1}$$

where the kinetic energy term, T, is

$$T = \frac{p_1^2}{2M_{\mathrm{CH}}} + \frac{p_2^2}{2M_{\mathrm{CN}}} - \frac{p_1 p_2}{m_{\mathrm{C}}}, \tag{5.2}$$

where $M_{\mathrm{CH}} = m_{\mathrm{C}} m_{\mathrm{H}}/(m_{\mathrm{C}} + m_{\mathrm{H}})$ and $M_{\mathrm{CN}} = m_{\mathrm{C}} m_{\mathrm{N}}/(m_{\mathrm{C}} + m_{\mathrm{N}})$ denote the associated reduced masses.

The potential energy, V, consists of two uncoupled Morse functions

$$V = D_1 \left(1 - e^{-\alpha_1 q_1}\right)^2 + D_2 \left(1 - e^{-\alpha_2 q_2}\right)^2, \tag{5.3}$$

where D_1 and D_2 are the CH and CN dissociation energies, and α_1 and α_2 constants related to the CH and CN harmonic vibrational frequencies.

	Coordinate	
	1 (CH)	2 (CN)
D	0.209	0.404
α	1.554	1.940
r^e	2.014	2.179

Table 5.1: Numerical values for the parameters in the potential of this Hamiltonian model for HCN in Eq. (5.3) for the two relative coordinates $q_1 = r_{\rm CH} - r^e_{\rm CH}$ and $q_2 = r_{\rm CN} - r^e_{\rm CN}$. They have been taken from Ref. [Far09] and are given in a.u.

Figure 5.2 depicts the potential energy corresponding to the Morse function, and its relation to a harmonic oscillator. It can be observed that at a certain energy level the internuclear separation tends to increase eventually leading to molecule dissociation.

The numerical values for the parameters entering in Eq. (5.3) have been taken from Ref. [Far09], and are summarized in Table 5.1. Atomic units will be used henceforth unless stated otherwise.

The interaction with the laser, $\mathcal{H}_I(t)$, is described within the dipole approximation as

$$\mathcal{H}_I = \lambda_F \, \mu(q_1) \, \cos\omega_F t \tag{5.4}$$

being ω_F the frequency of the laser field, λ_F its amplitude, and $\mu(q_1)$ the HCN dipole function, which in our case is approximated as

$$\mu(q_1) = e^{-\eta(q_1 + r^e_{\rm CH})} \sum_{j=1}^{4} A_j (q_1 + r^e_{\rm CH})^j \tag{5.5}$$

being $\eta = 1$ bohr^{-1}, and A_j additional parameters whose values can be found in Ref. [Set12]. In this way, the system is non-autonomous and the motion, therefore, evolves in the five-dimensional space, so that the system is sometimes referred to as a system of 2.5 degrees of freedom.

The potential energy surface is shown in Figure 5.3 in the form of a contour plot. As can be seen, it presents a well $V = 0$ at $(q_1, q_2) = (0, 0)$ corresponding to the Li–C–N isomer linear equilibrium configuration, and the equipotential lines pack close together at the dissociation of the Morse functions in both modes, $V = D_1$ at $(0, \infty)$, and $V = D_2$ at $(\infty, 0)$, respectively.

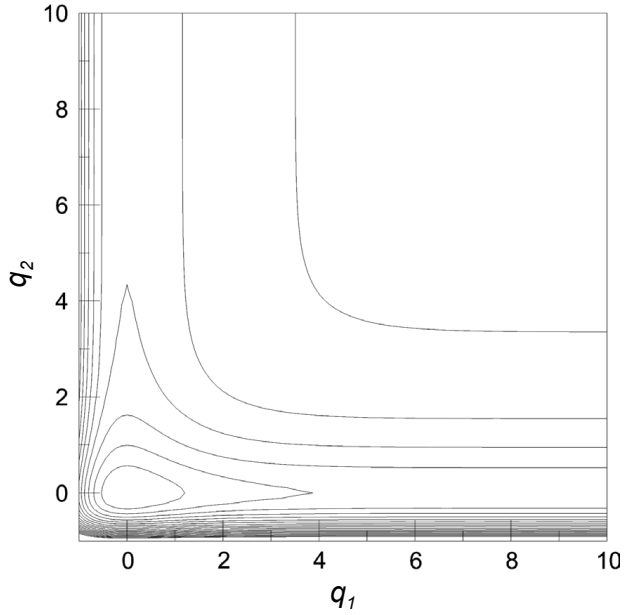

Figure 5.3: Contour plot of the HCN potential energy surface defined in Eq. (5.3) using the parameters of Table 5.1.

It should be noted that the molecule vibrational dynamics described here corresponds to the plant of the system to be controlled according to the definition in section §3. In this case, the laser is the actuator in the referred scheme, while the algorithm selecting the laser frequency corresponds to the controller. Since there is no sensor here to measure the dynamics regime and to close the loop, the whole setup acts as an open loop control system. In the following chapters, the rationale for the actuation of the laser in the control of the molecule vibrational dynamics is described in depth.

Chapter 6

HCN control results

6.1 HCN molecule without laser interaction

In this thesis the presentation of results of the conducted analysis starts by considering first the dynamics of the HCN without laser excitation, in order to obtain a reference for comparison with the results in subsequent chapters, in which the effects of the field on the molecule are examined. One key parameter in this study is the energy of the system, which plays the role of a perturbation, in the sense of the KAM theorem. Notice that in this case increasing the value of E not only represents a perturbation, but it has also the effect of open access to larger portions of phase space, this bringing about eventual new dynamical structures, such as for example those arising in bifurcations.

6.1.1 Classical trajectories and Poincaré surfaces of section

Classical trajectories for this Hamiltonian model of HCN are calculated by numerical integration of the corresponding Hamilton equations of motion (see Eqs. 2.21) where in this case $(\mathbf{q}, \mathbf{p}) = (q_1, q_2, p_1, p_2)$. The results presented in this thesis are obtained by using the symplectic algorithm defined by Störmer-Verlet [Hai03] for the propagation of the trajectories. The use of this prevents any eventual energy drifting induced by the numerical integration procedure.

In the case that there is no interaction of the molecule with the laser, the Hamiltonian $\mathcal{H} = \mathcal{H}_0$, does not depends explicitly on time, and then the system is two dimensional. Then, the corresponding dynamics can be conveniently monitored by computing composite Poincaré surfaces of section

(PSOS) at different values of the vibrational energy. This implies the definition of a Poincaré map consisting on the transversal intersection points of many trajectories, all computed at the same value of the energy, with a suitably defined codimension 2 hypersurface, $\mathcal{C}$, this reducing the dimensionality of the phase space flow to 3D. Accordingly, a periodic trajectory in the phase plane corresponds to a finite number of dots in the PSOS, while quasiperiodic orbits lying on invariant tori are represented by closed curves in the PSOS. (Notice that they constitute impenetrable barriers for the flux of trajectories across.)

For the case of the HCN model that are considered we take $\mathcal{C} : q_2 = 0, p_2 > 0$ as the sectioning plane, thus obtaining the corresponding (q_1, p_1) PSOS. As explained in section §5.2, when the interaction with the laser is taken into account the dimensionality of the system increases to 2.5 dimensions and the above described rationale no longer holds, since the invariant tori do not partition the phase space into distinct and unconnected regions. Alternative indicators, such as those described in the next subsections, should then be used.

Figure 6.1 depicts some composite PSOSs, as defined in Sect. §6.1.1, for the model of the isolated HCN molecule. From (a) to (c) three values of the vibrational energy are considered, namely $E = 0.1$, 0.135 and 0.21 respectively. In each plot a uniform grid of 10,000 initial conditions within the available PSOS was used as starting points to propagate the corresponding trajectories for 8192 steps of size $\Delta t = 4$, resulting in a total time span of 32768, which corresponds to 0.8 ps. For each trajectory $\sim$1000 intersections with the SOS were recorded and plot in the different panels. The same numerical values of the parameters will be used in the rest of the calculations of this thesis, unless otherwise stated.

As can be seen, for the lowest energy considered, $E = 0.1$, the system is mostly regular, and only invariant (KAM) tori and PB chains of islands are visible. For example, two main elliptic points can be observed in panel (a), at $(q_1, p_1) = (0.55, -10.59)$ and $(-0.075, 5)$, respectively. They are associated to the primary resonance, $\omega_1 : \omega_2 = 1 : 1$. The first one corresponds to the asymmetric normal mode trajectory (see discussion in [Jaf80, Sib82, Dav81]), while the second is mainly a slightly distorted C-H local mode trajectory. Moreover, a chain of 5 islands around the first fixed point, corresponding to a 1:5 secondary resonance, is also observed. And similarly, two more chains of islands are visible around the second fixed point, corresponding to 1:3 and 1:4 secondary resonances. For $E = 0.135$ [Figure 6.1(b)] the

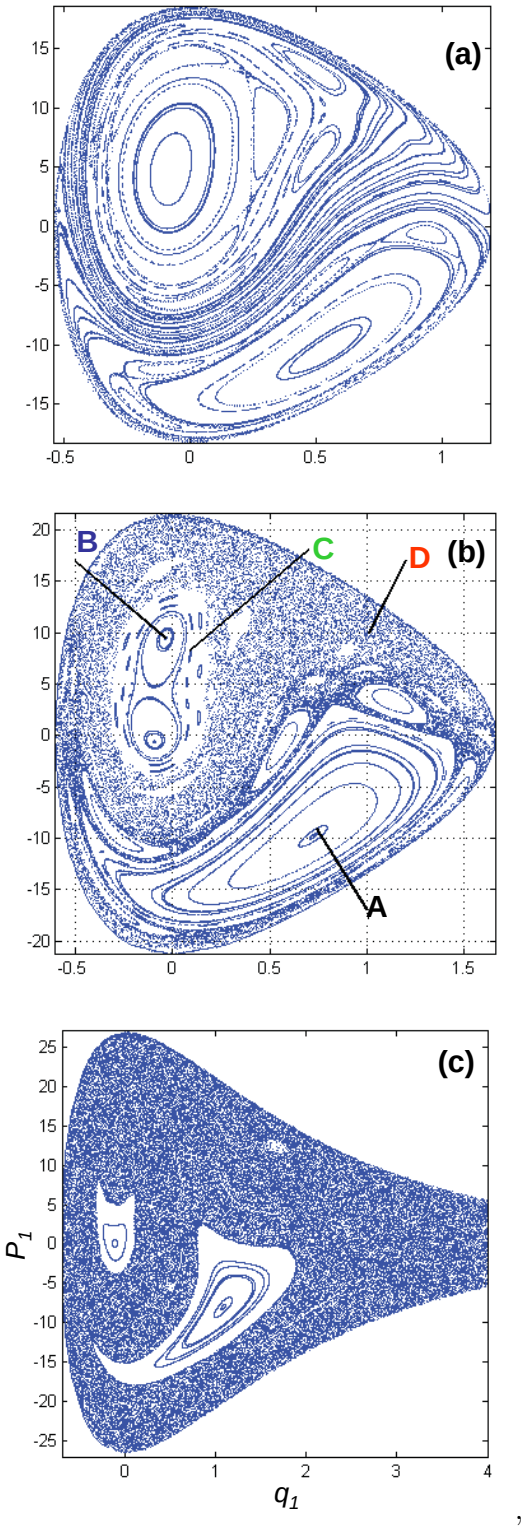

Figure 6.1: Composite Poincaré surfaces of section, as defined in Subsect. §6.1.1, corresponding to intersections with the plane $q_2 = 0$ with $p_2 > 0$ for the HCN molecule without interaction with the laser at $E = 0.1$ (a), 0.135 (b), and 0.21 (c). Four representative trajectories, marked A–D in panel (b), are analyzed in the text. (Atomic units are used in all figures of this thesis.)

Table 6.1: Initial conditions on the PSOS for the four trajectories of HCN at $E = 0.135$ marked A–D and colors black-blue-green-red in Figure 6.1, which are representative of regions of the phase space with different dynamical character (this being indicated in the last column).

Trajectory	q_1^0	p_1^0	Phase space region
A	0.74	–9.13	1:1 resonance
B	–0.036	9.49	3:2 resonance
C	0.09	8.26	torus around 3:2 resonance
D	1.01	10.00	Chaotic region

perturbation grows. However, the broad region of regularity around the first 1:1 resonance, located in the lower right part of the plot, as well as the 1:5 chain of island structure around it, mostly survive. On the other hand, the second region of regularity, located in the upper left part of the figure, has suffered more profound changes. Actually, a pitchfork bifurcation has taken place, turning the central elliptic point into unstable, with the simultaneous emergence of a resonance region around. This new region consists of two new elliptic points corresponding to a 3:2 resonance (as it will be explained in more detail below). Also, a vast region around this structure, that was regular at $E = 0.1$, has become chaotic. As a consequence, from the two prominent 1:3 and 1:4 secondary resonances clearly visible at $E = 0.1$ only remnants of the former now persist. Finally, in Figure 6.1(c), corresponding to $E = 0.21$, the vast majority of phase space is dominated by chaotic behavior. The two main regular regions described before have been greatly reduced in size, corresponding to motions around the equilibrium point, $(q_1, p_1) = (0, 0)$ and around $(q_1, p_1) = (1.08, -8)$, respectively. Nevertheless two very small island of regularity are visible around $(q_1, p_1) = (0.5, -5.0)$ and $(q_1, p_1) = (1.65, 12.3)$.

To further continue the investigation of the phase space of HCN without the laser, let us examine next some representative trajectories in these PSOS's. For this purpose, four trajectories have been chosen at the intermediate energy $E = 0.135$ (very close to that used in Ref. [Set12]), since the other two cases considered in Figure 6.1 are either too regular or too chaotic. These trajectories have been marked with the letters A–D and colors black-blue-green-red in Figure 6.1(b), and their numerical initial conditions (in the PSOS) and dynamical character of the phase space regions in which they are located have been summarized in Table 6.1. The corresponding orbits

and PSOS are shown in the top and bottom rows, respectively, of Figure 6.2 using the same colors as in Figure 6.1. As can be observed, trajectory A (left tier) corresponds to a asymmetric normal mode 1:1 resonance with values of the frequencies at this resonance equal to $\omega_1^{[1:1]} = \omega_2^{[1:1]} = 0.012371$. Trajectories B and C are located in the region associated to the bifurcated (mainly C-H local mode) 3:2 resonance. The former corresponds to the stable new periodic orbit oscillating three times in q_1 while repeating only twice in q_2, in a Lissajous-like pattern. The corresponding two fundamental frequencies have been computed using the method of Laskar (see Subsect. §2.4.3) resulting in $\omega_1^{[3:2]} = 0.005$ and $\omega_2^{[3:2]} = 0.00333$, which are very approximately in the expected 3/2 ratio. On the other hand, trajectory C corresponds to a quasiperiodic motion (torus) around the whole structure born in the pitchfork bifurcation described above. This orbit has been plotted (in green) in the middle tier of Figure 6.2 superimposed to B (in blue). As can be seen, it presents a box-filling type of orbit, wiggling around the 3:2 resonance, thus revealing the irrational frequency ratio dominating that area of phase space. This is even more apparent in the bottom plot, where the corresponding

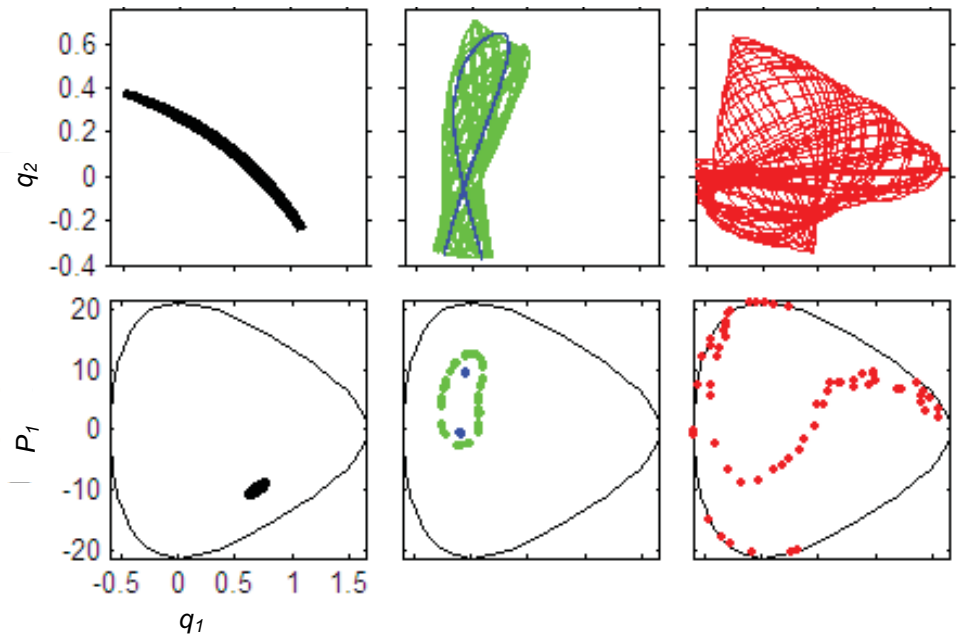

Figure 6.2: Trajectories A (left tier), B and C (middle tier), and D (right tier) for the HCN molecule without interaction with the laser marked in Figure 6.1. The top row plots show the orbits in configuration space, while those at the bottom corresponds to Poincaré surfaces of sections.

PSOSs are presented. Finally, trajectory D corresponds clearly to an irregular orbit, filling the chaoticity band where its initial condition was chosen. It can also be observed that its evolution in the PSOS is consistent with the areas marked as chaotic in the SALI map discussed in Figure 6.3 below. In subsequent sections of this thesis, these four trajectories will be used as reference cases for a further characterization in the presence of the laser field.

6.1.2 SALI indicator and diffusion coefficients

This subsection presents results corresponding to PSOS colored with SALI and diffusion coefficient $\mathcal{D}$ maps, (as defined in Subsects. §2.4.2 and §2.4.3 respectively) for the vibrational dynamics of HCN at $E = 0.135$ without interaction with the laser. Accordingly, they should be compared with those in Figure 6.1(b). The reason for this choice of the energy value is threefold. First, at this energy there is no dissociation when the laser is off. Second, the fraction of chaotic trajectories, which are the most likely candidates for dissociation, is relatively large. Third, it has two sizable regular regions corresponding to different dynamical characteristics (order of the main resonance in the region).

The results, computed using the same numerical parameters of the previous subsection, are presented in Figure 6.3. The logarithmic scales of colors used to code the numerical obtained values are given in the right part of the plots. As can be seen, the SALI map [panel (a)] shows, as a priori expected, a remarkable resemblance with the PSOS in Figure 6.1(b), with all areas of regularity appearing in pale colors. Indeed, even the existing PB structures are clearly delineated by the existence of darker tones. The areas of chaos, also appear in darker colors, but even here a tonality variation is found, this indicating the existence of different types of chaotic behavior in the system [Beni15].

Furthermore, Figure 6.3(b) shows the corresponding diffusion coefficient map. Recall that here the color scale should be represented in an inverted way, since larger values of $\mathcal{D}$ correspond to chaos. Similarly to the case of the SALI indicator in the panel (a), this map is informative and useful, but the resemblance with the PSOS and the number of different details that can be appreciated is lower. Regular areas, regions of stochasticity, and even much of the detail of the PB structures are clearly visible, however.

6.2 HCN molecule interacting with laser

The previous section discussed different aspects of the vibrational dynamics of the model for HCN when there is no interaction with a laser. The rest of

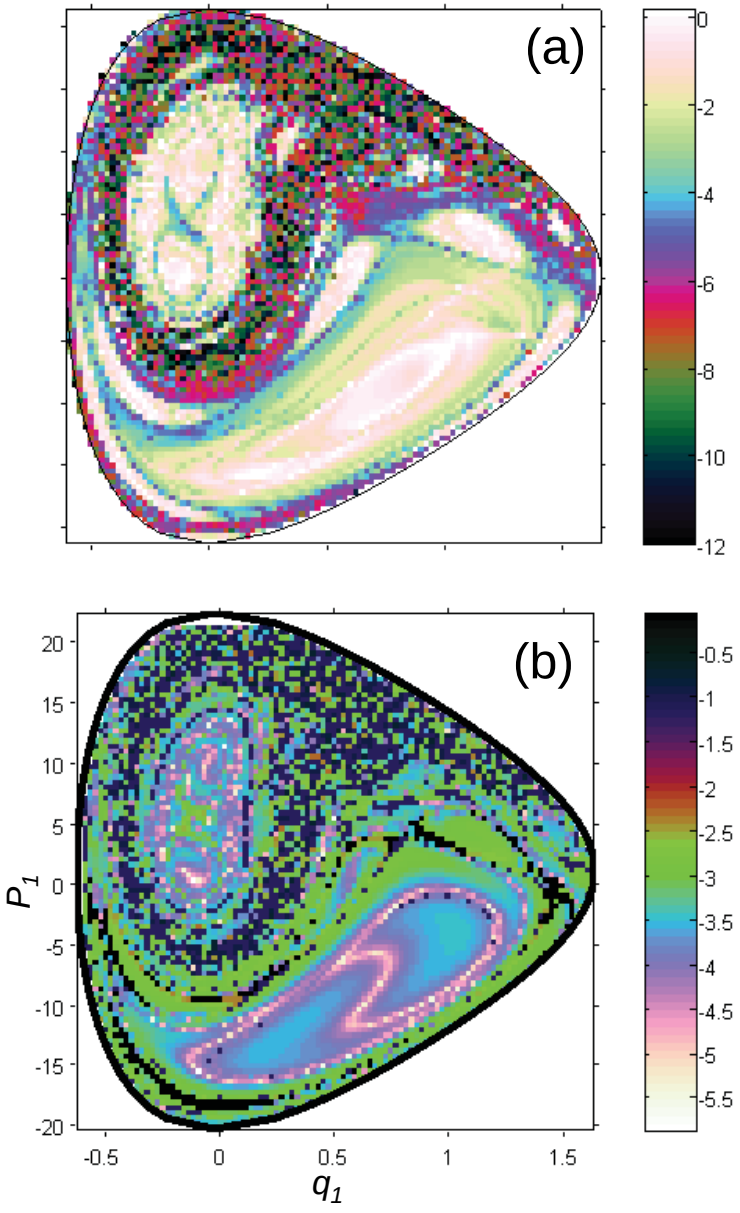

Figure 6.3: SALI (a) and diffusion coefficient (b) colored PSOS maps, as defined in Subsects. §2.4.2 and C, for the HCN molecule without interaction with the laser, for $E = 0.135$ [this corresponding to Figure 6.1(b)]. Values are shown using the color code given on a logarithmic scale at the right of the plots.

the chapter is devoted to study the influence of a laser radiation field on this dynamics, paying special attention to the effect of the laser frequency. A fixed value of the amplitude of the laser field, equal to $\lambda_F = 0.009$ corresponding to $\simeq 3$ TW/cm^2 (the same value as that considered in Ref. [Set12]), will be used throughout. On the other hand, the laser frequency, ω_F, will be varied, and six particular values of it will be considered, except in Figure 6.8, where a larger number of frequencies is studied.

As commented in chapter §5, in this system the actuator of the control scheme corresponds to the laser exciting the molecule vibrational dynamics. The system controller is represented by the strategy in the selection of the laser frequency, whose physical justification is provided in the following sections.

6.2.1 SALI indicator

Let us first focus on the sensitivity of the SALI index to the laser frequency; other features will be considered afterwards. The same scheme will be followed in other subsections.

When the effect of the laser is considered, the resonances in the system are more complex, since now the frequency of the laser, ω_F, must also be included in the discussion. Also, some care should be paid to the notation. In this case, the standard vectorial notation will be used, in which fulfillment of the resonance condition: $n_1\omega_1 + n_2\omega_2 + n_F\omega_F = 0$ is abbreviated as (n_1, n_2, n_F) for short. In this way, the previously introduced resonances without the laser, $n_1 : n_2$, will be denoted hereafter as $(n_2, -n_1, 0)$.

Figure 6.4 presents the results of the SALI colored PSOS map for increasing values of laser frequency. These values have been carefully chosen in a dynamical sense, as described when the results in each panel are discussed below. The initial energy without the interaction with the laser, i.e. that corresponding to $\mathcal{H}_0$ in Eq. (5.1), is taken in all cases equal to $E_0 = 0.135$, which is the same one as in Figure 3(b).

A first comment regarding Figure 6.4 is in order. As can be seen, as the value of the laser frequency increases the structure of the associated phase space changes. The region corresponding to the 1:1 resonance is the most robust one, and its structure changes little under the effect of the laser; however, the area of influence of this resonances decreases with ω_F. Another interesting observation is that the region corresponding to the 3:2 resonance

first disappears as ω_F increases, but then it reappears for the highest values of this parameter. Let us consider this striking effect in more detail.

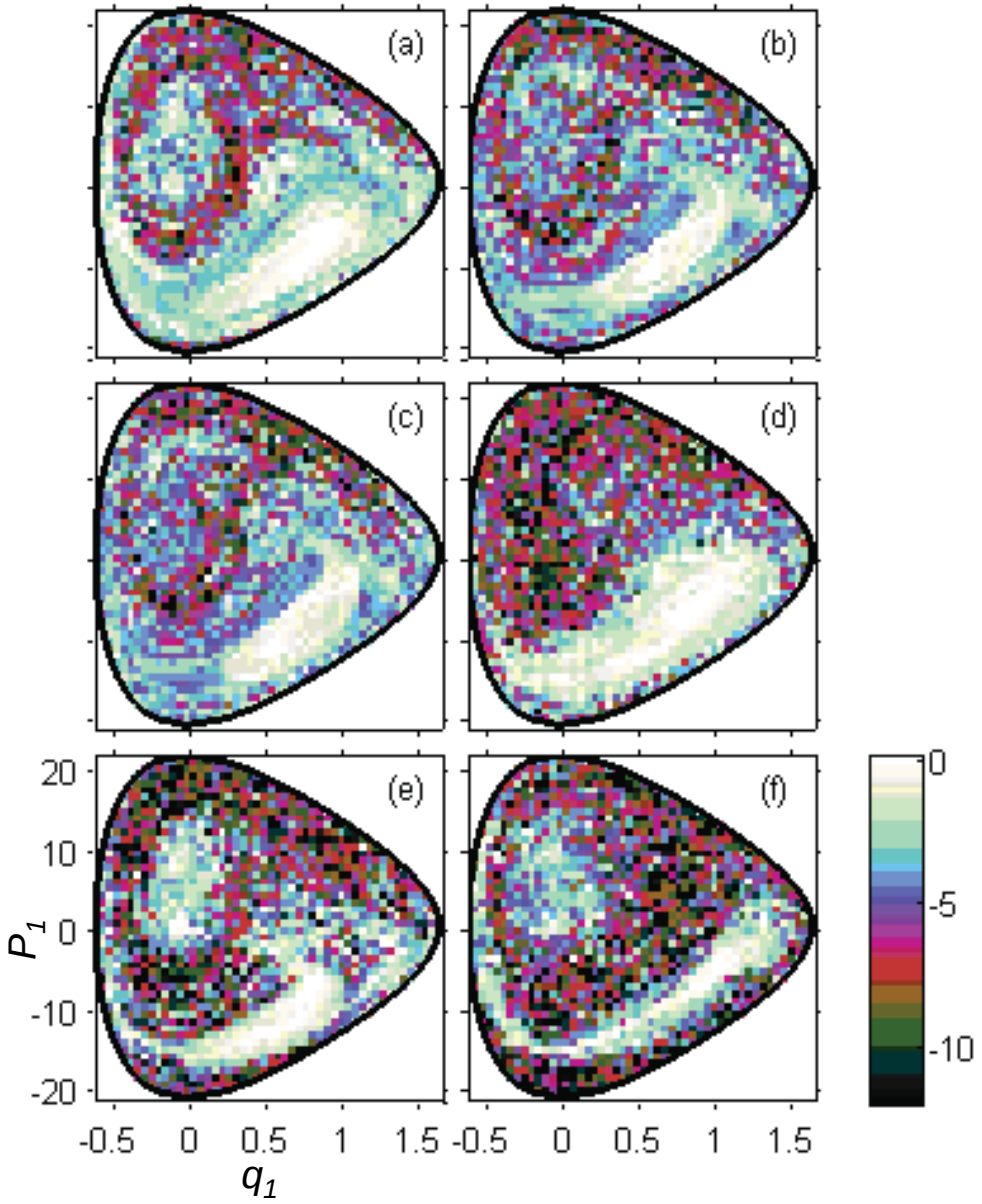

Figure 6.4: SALI colored Poincaré surface of section map, as defined in Subsect. §2.4.2,for HCN in the presence of a laser with the following values of the frequency: $\omega_F = 0.003333$ (a), 0.004123 (b), 0.009278 (c), 0.010000 (d), 0.014430 (e), and 0.018556 (f), respectively. In all cases the initial energy without the interaction with the laser is taken equal to $E_0 = 0.135$.

In panel (a), we have that $\omega_F = \omega_2^{[3:2]} = 0.003333$, i.e. the laser is in an integer resonance with the dynamics in the 3 : 2 area of influence. Despite the existence of this resonance, the effect of the laser is very small, and then the structure of the phase space is not largely altered, as can be ascertain by comparing panels (a) in Figs. 6.3 and 6.4. This persistence is due to the fact that the value of the laser frequency/perturbation is very small, and then many tori survive according the prescription of the KAM theorem [Ber78].

In panels (b) and (c) we have that the value of the laser frequency, and then its effect in the HCN dynamics, has increased. As a result, more tori that in the previous case are destroyed. This is even true for the robust 1:1 resonance zone, since now we have that $\omega_F = (1/3)\ \omega_{1,2}^{[1:1]}$ and $\omega_F = (3/4)\ \omega_{1,2}^{[1:1]}$, respectively for panels (b) and (c). Also, it should be remarked that although the region corresponding to the 3:2 resonance appears highly destroyed, this is not so much the case, since when the actual numerical values of the SALI are carefully examined they are seen to be not too small.

The situation is completely different in panel (d), where the 3:2 region appears totally destroyed, while the size and regularity of the 1:1 has largely increased. The first observation is in agreement with the fact that the perturbation has increased, but by the same token the second is totally unexpected. This result can be understood if we take into account the dynamical relationships existing between the different motions. In this case, one has that $\omega_F = 2\ \omega_1^{[3:2]} = (\gamma/2)\ \omega_{1,2}^{[1:1]}$, being $\gamma = (1 + \sqrt{5})/2$ the golden mean. The first relation enhances the destruction of tori in the first region, while the (very irrational) second prevents the destruction of the second. Moreover, the colors corresponding to the SALI indicates that the destruction of the 3:2 area is very high.

This balance of larger or smaller destruction of regular tori as a function of the irrationality of the ratio between laser and vibrational frequencies of the isolated molecule is also very well illustrated in the remaining panels of the figure. In panel (e), $\omega_F = (7/6)\ \omega_{1,2}^{[1:1]} = (7/\gamma)\ \omega_2^{[3:2]}$. As a result, now the 1:1 region appears much destroyed than before, while the irrational ratio with the 3:2 resonance ensures the revival of the corresponding region that it is seen in the results. The situation is totally similar in panel (f), where $\omega_F = (3/2)\ \omega_{1,2}^{[1:1]} = (9/\gamma)\ \omega_2^{[3:2]}$.

6.2.2 Frequency map analysis

The structure of nonlinear resonances in phase space, such as the one just discussed for the HCN vibrational dynamics in the presence of a laser, does also

appear usually clearly displayed in the maps derived from frequency analysis [Las92, Dum93, Los98]. With this motivation in mind, we will use now the procedure described in Sect. §2.4.3 to compute frequency maps to present an alternative, but nevertheless complementary, analysis to the results discussed in the previous subsection.

Accordingly, Figure 6.5 presents computations for the ratio between the two fundamental frequencies, ω_1 and ω_2, and the laser frequency, ω_F, for the same set of trajectories in the grids of the different panels in Figure 6.4. For comparison, each of these points is painted with the color of the corresponding SALI parameter, using the color scale indicated in the right part of the figure. Additionally, in the different plots of the figure it is included three straight lines corresponding to the resonance conditions $(1, 0, \gamma/2)$, $(1, -1, 0)$, and $(2, -3, \gamma)$. Actually, the first one indicates an irrational frequency ratio between mode CH and the laser; in the second one, modes CH and CN are in a 1:1 resonance; and finally, in the third line there is an irrational ratio between the laser and the 3:2 molecular resonance. These lines correspond to invariant tori, typical of the Arnold web, separating the available frequency space in different relevant zones where the trajectories accumulate.

Two previous comments regarding Figure 6.5 are in order. For one thing, it seems at first sight that now the number of points in the different plots of the figure has been reduced with respect to those in Figure 6.4. However, this is not the case at all, and the apparent reduction is just a visual effect due to the fact that several trajectories may now have very similar fundamental frequencies. Second, notice that although the structure in the panels is (more or less) conserved, the corresponding region in the frequency space are significantly changing. This is due to the fact that the axis presents the values of the frequencies ω_1 and ω_2 scaled with respect to the value of the laser frequency, which is different in each panel.

Now, let us discuss the results in the different panels of Figure 6.5. For the smallest value of the laser frequency, in panel (a) it is observed that the calculated points cluster in four different groups. The first two are located in the upper part of the plot, close to the value $\omega_2/\omega_F \simeq 1$, respectively on the $(1, -1, 0)$ and $(2, -3, \gamma)$ resonance lines. As can be seen by the color indicating the value of the SALI they are all regular trajectories, the first group being associated to the 1:1 resonance region and the second one to 3:2 [see Figs. 6.1(b) and 6.4(a)]. The other two groups of points, appear respectively on the $(1, 0, \gamma/2)$ and (slightly) to the right of the $(2, -3, \gamma)$ lines, respectively. They correspond to chaotic motion, as inferred from the SALI

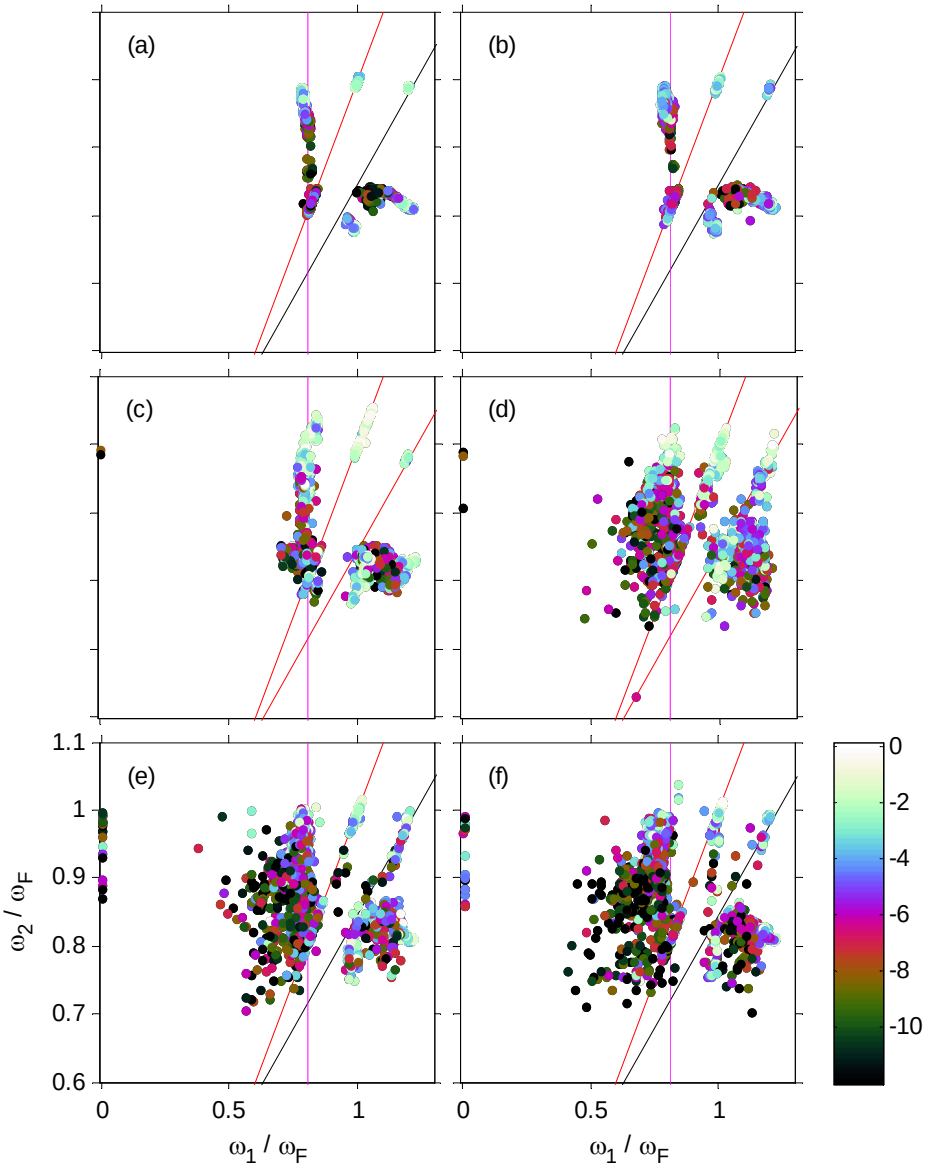

Figure 6.5: Frequency map, as defined in Subsect. §2.4.3, for the vibrational dynamics of HCN interacting with a laser, using the same parameter values as in Figure 6.4. For comparison purposes, it is also indicated the value of the SALI coefficient corresponding to each of trajectory using the same color scale as in Figure 6.4. To help in the discussion three straight lines, corresponding to the resonance conditions $(1, 0, \gamma/2)$ (pink), $(1, -1, 0)$ (red), and $(2, -3, \gamma)$ (black), have been plotted superimposed.

values, around the same two molecular resonances, 1:1 and 3:2. Moreover, the later region corresponds to what Sethi and Keshavamurthy called the NH in Ref. [Set12], while the vicinity of the former would be the DH, although as can be seen no dissociating trajectories (that should appear on the $\omega_1 = 0$ line) are observed at this value of ω_F. When the laser frequency is increased, in panels (b) and (c), the results obtained are very similar, and only a small increment in the dispersion of the data, indicating a growth of the available frequency space, is observed. Two new facts are, however, worth mentioning. First, same points on the $(1, 0, \gamma/2)$ line drift to the left, i.e. to smaller values of ω_1/ω_F. Second, a few points appear at $\omega_1 = 0$ indicating dissociation of the CH bond. The situation is completely different in panel (d). Here, the number of dissociating trajectories increases significantly. The dispersion and drift to the left of the points over the $(1, 0, \gamma/2)$ line largely increases, and the regular trajectories, i.e. points in light colors, at $\omega_2/\omega_F \simeq 1$ still persists. Also, the resonant line $(1, -1, 0)$ seems to constitute a strong barrier, or bottleneck for IVR, separating the DH from the rest of regions in the frequency space. This tendency continues in panels (e) and (f) as the frequency of the laser is increased, and the same comments made above also apply here.

To conclude this subsection, let us now discuss how the conclusions drawn from the results of Figure 6.5 translate into phase space. For this purpose, a more precise definition of the NH and the DH hubs is needed. In this case, it is considered that a trajectory belongs to the NH when it is below the $(2, -3, \gamma)$ line, while trajectories in the DH are taken as those with $\omega_1/\omega_F < 3/4$. The corresponding analysis is shown pictorially in Figure 6.6, where the trajectories (initial conditions over the PSOS) contained in the NH and DH are plotted in blue and brown, respectively. As can be seen, the NH points cluster in the 3:2 resonance zone, this being a further confirmation of the conclusion drawn previously in connection with the results of Figure 6.5. However, this region is also filled with DH trajectories (brown points) for $\omega_F = 0.010000$ [panel (d)], since at this value the laser is in resonance with the 3:2 molecular motion. Notice how this region is avoided by the same class of trajectories for the rest of values of the laser frequency (panels). These trajectories fulfill the chaotic region, result which is also inferred from the SALI values (dark colors) in Figure 6.4.

6.2.3 Molecular dissociation and chaotic dynamics

The main conclusion of the previous subsection is that resonance $(1, -1, 0)$ constitutes a robust bottleneck dividing the frequency space of the HCN in the presence of a laser into two different regions, namely the NH and the DH,

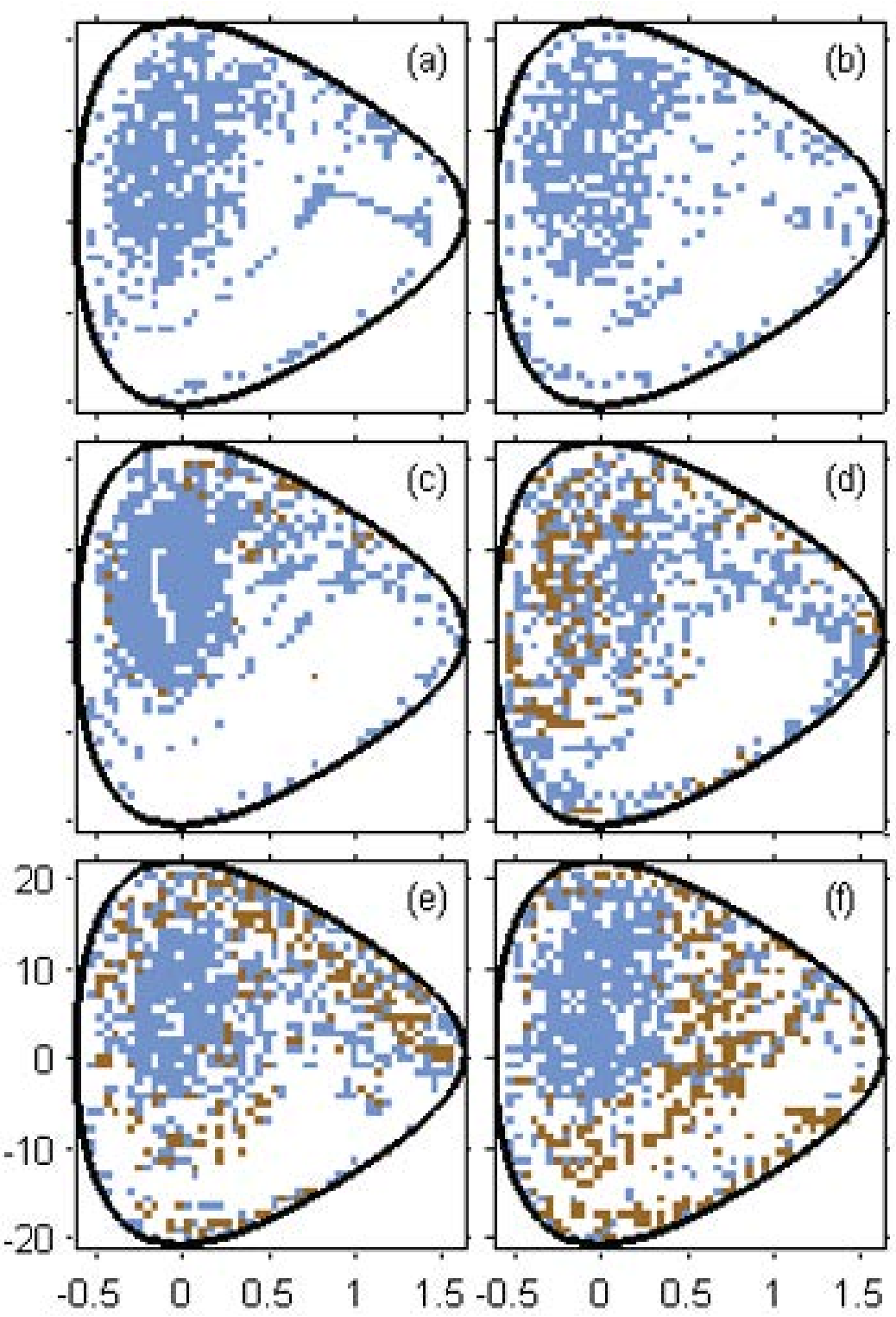

Figure 6.6: Phase space picture of the trajectories (initial conditions represented over the Poincaré surface of section) in the noble (blue dots), and dissociation hubs (brown dots) for the vibrational dynamics of HCN interacting with a laser, using the same parameter values as in Figure 6.4.

being the later formed by a mixture of chaotic and dissociating trajectories. Let us examine now in more detail this region.

For this purpose, the previous calculations have been up to a much longer time than that used in the frequency analysis, in order to allow for a proper assessment of the dissociation process. Trajectories will then be considered dissociative when the displacement in the bond of interest exceeds a certain threshold, which are set here to 15 a.u. for the CH bond. The corresponding results are shown in Figure 6.7 where the dissociation times are shown in a color scale for the same laser frequencies considered before. Several comments are in order.

In the first place, it can be observed that the laser is not able to dissociate the molecule until a value of $\omega_F = 0.009278$ [panel (c)]. Second, by comparing the results in Figure 6.7 with those in Figure 6.6, it can be concluded that in all cases the dissociating trajectories correspond to initial conditions in the DH. Moreover, all the dissociative trajectories present a large degree of chaoticity, as assessed by the SALI value, given in Figure 6.4. Third, it can be noticed that trajectories in the NH and the 1:1 resonance zone do not lead to dissociation. And fourth, notice how dissociation also reflects the fact that when the laser frequency is $\omega_F = 0.010000$ [panel (d)] the resonance with the 3:2 vibrational molecular motion destroys the regularity in this region. Notice that the lapse of time in which the dissociation takes place has nothing to do with the fact that the initial value of p_1 is small or large, since in the corresponding region the dynamics is very chaotic and the values of the coordinates may change quickly. For example, consider in Figure 9 (f) the region near $(p_1 = 0; q_1 \approx 0.75)$, where the frequency ratio indicates that it belongs to the dissociation hub, where the escape is very fast.

To obtain a clearer idea of the dependence of dissociation on the laser frequency, this subsection is finished by presenting in Figure 6.8 the fraction of dissociative and chaotic trajectories for a number of frequency values much larger than those considered in the analysis of Figs. 6.4 and 6.7. These results are computed by considering that a trajectory is chaotic when its SALI coefficient is smaller than 10^{-5}.

As can be seen, there is no dissociation (black circles) until the laser frequency reaches 0.009. This threshold value, which depends on the laser intensity (recall that in this work only one value of this parameter is considered), is in good agreement with the result of Brezina and Liu [Brez04], despite the fact that the present representation of the dipole is much simpler that the

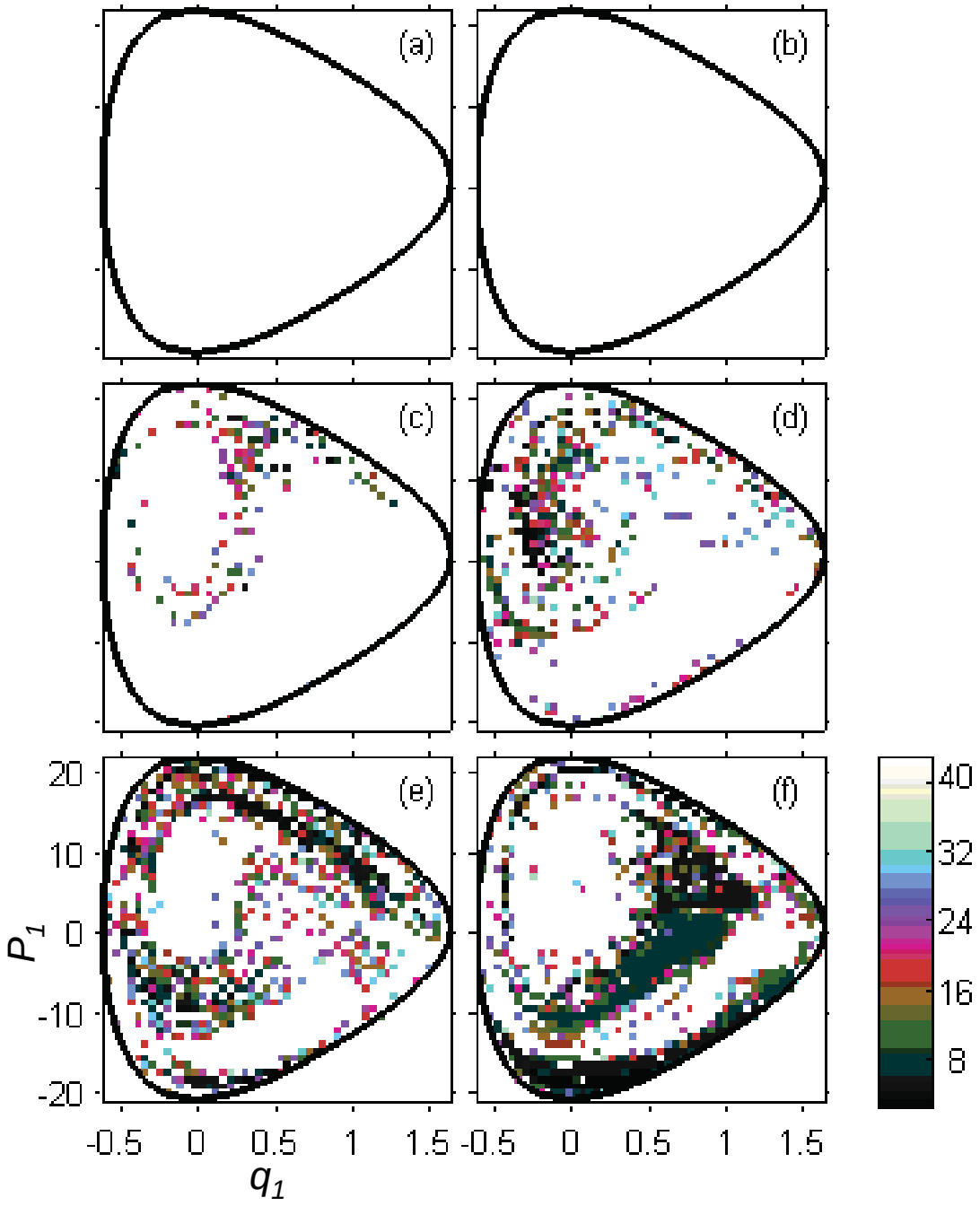

Figure 6.7: Dissociation times for the vibrational dynamics of HCN interacting with a laser, using the same parameter values as in Figure 6.4. White dots indicate initial conditions not leading to dissociation. The color scale is represented in units of 10^3 a.u. of time.

one used by those authors. Beyond the threshold, the fraction of dissociative trajectories presents two peaks, at $\omega_F = 0.018556$ and 0.022266, respectively, with a minimum in between for 0.020000. These values correspond, respectively to the integer frequencies $\omega_F = (3/2)\ \omega_{1,2}^{[1:1]}$, $\omega_F = (9/5)\ \omega_{1,2}^{[1:1]}$, and the noble ratio $\omega_F = \gamma\ \omega_{1,2}^{[1:1]}$, respectively.

With respect to the fraction of chaotic trajectories (blue circles), it can be observed that for $\omega_F > 0.009$ the curve follows the same behavior as that for dissociation. Below that value, the curve presents a numerous series of peaks and valleys, that can always be associated with laser-molecule resonances, as labeled in the figure, being those resonances of integer oder for the peaks and of noble ratios for the valleys.

From a dynamical point of view, Figure 6.8 can be seen as summarizing the balance of larger or smaller destruction of regular tori as a function of the irrationality of the ratio between laser and vibrational frequencies of the isolated molecule, as stated at the end of Sect. §6.2.1, since the effect of the laser is different for the two regular regions around the 1:1 and 3:2 HCN resonances. When ω_F is in resonance with any of the associated frequencies (see labels at the top of graph in the figure) the corresponding fraction of destroyed tori increases. For example, there is near $\omega_F = 0.0023$ a small peak encircled in red indicating that when $\omega_F = (2/3)\ \omega_2^{[3:2]}$ part of the regular 3:2 region turns chaotic. This effect is, however, much larger when the laser is in resonance with the motion in the 1:1 region 1:1, as for example at the nearby frequency where $\omega_F = (1/3)\ \omega_{1,2}^{[1:1]}$.

Concerning dissociation, it can be observed for example that for $\omega_F = 0.010000$ there is a small peak of dissociating trajectories that coincides with a minimum in the chaotic fraction. Again, this is explained in a similar way as before, since at this value of ω_F, the laser is in resonance with one of the frequencies of the 3:2 resonance. This is in agreement with the results of Figure 6.4(d), where the corresponding region is seen to be almost completely destroyed and filled with (chaotic) trajectories with high values of the SALI, which are also seen in Figure 6.7(d) to lead to fast dissociation. The (larger) phase space region corresponding to motion around 1:1 is however largely unaffected, since there the ratio between laser and molecular motions is very irrational, i.e. $\gamma/2$. This tendency reverses for the next point in the graph, i.e. $\omega_F = 0.0103$, where laser and molecular motions are not in resonance any more.

The global maximum for dissociation, which is also a global maximum for chaotic trajectories, appears at $\omega_F = 0.01857$. This corresponds to a 3:2

resonance between laser and HCN. Notice, also that this value is different from that of 0.011, chosen in Ref. [Set12] only on the criteria that the laser is out of resonance with the CH harmonic frequency. The results presented in this thesis clearly indicate that this 1:1 resonance at low energy with the laser, although important, is not necessarily crucial. The reason for the relevance of the 3:2 resonance is not totally clear, and certainly deserves further investigation. However, this finding is not unreasonable. Resonance 3:2 is the first one in the layer of the Farey tree originated by the 1:1 (with a large area of influence) and the 2:1 (where dissociation severely decreases) parent resonances, then sharing the dynamical characteristics of both of them. Also, one should be aware that the relevance of the 3:2 resonance may change, for example, when considering other values of the laser amplitude.

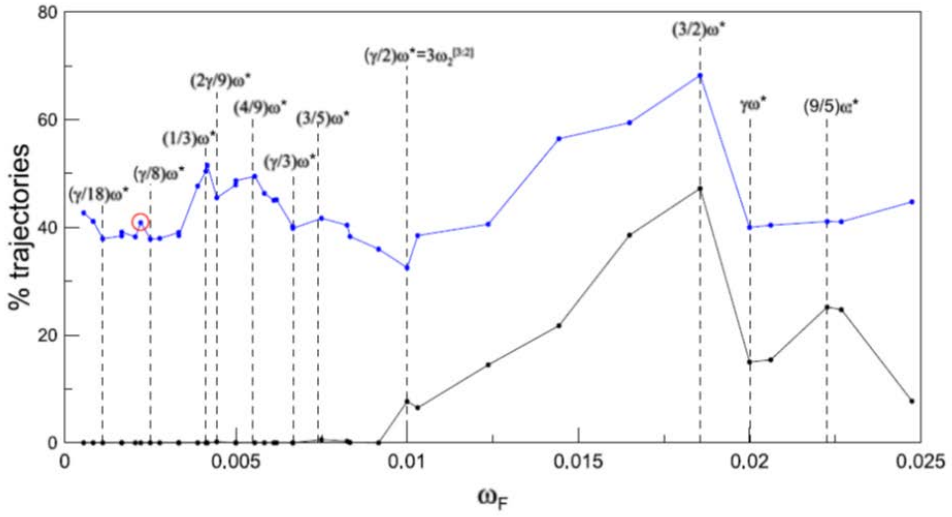

Figure 6.8: Fraction of dissociative (black circles) and chaotic (blue circles) trajectories as a function of the laser frequency, ω_F. All peaks and valleys are found to be correlated with resonances between ω_F and $\omega^* = \omega_{1,2}^{[1:1]}$, as indicated by the labels, except for the case of the peak encircled in red, where the resonance condition corresponds to $\omega_F = (2/3)\omega_2^{[3:2]}$. (See text for details.)

To conclude, it should be emphasized that Figure 6.8 is very important, since it summarizes all the relevant dynamical information on the laser interaction with the HCN vibrations. Indeed, it allows to predict which laser frequency values are the most effective in promoting/avoiding molecular dissociation in this system. Moreover, Figure 6.8 clearly illustrates the process of tori persistence and destruction with respect to the variation of an external

parameter, in the spirit of the KAM theorem. In this sense, the results are analogous to those presented in this multifractal analysis of the frequency map as a function of the excitation energy [Tar01], showing peaks and valleys associated to the density of regular tori in a similar, although laser free, molecular system.

Part III

Control of Dynamics on Complex Networks

Chapter 7

Complex Networks

Complex systems are ubiquitously present in natural and human-related phenomena, and complex networks are considered the backbone of such systems in a wide range of scenarios ranging from social and ecological to biological and technological systems. For example, the brain can be modelled as a network where each neuron is represented by a node and links represent the interaction among neurons, while the power grid is designed to be a network where the generators are the nodes and the transmission lines are abstracted as links. Thus, the study of complex networks has become one of the major topics of interdisciplinary research in the XXI century. Nevertheless, the theory of networks goes back to graph theory, a branch of discrete mathematics that focuses on the analysis of networks since 1736, when Leonhard Euler famously found the solution of the problem of the seven bridges of Königsberg.

The explosion in the development and application of network theory in recent years is not due to the appearance of new systems to study, such as the cell-phone calls network. It should be noted that most of the systems under study are by no means new. For example, metabolic networks date back to the origins of life, sociologists have been studying social networks for decades and the Internet is now over four decades old. In contrast the reason for this explosion of network science is the availability of large amounts of data. In the past the ability to build accurate maps was limited by the absence of high resolution data. Hence, the lately acquired ability to store and share data prompted the evolution of network science. Nowadays Internet and the emergence of cheap digital storage have enhanced the storage and share of data, permitting its analysis in the shape of networks. Another key issue that has promoted network science is that, despite most complex systems largely differ in their nature goals and scope, after abstracting them as a

Figure 7.1: Barcelona Metro network

network they share many properties. Given the diversity of the systems studied by network science, one would expect that their properties will largely differ. However, one of the most important discoveries of network science was that this is not the case. On the contrary, the network emerging from diverse systems are rather similar to each other, allowing us to use a common formalism and mathematical tools to explore them. Hence, the universality of networks is a fundamental principle that has guided the explosion of network science in the past two decades.

7.1 Networks and graphs

A network is an abstraction of a system in which we represent its elements as nodes or vertices and the interactions between them as links or edges. Formally this is defined by the triple (V, E, f) where V is a finite set of *nodes* or *vertices*, $E \subseteq V \times V = \{e_1, e_2, ..., e_L\}$ is a set of *edges* (also named *links*) and f is a mapping which associates some elements of E to a pair of elements of V, such as that if $v_i \in V$ and $v_j \in V$ then $f : e_p \to [v_i, v_j]$.

The number of nodes or vertices of the network is given by N which is the size of the network. Nodes are usually referred to by an integer $i \in \{1, 2, ...N\}$, but the labelling is completely arbitrary. The number of links or edges is denoted by L, with $0 \leq L \leq N(N-1)/2$. In a undirected graph, each of the edges is defined by a couple of nodes v_i and v_i, and we say that the edge $e_k = (v_i, v_j)$ connects nodes v_i and v_j or is incident in them. On

the other hand, in a directed graph, the order of the two nodes in a edge has to be taken into account, and then we distinguish between edges (v_i, v_j) and (v_j, v_i). Two nodes connected by an edge are referred as *adjacent* nodes. For network and vertex $v \in V$, the neighbour set N_v of v is the set of vertices (other than v) adjacent to v.

Networks usually have at most one edge between two nodes. In case that there are more than one edge between the same pair of vertices we refer to them as a *multiple edges*. On the other hand, if a link connects a node to itself, it is called a *loop*. A network that has neither loops nor multiple edges is called *simple*. A *bipartite* network has two kinds of vertices, one representing the original vertices and the other representing the groups to which they belong [New10].

There is a type of real networks for which it is useful to represent edges as having a strength, weight, or value to them, usually a real number. This is for example the case of the Internet network, where edges can be assigned to weights representing the amount of data flowing along them or their bandwidth. These are called weighted networks, which are formally described by the quadruple $(V, E, \overline{W}, f)$, with V, E, f previously defined and $\overline{W} = \{w_1, w_2, \dots w_L\}$ being the set of weights associated to each edge in the network. In matricial representation, the network is described by the weight matrix W is an N x N matrix whose entry $w_{ij} \in \mathbb{R}$ is the weight associated to the link (v_i, v_j).

Another important concept to be defined is that of reachability of two different nodes in a network. A *walk* $\mathcal{W}$ from node v_i to node v_j is an alternating sequence of nodes and edges (a sequence of adjacent nodes) that begins with v_i and ends with v_j [Har94]. Formally, we have:

$$\mathcal{W} : v_i \to v_{i+1} \to \cdots \to v_{j-1} \to v_j \tag{7.1}$$

A walk $\mathcal{W}$ between edges v_i and v_j is *closed* if $v_i = v_j$. A *trail* is a walk in which no edge is repeated. A *path* is a walk in which no node is visited more than once: $v_m \neq v_n \ \forall \ m \neq n$. A walk $\mathcal{W}$ is a *cycle* if it is closed and $v_m \neq v_n \ \forall \ m \neq n$ except $v_i = v_j$. The *distance* or *length* of a path is defined as the number of links that the path contains. The shortest path (or *geodesic*) between two nodes refers to the path with fewer links that connects the two nodes. Then, a network is said to be *connected* if, for every pair of distinct nodes i and j, there is a path from i to j, otherwise the network is said to be *unconnected* or *disconnected*. Furthermore, a network is called *acyclic*, if it has no cycles. An acyclic network is also called a $forest$. A *tree* is a connected acyclic network [Har94].

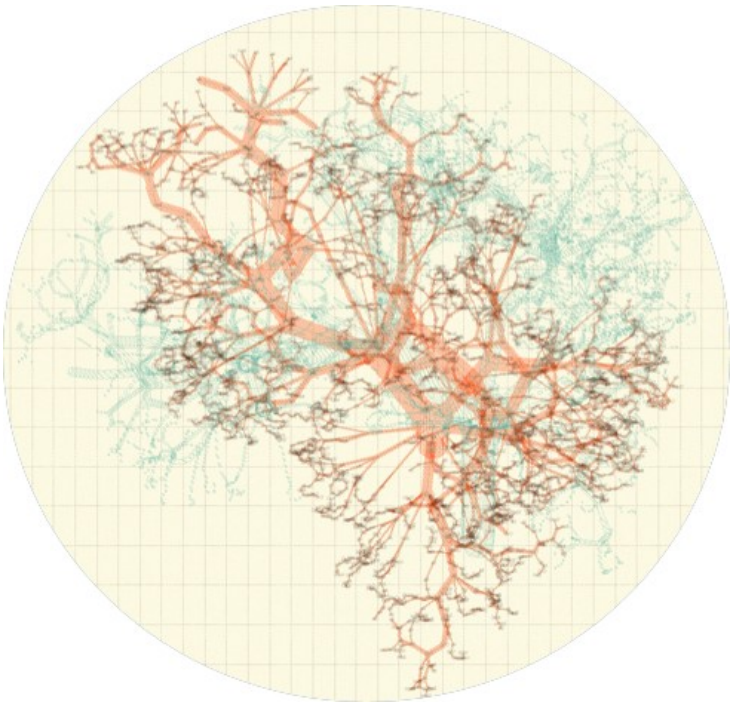

Figure 7.2: Robert Fischer's chess game tree (Arbor Ludi) [Ser18]

The concepts above are illustrated here with two graphical examples. Figure 7.1 shows the network of Metro transportation in Barcelona, with the nodes being the stations and the links being the lines between them. This network is connected (any station can be reached from any other one), undirected (trips can be done in both ways), and passengers choose the route (path) with the shortest (geodesic) distance between origin and destination. On the other hand, figure 7.2 depicts the so called *Arbor Ludi* (game tree) of the World's champion chess player Robert Fischer considering the games he played during his professional career. The links represent the moves during a given game that he would perform, while the edges corresponds to intermediate positions, and the ramifications represents the evolutions and variants of the game from the beginning and aperture to the end. Thicker links correspond to moves that Fischer most frequently used. The two colors orange and green on the graph correspond to either playing white or black pieces (therefore there are two type of edges in the network). This plot represents indeed two superimposed networks (one per color) both of them being a weighted directed tree (note that it is not a bipartite network since there are no links between the two types of nodes).

7.2 Degree of a node

The main property of each node is its *degree* k. The degree of a node represents the number of links that the nodes has to other nodes in the network. The average degree for undirected graphs is given by:

$$\langle k \rangle = \frac{1}{N} \sum_{n=1}^{N} k_i = \frac{2L}{N} \tag{7.2}$$

For directed networks, we can extend the definition of degree by distinguishing between in-degree (k_i^{in}) and out-degree (k_i^{out}). The first one measures the number of links that point to node i, while the second one measures the number of links that point out from node i. The sum of a node in and out degree is equal to its degree:

$$k_i = k_i^{in} + k_i^{out} \tag{7.3}$$

If every vertex has the same degree, the graph is called *regular*. In a k-regular network each vertex has degree k.

The *degree distribution*, $P(k)$, represents the probability of randomly selecting a node with degree k. Hence, in a network of size N, $P(k)$ is given by the following expression:

$$P(k) = N_k/N \tag{7.4}$$

where N_k represents the number of nodes in the network with degree k. The degree distribution plays a key role in network science, as it is used to calculate many network properties, such as the average degree.

7.3 Matricial description of Networks

A representation of the graph can be given in terms of an *adjacency matrix* A, which is a N x N binary matrix whose entry A_{ij} is 1 if $(i, j) \subset E$ and 0 if nodes i and j are not connected. Note that for undirected graphs the adjacency matrix is symmetric, and that for networks without loops (as we consider in this thesis), the diagonal entries of the adjacency matrix are zero.

The degree of a node can be easily obtained from the adjacency matrix. In the simplest case of an undirected network the degree (k_i) of node i is either the sum over the rows or columns of the matrix:

$$k_i = \sum_{j=1}^{N} A_{ij} = \sum_{j=1}^{N} A_{ji} \tag{7.5}$$

Thus for directed networks, $k_i = k_i^{in}$ and k_i^{out} can be expressed as:

$$k_i^{in} = \sum_{j=1}^{N} A_{ji}\ k_i^{out} = \sum_{j=1}^{N} A_{ij} \tag{7.6}$$

An alternative procedure to describe a network is via its *incidence matrix*. For the case of an undirected graph is a N x L matrix B, such that $B_{ij} = 1$ if the vertex v_i and edge v_j are incident and 0 otherwise. For the case of a directed graph, the incidence matrix B is also N x L such that $B_{ij} = 1$ if the edge e_j is incoming to vertex v_i, $B_{ij} = -1$ if the edge e_j is outcoming from vertex v_i, and 0 otherwise.

Other relevant matrices associated to a network are the *Normal* matrix, defined as $N = D^{-1}A$, where D is the diagonal matrix with elements $D_{ii} = k_i$ and the combinatorial *Laplacian* matrix (also known as Kirchhoff matrix) defined as $\Delta = D - A$. The Laplacian can also be expressed in terms of the incidence matrix as $\Delta = BB^T$, and thus it is a semidefinite positive matrix.

A key concept in matrix theory is that of eigenvalues and eigenvectors, which renders relevant information of matrices in general, and also particularly of network structure and features. The spectrum of a network is defined as the set of eigenvalues of its adjacency matrix A. When the network is undirected, without loops or multiple edges, A is real and symmetric, and thus the graph has N real eigenvalues $\mu_1, \mu_2, \ldots, \mu_N$, and the eigenvectors corresponding to distinct eigenvalues are orthogonal. On the contrary, when the network is directed, the eigenvalues can have imaginary part.

The Perron Frobenius theorem states that the adjacency matrix of network has a real eigenvalue μ_N associated to a real nonnegative eigenvector, and such that $|\mu| \leq \mu_N$ for each eigenvalue. If the graph is connected, then μ_N has multiplicity 1 and $|\mu| < \mu_N$ for all eigenvalues different from μ_N. The value of μ_N decreases when vertices or edges are removed from the graph. For a connected undirected graph, this means that the largest eigenvalue μ_N is not degenerate.

The spectrum of the Laplacian matrix $\lambda_i(\Delta)$ also captures many topological properties of the network. It must be noted that Δ is always positive semidefinite. All the eigenvalues of Δ are real and non-negative, and Δ has

a full set of N real and orthogonal eigenvectors. Since all rows of Δ sum to zero, the Laplacian always admits the lowest eigenvalue $\lambda_1(\Delta) = 0$, with associated eigenvector composed of N ones. The algebraic multiplicity of this eigenvalue is equal to the number of connected components in the network. Furthermore, the first non-zero eigenvalue $\lambda_2(\Delta)$ (also referred as the Fiedler eigenvalue or algebraic connectivity) gives a measure of the connectedness of the network.

7.4 Clustering Measures

The clustering or transitivity of a network indicates the relation between the neighbours of an edge among them. If the edge connection is transitive among three vertices v_i, v_j, and v_k, it implies that if vertex v_i is connected to vertex v_j, and v_j is connected to v_k, then v_i is also connected to v_k. Thus, transitivity measures the total number of closed triangles in a network. Random networks, such as the Erdös - Rényi network, do not present a clustering structure, while most of the complex networks present in nature do. The clustering of a network can be defined in several ways. Following the previous example of three vertices, If the transitivity relation holds among them, there is a path which forms a loop of length three, and we say that the path is closed. The *clustering coefficient* is then defined to be the fraction of paths of length two in the network that are closed.

The clustering coefficient is obtained as follows : we count all paths of length two, and we count how many of them are closed, and we divide the second number by the first to get a clustering coefficient C that lies in the range from zero to one :

$$C = \frac{\text{number of closed paths of length two}}{\text{number of paths of length two}} \tag{7.7}$$

C = 0 implies no closed triads, while C = 1 implies perfect transitivity.

An alternative description of the clustering coefficient is given as follows:

$$C = \frac{\text{number of triangles x 6}}{\text{number of paths of length two}} \tag{7.8}$$

In other words, the clustering coefficient measures the fraction between the actual triangles in the network and the potential triangles that could be closed

The clustering coefficient can also be defined locally for a single vertex i, as follows:

$$C_i = \frac{\text{number of pairs of neighbors of i that are connected}}{\text{number of pairs of neighbors of i}} \tag{7.9}$$

In this definition, for those vertices with degree equal to 0 or 1 (in which case the numerator and denominator of the above expression is zero) we set $C_i = 0$. The coefficient for the overall network is then computed as the average value of the individual clustering coefficients:

$$C = \frac{1}{N} \sum_{j=1}^{N} C_i \tag{7.10}$$

7.5 Centrality Measures

In the context of network science there are several measures that quantify how central each node is in a given network. The goal of centrality measures is to determine the importance or influence of a given node in the network. The most basic measure of centrality is the degree already described previously. Other measures of centrality include closeness centrality, betweenness centrality, eigenvector centrality and page rank centrality. They are described in subsequent sections.

7.5.1 Betweenness Centrality

Betweenness is a centrality measure of influence of a node within a networks (it can also be defined for links). This measure quantifies the number of times a node acts as an intermediary along the shortest path between two other nodes.

$$b_i = \sum_{j=1}^{N} \frac{n_{jk}(i)}{n_{jk}} \tag{7.11}$$

with n_{jk} being is the number of shortest paths connecting j and k, while $n_{jk}(i)$ is the number of shortest paths connecting j and k and passing through i.

7.5.2 Closeness centrality

This measure quantifies how close (or far) is a node from the rest of the nodes in the network. Intuitively, it represents how long it will take a node

to spread information to all other nodes. In connected networks we can define a natural distance between all pairs of nodes. This distance is given by the length of the shortest path connecting each pair of nodes. Thus, the closeness of a node is defined as the inverse of the sum of its distances to all other nodes. Therefore, the more central a node is the lower its total distance to all other nodes.

7.5.3 Eigenvector centrality

Eigenvector centrality measures the influence of each node in a network. This measure assigns scores to nodes in the network based on the concept that connections to central nodes contribute more to the score of the node in question than the same number of connections to peripheral nodes. In many circumstances a vertexs importance in a network is increased by having connections to other vertices that are themselves important. Taking this rationale into account, eigenvector centrality of a vertex is defined to be proportional to the sum of the centrality of its neighbours. The derivation of its formal definition is as follows. In a first iteration, each vertex is assigned the same centrality, for example $x_i = 1, \forall i = 1 \dots N$. We then compute a second iteration for the i^{th} vertex by means of the sum of its neighbours, as follows:

$$x'_i = \sum_{j=1}^{N} A_{ij} x_j \tag{7.12}$$

This expression can be cast in matricial form as $\mathbf{x}' = A\mathbf{x}$ with A being the adjacency matrix and $\mathbf{x}$ the vector with elements x_i. The process can be repeated t times to make better estimates, resulting in the evolution of the eigencentrality as:

$$\mathbf{x}(t) = A^t \mathbf{x}(0) \tag{7.13}$$

Since A is symmetric matrix, its normalized eigenvectors $\mathbf{v_i}$ form an normalized basis that span $\mathbb{R}^N$. Thus, $\mathbf{x}(0)$ can be expressed as follows for some constants c_i

$$\mathbf{x}(0) = \sum_{j=1}^{N} x_i \mathbf{v_i} \tag{7.14}$$

Based on linear system theory and the expressions above, we have that

$$\mathbf{x}(t) = A^t \sum_{j=1}^{N} c_i \mathbf{v_i} = \sum_{j=1}^{N} c_i \lambda_i^t \mathbf{v_i} = \lambda_1^t \sum_{j=1}^{N} c_i (\frac{\lambda_i}{\lambda_1})^t \mathbf{v_i} \tag{7.15}$$

with λ_i being the eigenvalues of the A matrix and λ_1 the largest one. Thus, the series converges to $c_i \lambda_1^t \mathbf{v_i}$

In matrix form, it can be stated that the centrality vector satisfies $A\mathbf{x} = \lambda_1 \mathbf{x}$

Therefore we have that eigencentrality of node i is indeed proportional to the average eigencentrality of its neighbours:

$$x_i = \frac{1}{\lambda_1} \sum_{j=1}^{N} A_{ij} x_j \tag{7.16}$$

In general, there will be many different eigenvalues for which an eigenvector solution exists. However, all the entries in the eigenvector need be positive since negative centralities make no sense. Hence, this implies (by the Perron Frobenius theorem) that only the eigenvector associated to the greatest eigenvalue results in the desired centrality measure. Thus, the centrality score of node i is given by the ith term of the related eigenvector

It should be noted that PageRank (used by Google) and Katz centrality are variants of the eigenvector centrality.

7.6 Network models

7.6.1 Random Networks

One of the goals of network theory is to develop models that reproduce the network structure of the complex systems that we encounter in nature. Real networks do not present a regular crystal structure, such as the lattice forming the net of a goal. In contrast, the networks we find in nature present a much more random structure.

Random network can be defined as a set of nodes N where each pair of them is connected with the same probability p. In other words, a random network consists of N nodes with L randomly placed links. Thus, we can easily build a random network in the following way. We first create a set of N nodes. Next, we select all possible pair of nodes and generate a random number between zero and one for each pair. If the number is smaller than

a fixed probability p we link the pair of nodes, otherwise we do not connect them.

Paul Erdös and Alfréd Rényi significantly contributed to the knowledge on random networks properties, and for this reason these networks are usually referred as Erdös - Rényi (ER). It should be emphasized that a given network is one outcome of the possible realizations.

The average degree $\langle k \rangle$ of a random network is determined by the size of the network N and the parameter p that controls the density of the network. Hence, $\langle k \rangle$ results from the product of p and the maximum number of links a node can have (N-1). It can be expressed in the following way:

$$\langle k \rangle = \frac{2L}{N} = p(N-1) \tag{7.17}$$

The degree distribution of a random network is given by the binomial distribution

$$P(k_i = k) = C_{N-1}^{k} p^k (1-p)^{N-1-k} \tag{7.18}$$

Therefore, by using the properties of the binomial distribution we can calculate the average degree and its standard deviation. It is well known from probability theory that for fixed $\langle k \rangle$ and large N, we can approximate the degree distribution by the Poisson distribution given by the following expression:

$$P(k) = e^{-\langle k \rangle} \frac{\langle k \rangle^k}{k!} \tag{7.19}$$

The Poisson distribution is only an approximation to the degree distribution of a random network. However, due to its analytical simplicity in comparison to the binomial distribution, it is usually the preferred form.

7.6.2 Small-World networks

The small-world effect is an interesting phenomenon observed in social networks that was first reported within an experimental approach by Stanley Milgram in the 1960s [Tra69, Mil67]. Milgram conducted an experiment in which a series of individuals on Kansas and Nebraska had to send letters to individuals who they did not know living in Boston, Massachusetts. The letters passed from person to person and surprisingly were able to reach the designed target in a few steps (around six on average). A similar phenomenon is also found in the well-known parlor game called the Six Degrees of Kevin

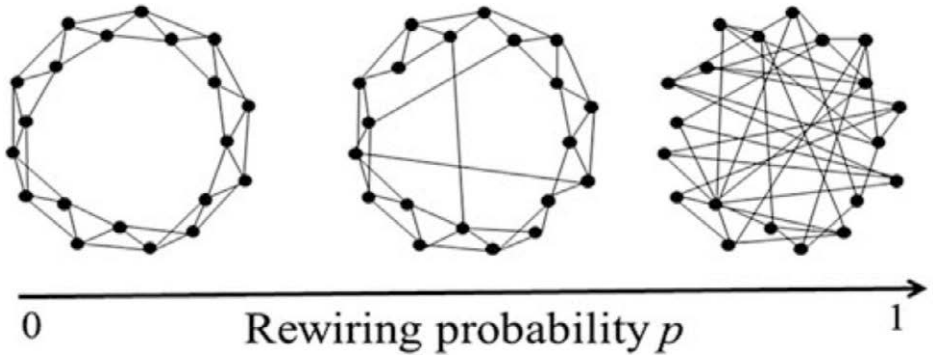

Figure 7.3: Rewiring process in the Small World model. Adapted from [Est15]

Bacon, in which one attempts to connect pairs of actors A and B via chains of costars, such that each intermediate pair collaborated in at least one movie, in such a way that chain ultimately links actors A and B.

Similarly, there is a well-known reference within the mathematicians community (referred as Erdös number), which is related to the scientific papers an author has published, and the links of its co-authors established via their own publishing record. To be assigned an Erdös number, someone must be a co-author of a research paper with another person who has a finite Erdös number. The procedure goes as follows: Paul Erdös is assigned an Erdös number of zero. Anybody else's Erdös number is $n + 1$ where n is the lowest Erdös number of any co-author. Thus, such number provides an indication of the closeness with respect to Paul Erdös. It is interesting to notice that even Nobel prizes of quite unrelated fields (such as medicine) have an average Erdös number lower than six.

This concept was formalized by Watts and Strogatz [Wat98], which introduced the so-called small-world property of networks, and showed its relevance in biological and technological applications. The model is based on a rewiring procedure of the edges implemented with a probability p. The starting point is a N nodes ring, in which each node is symmetrically connected to its $2m$ nearest neighbours for a total of $K = mN$ edges. Then, for every node, each link connected to a clockwise neighbour is rewired to a randomly chosen node with a probability p, and preserved with a probability $1p$. In the case with p =0 we have a regular lattice, while for $p = 1$ the model produces a random graph with the constraint that each node has a minimum connectivity $k_{min} = m$. For intermediate values of p the procedure generates graphs with the small-world property and a non-trivial clustering

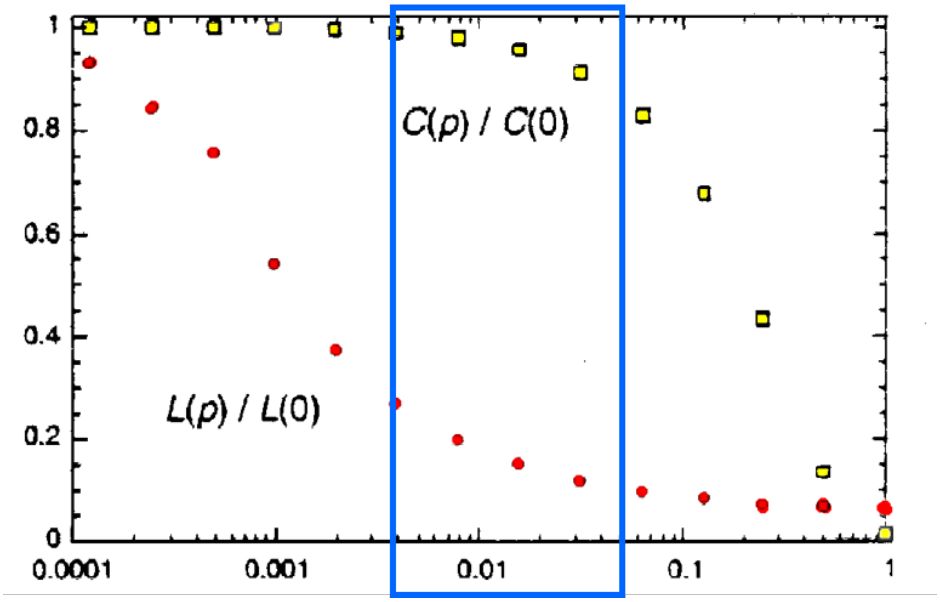

Figure 7.4: Small World normalized clustering coefficient (yellow squares) and average path length (red circles) versus the rewiring probability p. Adapted from [Wat98]

coefficient.

Small-world networks combine a high level of clustering with a small average path length (see figure 7.4, where this effect occurs in the middle of the p probability range). It turns out that the existence of shortcuts in a network allows for the coexistence these two apparently incompatible features. Indeed, adding a few links between distant regions to a highly clustered regular network may be sufficient to drastically reduce the average geodesic distance without significantly altering the high clustering in the network.

7.6.3 Scale-free networks

It has been observed in many examples in the network literature [New03] that the degree distribution of many real networks do not follow the profile associated to random networks. For example, when plotting the degree distribution of many networks associated to internet (web pages in a certain field, distribution of clients, etc.) it is observed that most of the vertices in the network have low degree but there is a significant tail to the distribution, corresponding to vertices with substantially higher degree. We

call such a well-connected vertex a hub and this new type of networks as *scale-free networks*. This term refers to any functional form that remains unchanged to within a multiplicative factor under a rescaling of the independent variable. For this reason they are also called *power-law networks*, since these are the only functions that comply with such requirement. It is worth mentioning that small world effect (in terms of low average path length) can also be observed in these networks, although it is not obtained by rewiring as in the Watts and Strogatz model.

The main difference between these scale-free networks and random graphs appears in the tail of the degree distribution. While for random networks the probability of finding a node with degree k rapidly decreases, the pattern is significantly different in the scale-free case. For scale free networks the probability of finding high degree nodes, or hubs, is several orders of magnitude higher than in random networks. For scale-free networks, we say that the degree distribution is right-skewed, which means that their distribution has a long right tail of values far above the mean.

There are two basic assumptions in the Erdös - Rényi model that do not occur in real life. The first assumption is that networks are static. The ER model fixes the number of nodes that does not vary during the forming process of the network. This is not true in nature, where systems continually grow with the addition of nodes. The second one is that the ER model assumes that we randomly choose with whom we interact. However, this is not true, as new nodes prefer to connect with those that are already highly connected (hubs). This is known as the preferential attachment rule. In summary the ER model fails to explain the growth of real networks and the emergence of hubs. Yet, these properties emerge from preferential attachment rules. The first network growth model based on preferential attachment was proposed by Price. However, preferential attachment did not become widely accepted as a mechanism for generating power laws in networks until the 1990s, when it was discovered by Barabási and Albert [BaAl99].

The model proposed by Barabási and Albert is defined as follows. At each time step a new node is created with m links that will connect the new node to the previously existing ones. The probability that the new node becomes connected to a node i of degree k_i is

$$P(k_i) = \frac{k_i}{\sum_{j=1}^{N} k_j} \tag{7.20}$$

The model is based on a probabilistic rule that determines that a node

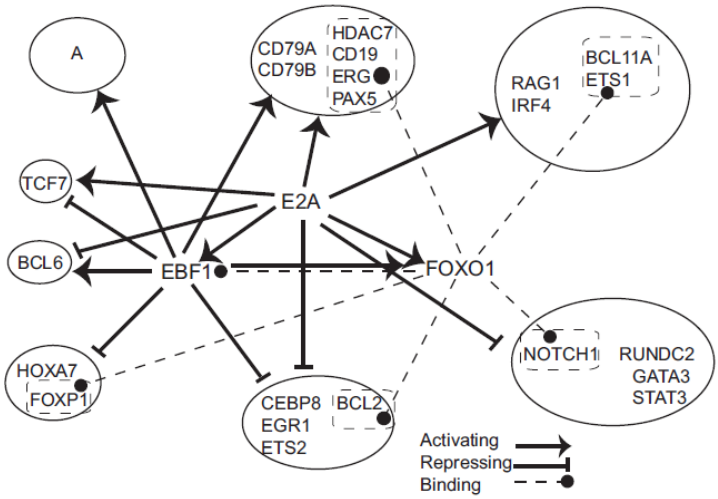

Figure 7.5: The network of protein-DNA interaction in B-cell development [Rav13]

can connect to any other node in the network, being more probable that it connects to a hub than to a low degree node.

Reference [Sant08] presents a framework for the extension of the Barabási-Albert model to heterogeneous complex networks. In this case, the m links attached to a new node v_a are randomly connected to the network nodes following a distribution $\Pi(v_i)$ given by an extended attachment rule:

$$\Pi(v_i) = \frac{\pi(v_i)}{\sum_{j=1}^{N} \Pi(v_j)} \tag{7.21}$$

The attachment kernel or visibility π of a node v_i in the rule is given by the product of its degree k_i and its affinity σ with the newly added node v_a, which is itself a function of the states of nodes i and a (x_i and x_a, respectively):

$$\pi(v_i) = k_i \sigma(x_i, x_a) \tag{7.22}$$

7.7 Processes on Networks

The concepts introduced in previous sections list some of the most relevant features that describe the topology of a complex network. Nevertheless, equally important in the study of complex networks is the description and

analysis of processes taking place on their structure. The types and practical examples of such processes are numerous, ranging from social, economic, technological to biological fields ([Rav13, Gros11, Noe1918, Bar08, Hav10, Est15]). As an example of such processes we can mention those associated with Gene Regulatory Network (GRN), as the one shown in figure 7.5). This section reviews some important ideas regarding the processes that frequently take place within the structure of a network.

7.7.1 Percolation and network resilience

A percolation process is one in which vertices or edges on a graph are randomly designated either occupied or unoccupied and one asks about various properties of the resulting patterns of vertices [New03]. An example is related to the immunization of individuals against a certain disease, or the removal of a fraction of the vertices in a network, as in the case of failure in Internet routers (cf. [New10]). The dual phenomenon is bond percolation, in which some of the bonds or links of the network are occupied (see figure 7.6).

This process has important implications regarding the resilience of a network. For example, in case of removal of nodes with a high degree, the connectivity of the network can be seriously affected. Regarding nodes removal, a network is said to be robust if it can tolerate the loss of a large fraction of its nodes and still being connected. Scale-free networks are said to be highly robust because they keep a giant component even after removal of many of its nodes [New03]. On the other hand, in case of intentional attacks, a scale-free structure can cause more damage than a random attack

A similar problem is that of diseases spreading (or internet virus propagation, for that matter) which can be controlled in a smart way by proceeding to vaccination only of nodes with highest degree. This is the so called herd immunity effect. In this case power-law networks cause more problems because they require a vaccination of a larger number of elements in the network to prevent the disease dissemination [Hav10].

7.7.2 Consensus dynamics

Consensus is a dynamical process between the elements within a group or network that try to reach an agreement on a certain quantity of interest [Olf07]. The most standard consensus dynamics mechanism for a network of N nodes and adjacency matrix A is given by:

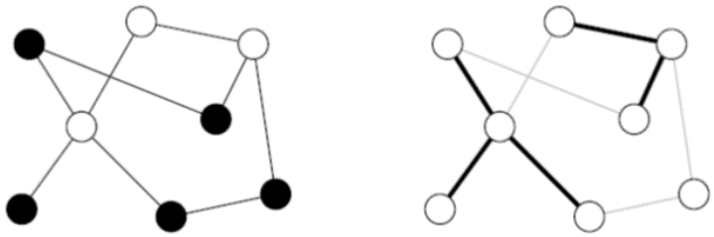

Figure 7.6: Site (left) and bond (right) percolation. Adapted from [New03]

$$\dot{x}_k(t) = \sum_{l \subset N_k} A_{kl}(x_l(t) - x_k(t)) \tag{7.23}$$

which can be cast in matrix form as:

$$\dot{\mathbf{x}} = -\Delta \mathbf{x}(t) \tag{7.24}$$

where Δ is the Laplacian matrix of the network, defined in §7.3. The equivalence of this equation to the classical Fourier law for heat diffusion equation leads to the use of the Laplace operator to denote also the Laplacian matrix.

The discrete time equivalent of these consensus dynamics is given as follows (also presented in section §8.1.1):

$$x_k(n+1) = x_k(n) + \epsilon \sum_{l \subset N_k} A_{kl}(x_l(n) - x_k(n)), \tag{7.25}$$

Diffusive phenomena in networks for instance as described by the equations above) have been extensively studied (e.g. [Del15, Bar08]).

A consensus is reached whenever the following condition holds after a given time t [Olf07] :

$$x_1 = x_2 = \cdots = x_N \tag{7.26}$$

In other words, the network nodes states converge to the subspace $\mathbf{x}$ = span($\mathbf{1}$) with $\mathbf{1} = (1, \cdots, 1)^T$. When the equilibrium condition is met, the state reached by every node is equal to the average of the initial state value of all nodes. As explained in section §7.3, Perron-Frobenius theorem

states that **1** is an eigenvector of the Laplacian matrix associated with the zero eigenvalue λ_1. For a connected network, the rest of the eigenvalues of the Laplacian matrix $(\lambda_2, \cdots, \lambda_N)$ are positive. The time convergence of consensus dynamics is dictated by the second smallest eigenvalue of the Laplacian matrix λ_2 (algebraic connectivity of the network, introduced in §7.3) because it defines the rate of convergence of the slowest mode [Olf07].

7.7.3 Synchronization on networks

Historically, research on synchronization phenomena have been conducted since the earlier days of physics. Already in the XVII century Christian Huygens discovered that two pendulum clocks hanging at the same beam were able to perfectly synchronize their phase oscillations [Stro03]. Synchronization is encountered in many natural phenomena (fireflies, semiconductor lasers, electronic circuits, etc. [Boc06, Stro03]). The approach started by Winfree [Win67] was based on a population of coupled nearly identical limit-cycle oscillators. This simple model capture with reasonable fidelity many observed real phenomena. As the coupling is increased, a certain threshold in the interaction strength is reached, above which the number of oscillators locking into synchrony continuously increases with the coupling intensity, ultimately reaching total synchronization. Kuramoto [Kur84] worked on the problem by means of a simple mathematical formulation in order to capture the rationale behind the onset of synchronization. His model is based on an all-to-all oscillators phase coupling, by means of the following governing equation for each of the N elements:

$$\dot{\theta}_i(t) = \omega_i + \frac{K}{N} \sum_{j=1}^{N} sin(\theta_j(t) - \theta_i(t)) \tag{7.27}$$

with ω_i being the natural frequency of oscillator i and K the coupling strength parameter. The frequencies ω_i are distributed according to some function g(ω), that is usually assumed to be unimodal and symmetric about its mean frequency Ω [Are08]. Kuramoto introduced a change of reference frame as $\omega_i \rightarrow \omega_i + \Omega$ so that the ω_is denote deviations from the mean frequency. The analytical treatment of the problem then follows the mean field approach. The collective dynamics of the whole population is measured by the macroscopic complex order parameter:

$$r(t)e^{i\phi(t)} = \frac{1}{N} \sum_{j=1}^{N} e^{i\theta_j}(t) \tag{7.28}$$

with $0 < r(t) < 1$ measuring the coherence of the population and ϕ(t) being the average phase, the higher its value the more overall synchronization is present among the oscillators. The Kuramoto equation can then be written as follows for each element i:

$$\dot{\theta}_i(t) = \omega_i + Krsin(\phi - \theta_i(t)) \tag{7.29}$$

Thus, each oscillator interacts with all the others only through the mean field quantities r and ϕ. It can be shown that [Are08] there is a critical value of the coupling parameter K at the onset of synchronization above which $r > 0$, whose value is:

$$K_c = \frac{2}{\pi g(0)} \tag{7.30}$$

The all-to-all connection considered above can be generalized to a set of oscillators embedded in a complex networks with a given wiring topology. Then, equation 7.27 is transformed into the following form:

$$\dot{\theta}_i(t) = \omega_i + \frac{K}{N}\sum_{j=1}^{N}\sigma_{ij}A_{ij}sin(\theta_j(t) - \theta_i(t)) \tag{7.31}$$

where σ_{ij} denotes the strength coupling between nodes v_i and v_j, and A_{ij} is the corresponding element of the adjacency matrix. In this case, critical coupling for synchronization depends also on the maximum eigenvalue of the adjacency matrix A (ibid.). Furthermore, analysis of the stability of the synchronization regime can be undertaken by means of Lyapunov functions and spectral graph theory, even for uncertain natural frequencies [Jad04]

A further extension of the Kuramoto problem is proposed in [Jad04, Hong11b]. There, all the oscillators are assumed to have the same natural frequency, but some of them (referred as contrarians) are negatively coupled to the mean field, while the rest of the elements (named conformists) are positively coupled. The observed dynamics in such case include travelling waves, complete incoherence, and full splitting of the population in two diametrically opposed factions. This alternative framework is used in [Louz12] for the study of techniques oriented to the suppression of undesired synchronization, based on the use of contrarians and either local or global information of the network status.

Synchronization phenomena are certainly not limited to the Kuramoto model briefly described here [Stro03]. Extensive research has been conducted in the field [Boc08], not only for regular dynamics but also for chaotic ones.

Stability of the synchronized state can in general be addressed by the so called Master Stability Function (MSF) [Are08, Boc08].

7.7.4 Spreading mechanisms

One of the processes most commonly found in real networks is that of spreading, which is also associated to percolation described above. This include spreading of epidemic diseases, via the susceptible-infected-susceptible (SIS) and the susceptible-infected-removed (SIR) models [Boc06]. In the first case, each element of the population is either susceptible (S) or infected (I). It is considered that an individual at the I group can infect its neighbours in the network with a rate λ, and be recovered to the S state at a rate μ. The SIR model corresponds to those diseases that result in an infected individual being removed (R) from the infection process, either because they become immune to the illness or they are removed for other reasons (they are deceased or translated outside of the network). In that case the recovery rate leads an individual towards the R group of the population. The dynamical equations for the SIR model are given by:

$$\begin{aligned} \dot{S}(t) &= -\lambda \overline{k} I(t) S(t) \\ \dot{I}(t) &= -\mu I(t) + \lambda \overline{k} I(t) S(t) \\ \dot{R}(t) &= \mu I(t) \end{aligned} \tag{7.32}$$

where S(t), I(t), and R(t) are respectively the fraction of susceptible, infected and recovered individuals at time t, and $\overline{k}$ is the number of contacts per unit time in the population.

In both models, the dynamics on complex networks of the infection mechanism depend on the network topology [Boc06]. For example, a reasonable assumption is that the infection rate λ depends on the degree of the node [Hav10]. Additionally, it can be found a certain threshold to the value of λ, below which the disease impact is null, and above which it reaches a certain finite value. A similar problem for the disease dynamics is rumour spreading [Boc06]. In this case the classes of individuals in the dynamics are ignorant (I) spreader (S) and stifler (R). Spreading dynamics are here again affected by equivalent transmission rates as for the disease models explained above.

7.7.5 Games on networks

Another case of dynamical processes undergoing over complex networks is that of games on networks [Jack14, Gal10, Grew10, Sli01]. A brief review

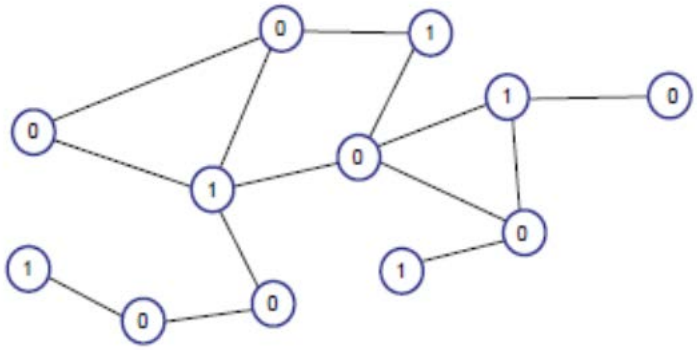

Figure 7.7: Equilibrium in the best-shot public game [Jack14]

of examples has been provided in chapter §1. The applications extend to a wide spectrum of topics such as transport phenomena, collaboration and market competition, imitation and altruism, social learning, strategic network formation, research collaboration among firms, etc [Goy07]. The classification on games on networks depends on whether they imply collaborative activities between nodes or not, if nodes have full or incomplete information (about other player's actions, payoff functions, network structure), whether the games are repeated or not, etc.

One of the most general approaches in the study of these processes is based on the analysis of the interaction among individuals who are connected via a network and whose behaviour is influenced by their neighbours. Other benchmarks include network formation [Sli01], agent-based models [Tesf06], etc. Here we will only review the games between nodes of the network, and in particular those related with the so called strategic complements and strategic substitutes, where the interaction in payoffs between players satisfies some natural and useful monotonicity properties [Jack14].

In the case of strategic complementarities, a player's incentives to take a certain action increase with the number of neighbours that take the same action, whilst strategic substitutes present the opposite incentives. A canonical example of the first case is the majority game, in which a player chooses a certain action (voting for a candidate, selecting a certain technology, etc) when the majority of its neighbours follows the same action. For the second case, a typical class include those described as "best-shot" public good games. For example, in this category we can consider the decision on buying a certain product or acquiring a piece of information that is easily shared or lent (strategy denoted as 1) or rather not do it (denoted as 0). Once a

neighbour has achieved the public good, it is not worth for the individual to expend the effort or the cost to procure it, and rather the logical strategy is to borrow it or have it directly from the other element. However, there is a penalty for each element if nobody takes the action, so that a player will rather follow this strategy if none of its neighbours has done it. It should be noted that in this type of games the strategies are always followed by selfish interests, regardless of the benefits or costs caused to other individuals in the network.

A Nash equilibrium is then achieved once the strategy of each element in the network is coherent with the overall game payoff rules and the selection of its neighbours. The case depicted in figure 7.7 shows an example of an equilibrium for a given network. It should be remarked that best-shot public goods games on a network always have pure strategy equilibria, which correspond to situations where the players who take action 1 form a maximal independent set. It can be shown that finding equilibria for the strategic complements type of game is relatively easy, while the same is not true for strategic substitutes, which in general is a computationally expensive task [Jack14].

Chapter 8

Game setup description

In this chapter we define a setup for games on networks where two teams compete over the state of a general population to which each of them has access. As explained in chapter §1, The layout of the problem under consideration is defined by a general population (GP) of elements which are connected between them by means of an arbitrary complex network whose adjacency matrix is denoted by $\overline{A}$. The state of each element in the GP depends on the consensus dynamics present between them, and some examples of these are given in section §8.1. The game also includes two teams whose connection to GP is given by the matrices S_P and S_M respectively, while their activity to impact the state of nodes in GP is denoted by the vectors $\mathbf{a_P}$ and $\mathbf{a_M}$, formed by the actuations of each of its agents. In order to ensure fairness in the game, the energy available to each team is fixed and equal, given by the square of the norm of the $\mathbf{a}$ vectors. Each team has to select the level of actuation of every agent so that the total payoff is maximized. The analysis considers that the topology of the GP corresponds to a connected graph. The GP is subject to consensus dynamics among its members (described by a matrix C) which ultimately lead to a steady state. Said C matrix depends on the influence mechanism between the GP members and on the GP network topology. A similar constraint on the norm of the $\mathbf{a_P}$ and $\mathbf{a_M}$ vectors is also applied to the S_P and S_M matrices, imposing that their Frobenius norms are equal.

As in the case described in chapter §5, in the framework described in this part of the thesis we also have a plant to be controlled, which here consists on the GP and the consensus dynamics ruling the state of its elements. Also, as commented in chapter §1 the strategies chosen by each of the two teams competing in the game correspond to one controller. In this case it is implicit that the teams have information of the state of the nodes in the GP

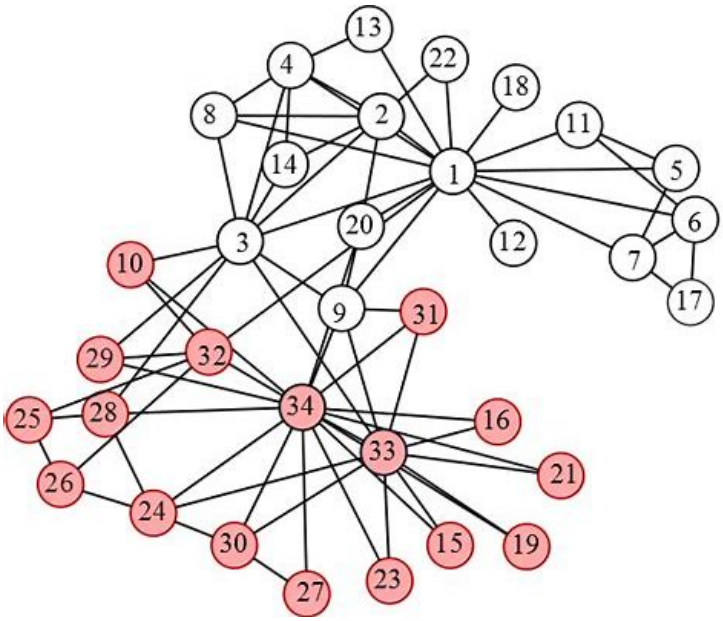

Figure 8.1: The social network of friendship within a 34-person karate club [Za77]

and thus a sensor is also present in the overall control layout. The members of each team are considered as the actuators in the system, which in this case corresponds to a closed loop architecture as defined in chapter §3. As it is always the case on any control problem, the actuators have a limited energy available, and this constraint is certainly considered, both teams having the same limitation as commented in the previous paragraph.

8.1 Consensus on Networks

This section describes three study cases of consensus dynamics, deriving their steady state and defining the concept of consensus function, which are analytically obtained for each of them.

8.1.1 Consensus based on damped influence

In reference [Zha14], a dynamical model for competitive dynamics on complex networks is presented. The competition between the two agents in the model is characterized by means of the relative impact of the competitors in the network. One of the competitors (x_{N-1}) consistently features a state value of $+1$, whilst the other competitor (x_N) holds a fixed -1 value, with N

being the number of nodes. The rest of the agents in the network start with a random value and each updates its state according to the equation:

$$x_k(n+1) = x_k(n) + \epsilon \sum_{l \subset N_k} A_{kl}(x_l(n) - x_k(n)) \tag{8.1}$$

with $x_k(n)$ being the state of agent k at time n while the parameter ϵ denotes the level of neighbors' influence, and N_k is the set of neighboring agents of agent k directly linked to this agent. Finally, A_{kl} denotes the elements of the adjacency matrix of the whole network. It is shown in [Zha14] that the state of each agent will reach a steady state value, provided that each normal agent has a path connecting to at least one competitor and that $0 < \epsilon < 1/D_{max}$, with D_{max} being the largest out-degree of agents in the network. The steady state value of the set of agents is given in matrix form as:

$$\mathbf{x}(\infty) = \left(\overline{D} - \overline{A}\right)^{-1} \left[\mathbf{c}_{i,N-1} - \mathbf{c}_{i,N}\right] \tag{8.2}$$

where $\overline{A}$ is a submatrix of the matrix A formed by the A_{kl} elements of equation 8.1, rearranged so that the two competitors correspond to the last two columns:

$$A = \begin{bmatrix} \overline{A} & \mathbf{c}_{i,N-1} & c_{i,N} \\ \mathbf{r}_{N-1,i} & 0 & a_{N-1,N} \\ \mathbf{r}_{N,i} & a_{N,N-1} & 0 \end{bmatrix} \tag{8.3}$$

Thus, column vectors $\mathbf{c}_{i,N-1}$ and $c_{i,N}$ contain the first N-2 elements of the last two columns of A, whilst row vectors $\mathbf{r}_{N-1,i}$ and $\mathbf{r}_{N,i}$ contain the first N-2 elements in the last two rows of the A matrix. Similarly, $\overline{D}$ is the diagonal matrix formed by the out-degrees of the non-competing agents. A study in competition between two nodes is then conduct with application to the classical karate club conflict problem ([Za77], see 8.1).

This thesis considers a different approach than the one considered in previous studies [Zha14], [Zha15] and [Far12]. As commented in the introduction, the problem under study has two teams P (Plus) and M (Minus), pulling for values $+1$ (-1) and with N_P (N_M) elements, respectively. Each team is connected to the same general population (GP) network by means of the adjacency matrix S_P and S_M, respectively. The elements of the general population (N in total) are linked to each other by a network with an adjacency matrix denoted by $\overline{A}$. Thus, we have that $\overline{A}$ is a $N \times N$ matrix, S_P is $N \times N_P$ and S_M is $N \times N_M$. Figure 8.2 depicts an example, with positive team represented by blue dots (left) and negative team by red dots (right), while the black nodes represent the general population. Their size has been

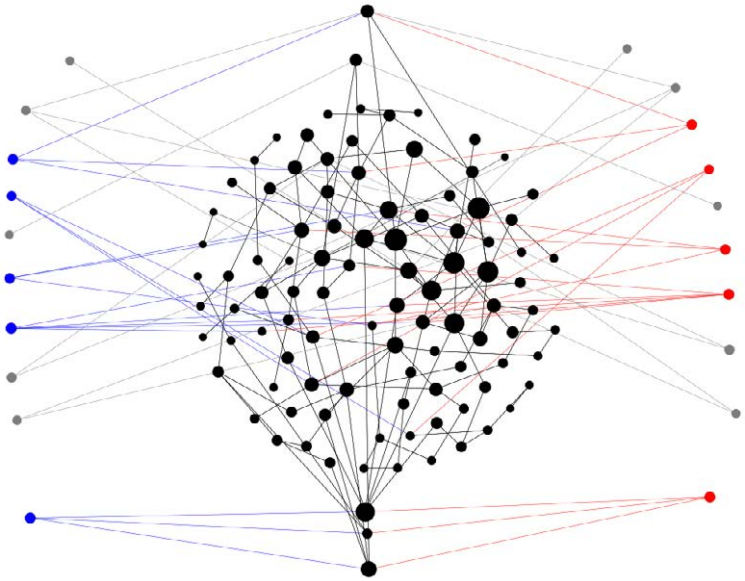

Figure 8.2: Competition diagram between two teams (blue and red) and connection to the general population (black).

set proportional to their eigencentrality. In this diagram, S_P and S_M are identical, associated with a configuration described in chapter §9.

The overall network is now given by this A matrix:

$$A = \begin{bmatrix} \overline{A} & S_P & S_M \\ S_P^T & 0 & 0 \\ S_M^T & 0 & 0 \end{bmatrix} \tag{8.4}$$

The goal of P team is to maximize the sum of states of the GP, whilst M team's objective is to minimize this value (maximize its negativity). Similarly to reference [Zha14], the stationary value for the GP state vector $\mathbf{x}$ is given by:

$$\mathbf{x}(\infty) = \left(\overline{D} - \overline{A}\right)^{-1} \left[S_P \mathbf{a_P} - S_M \mathbf{a_M}\right] \tag{8.5}$$

where vector $\mathbf{a_P}$ ($\mathbf{a_M}$) denotes the actions (values) taken by each of the elements of P (M) team, and $\mathbf{x}$ is the vector formed by all the states of the GP.

The justification of the existence of a steady state value of the state vector is equivalent to the demonstration shown in [Zha14], being the above equations a generalization of those presented in the mentioned reference.

In order to have a fair competition, the values of vectors $\mathbf{a}_P$ and $\mathbf{a_M}$ must be equally limited. This can be conceptually related to both teams having the same available energy E, according to the concept explained in chapter §1. This condition is given by the 2-norm of each vector being equal to $\beta = \sqrt{E}$. The limitation can be taken for integer values (as considered in chapter §9 in the case of genetic algorithms) or by means of continuous values, which is the case of the analysis from section 10.3 onwards.

It should be pointed out that in general, the particular function describing the specific dynamics of influence/consensus is not relevant for the analysis described in the following sections. Such consensus function will be noted as C, being for instance $C = \left(\overline{D} - \overline{A}\right)^{-1}$ in the present consensus case (eq. 8.5). This consensus function will also be derived for other cases in the following sections.

8.1.2 Consensus based on neighbours' average

Alternatively, the state of each element of the GP could be defined by means of a weighted average of its neighbours and the effect of the P and M teams, with ω_{kl} being weights for each link given by the A matrix:

$$\begin{aligned} x_k(n+1) = \; & \frac{1}{d_i} \sum_{l \subset N_k} w_{kl} A_{kl} x_l(n) \\ & + \sum_{l \subset N_k} S_{P,kl} a_{P,l} \\ & - \sum_{l \subset N_k} S_{M,kl} a_{M,l}. \end{aligned} \tag{8.6}$$

The equation 8.6 can be transformed in matrix terms as follows:

$$\mathbf{x}(n+1) = W \left(\overline{D}\right)^{-1} \overline{A} \mathbf{x}(n) + [S_P \mathbf{a_P} - S_M \mathbf{a_M}] \tag{8.7}$$

If the matrix $W \left(\overline{D}\right)^{-1} \overline{A}$ has all its eigenvalues within the unit disk, the above equation converges to the steady state vector:

$$\mathbf{x}(\infty) = \left(I - W\left(\overline{D}\right)^{-1}\overline{A}\right)^{-1}\left[S_P\mathbf{a_P} - S_M\mathbf{a_M}\right] \tag{8.8}$$

In this case, the consensus function is defined as:

$$C = \left(I - W\left(\overline{D}\right)^{-1}\overline{A}\right)^{-1} \tag{8.9}$$

8.1.3 Transport and trade consensus

Another case of consensus dynamics is presented herein. Let us consider a transport network in which a certain good (fruit, electricity, internet data, etc) is traded among the nodes within the network, whilst two teams compete as suppliers in the network, aiming to maximize their respective revenue. In particular, we can consider the following generic equation:

$$\begin{aligned} x_k(n+1) = & \left(1 - \sum_{l\subset N_k} A_{kl}\right) x_k(n) \\ & + \sum_{l\subset N_k} A_{lk}x_l(n) - F_{kk}x_k(n) \\ & + \sum_{l\subset N_k} S_{X,kl}a_k \end{aligned} \tag{8.10}$$

Thus, at each new step $n+1$ a fraction of the state x_k of previous step is transported to each neighbour node l according to A_{kl} (as given by the first term of eq. 8.10). The second term represents the transportation into node k brought from neighbour nodes, while the third term indicates the amount of the good that is consumed at node k itself at step n, with F_{kk} meaning the fraction of the good being consumed at that node. Finally, the last term denotes the sum of contributions of the considered good coming from supplier X through the matrix S_X. A similar equation is applicable for the second team with x_k being substituted by y_k, which corresponds to the amount of the traded good at each node k as introduced in the market by the second team. Note that in this case there are no Plus nor Minus teams, and they are named X and Y instead. The reason is that in this case the state variable corresponds to the amounts of the given good in the network (which must necessarily be positive), and the total amount is given by the sum of the vectors $X+Y$. The corresponding matrix equation for X is then given by:

$$\mathbf{x}(n+1) = \left(I - diag(\mathbf{1}\,\overline{A})\right)\mathbf{x}(n) + \overline{A}^T\mathbf{x}(n) - F\mathbf{x}(n) + S_X\mathbf{a_x} \tag{8.11}$$

where F is a diagonal matrix containing the F_{kk} elements on the k^{th} row and column. The described dynamics reach a steady state provided that the eigenvalues of the matrix $I - diag(\mathbf{1}\overline{A}) + \overline{A}^T - F$ have a magnitude smaller than 1. The resulting steady state is then given by:

$$\mathbf{x}(\infty) = \left(diag\left(\mathbf{1}\,\overline{A}\right) - \overline{A}^T + F\right)^{-1} S_X \mathbf{a_x} \tag{8.12}$$

Equivalent equations are applicable for Y (or any other additional competing team). In this case the consensus function is the following one:

$$C = \left(diag\left(\mathbf{1}\,\overline{A}\right) - \overline{A}^T + F\right)^{-1} \tag{8.13}$$

It is worth mentioning that the game corresponding to this consensus function is defined in a different way than the previous ones. Regarding the payoff, it could be given by the sum of the state of the targeted elements of the GP (as with the other cases). However, in this case the payoff could also be associated for example to the income obtained by each team depending on the price of the goods as purchased at each node. This price, on the other hand, depends on the supply available at the node as introduced by each team. The payoff can be computed as the product of the amount finally consumed at each node by the local price. Alternative payoffs could be considered too, but they are not further explored herein.

As a summary, table 8.1 presents the expression of the consensus function C for the three considered cases.

No.	Mechanism type	Consensus function
#1	Damped consensus	$C = \left(\overline{D} - \overline{A}\right)^{-1}$
#2	Average consensus	$C = \left(I - W\left(\overline{D}\right)^{-1}\overline{A}\right)^{-1}$
#3	Transport & Trade	$C = \left(diag(\mathbf{1}\,\overline{A}) - \overline{A}^T + F\right)^{-1}$

Table 8.1: Expressions of the considered consensus functions

Note that the reached steady state described above must be considered in the sense of thermodynamical reversible processes. As it will be seen in the following sections, such steady state can evolve in the long term based on variations of external conditions, affected by slower dynamics than those described in this section.

In summary, the game setup is defined by the adjacency matrices $\overline{A}$, S_P and S_M, actions $\mathbf{a_P}$ and $\mathbf{a_M}$ and the consensus function C. The following sections explore optimization of actions and adjacency matrices design.

Chapter 9

Numerical game optimization

In the previous section we have described a game between two teams acting on the general population GP, ultimately leading to a steady state of the elements of this network, which determines the payoff for each team. However, the first point to be noted is that in reality such game can be considered as a separate optimization problem for each of the two teams: team P has to choose $\mathbf{a_P}$ to maximize the value of the first term of eq. 8.5, regardless of the solution chosen by M team on the $\mathbf{a_M}$ vector. The reverse is valid for the M team. This is not the case on the last section of chapter §10, where the action of each team is to be selected as a function of the choice of the opponent, because the governing equations in that case are coupled, entailing dependency of the payoff for each team on both actions.

In the referred optimization process, several approaches can be taken. The most straightforward one is to evaluate the value of the sum resulting for the first term (for P team) for each of the combinations of $\mathbf{a_P}$ elements (similarly for M team) and select the option rendering maximum value. Assume that the number of elements in $\mathbf{a}_P$ to be set to 1 is given by $E \leq N_P$, the rest being left to zero. Thus, there are $N_c = \binom{N_P}{E}$ possible combinations. The associated payoff for each case can take quite a long time to be computed for a large network (depending also on E).

Besides this preliminary analysis, a more refined numerical approach can be followed based on Genetic Algorithms. The following sections provides the basics of the analysis and the obtained results, which are compared in chapter §10 with the analytical approach presented there.

9.1 Genetic Algorithms

A Genetic Algorithm (GA) is a numerical method for solving problems inspired by nature via natural selection through genes evolution, mutation mechanisms, and the survival of the fittest individuals. They are meant to look for the optimal solution and therefore are related with optimal search and control. This methodology can be applied to an extremely wide range of problems, and the fields of applications are numerous: VLSI chips layouts, image processing, robotics, water networks, spacecraft trajectories, etc.

Although there were some previous tries based on the same idea, the method was basically invented by John Holland in the 1960s and was subsequently developed by Holland and his students and colleagues at the University of Michigan. GAs are proven to be capable of solving many large complex problems where other methods experience difficulties. One of the keys of their popularity is the ability the prove to find global optimum within search spaces where many local optima are present. This feature establishes a relevant advantage with respect to gradient based methods (such as steepest descent, etc).

The typical procedure for a genetic algorithm that considers the following concepts:

Population definition. In order to properly look for the solution of the problem, the population of potential solutions has to be adequately defined so that optimal search is correctly conducted and the obtained solution has a proper correspondence with the nature of the problem.

Chromosome. This is a string of genes that fully describes a particular solution. Each gene in the chromosome controls a particular feature of the individual. An encoding method is used for this purpose, which typical follow a binary code.

Fitness function. Each solution consists of an individual with a number of genes that determines its fitness function, this being a function that quantifies the optimality of an individual in the population. Each solution has to be ranked against the rest of individuals. The fitness function must be defined according to the performance variable that is the subject of optimization in the problem.

Selection. This is the process that determines which solutions are to be preserved and allowed to reproduce and which ones deserve to die out.

On each iteration the worse solutions are eliminated while the overall population of solutions is kept constant. Several mechanisms can be considered for this purpose (e.g. [Mitc96]). In this thesis the procedure is based on a roulette wheel approach, in which parents whose chromosomes have a better fitness have higher chances to be selected for producing offspring.

Crossover. This is a mechanism by which the genes of the parents are crossed to obtain the chromosomes of the children individuals. There are many available methods for this purpose. One of the most popular ones (also used in this work) divides the two parent chromosome strings at some random point, and swaps each of the two resultant strings among the two parents.

Mutation. This mechanism occurs randomly and introduces new features in the chromosome of some individuals in the population by changing the value of one gene. This introduces an additional way to proceed towards the optimal solution of the problem (even if worse solutions can also be result from mutation), in order to further enhance the best solution search. It also allows to escape from local optimal points towards the global optimum.

Some of the advantages of GAs are: they do not require information on the derivative of the function being optimized, they are faster and more efficient than some traditional methods, have good parallel capabilities, and they are very useful when the search space is large involving many parameters.

The following figure depicts the typical process for a GA, which is also used in the next section.

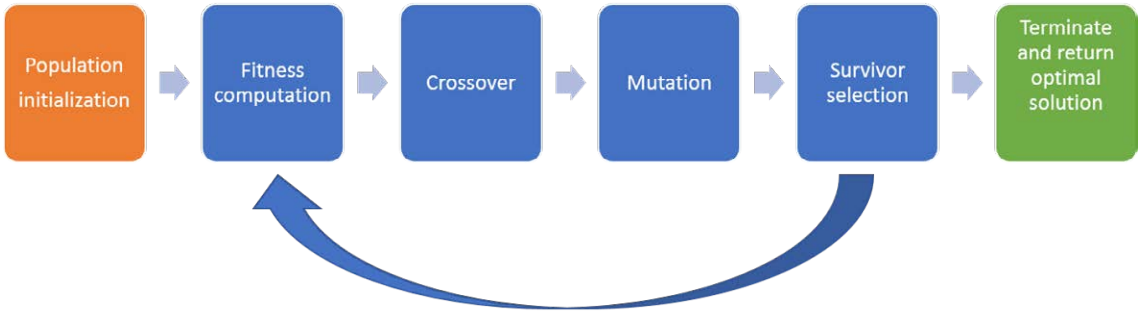

Figure 9.1: Genetic Algorithm general process

9.2 Optimal action based on GA

A numerical search scheme can be followed by means of genetic algorithms (GA), being the implemented procedure described herein. Each chromosome is defined as a vector of N_P elements, and the GA searches the best chromosome with optimal fitness against the opponent team action.

1. A population of N_{Chr} chromosomes is generated, of length N_P and number of 1's equal to E. Then a search cycle of N_{Gener} generations is repeated, with the following steps.

2. An array including the N_{Chr} chromosomes is stored, and the fitness of each chromosome a_P is computed as the sum of the state vector resulting from eq. 8.5.

3. At each new generation, two parents from the previous generation are chosen out of the chromosome pool, with a probability proportional to their fitness. In case all of them have the same fitness, any two of them are chosen and have two genes swapped. Then a point for dissection in the parent chromosomes is randomly chosen and the children of the new generation are obtained by joining the pieces of the two parents. The difference in 1's of the child with respect to E is randomly compensated among its genes. This is repeated to obtain $3 \times N_{Chr}$ chromosomes.

4. Out of the newly obtained chromosomes, the N_{Chr} with best fitness are selected for the next generation, and the rest are discarded. The best one of each generation is used for the computation of the state vector used in the following plots.

Figure 9.2 depicts an example of the GA result for the network shown in Figure 8.2 with $N = 200$, $N_P = N_M = 20$, $E = 5$, and $S_P = S_M$. The matrix A defines a random network with a 2 % probability of nodes being connected. The number of actions combinations is $N_c = 15504$, and the optimum resulting from an exhaustive search is depicted by the black horizontal line. Additionally, we proceed to search the optimum by means of GA starting with an initial random vector $\mathbf{a_P}$. The GA finds the same value as obtained before via an exhaustive search, but the efficiency of this method is proven because of the much shorter time used to obtain the optimal action (the computation time ratio between both methods is approximately 76).

The best value is obtained within a few generations, as represented by the blue line (first run). In the subsequent run of the GA search exercise, the same process is followed again, with $\mathbf{a_M}$ being set equal to the $\mathbf{a_P}$ vector

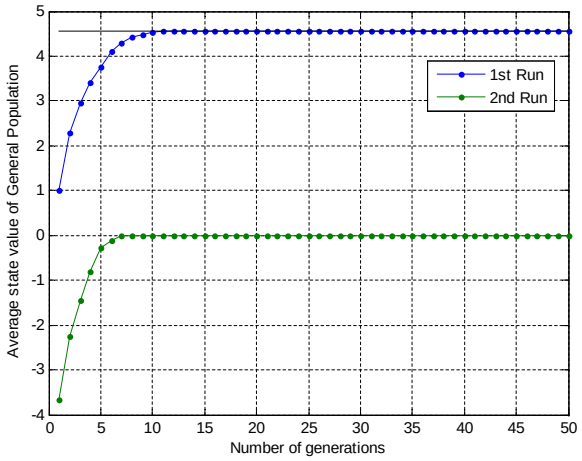

Figure 9.2: Search evolution by means of GA of optimal actuation solution.

obtained in the first run. This way we can establish an iterative process looking for the best response to the solution of the previous run, equivalent to a Nash equilibrium search. Since $S_P = S_M$, the solution results in a tie because the best response to $\mathbf{a_P}$ is an $\mathbf{a_M}$ vector with the same values on its elements, rendering a zero overall value (zero sum game).

Chapter 10

Algebraic game optimization

10.1 Singular Value Decomposition

In this chapter we address again the problem of optimal action on the consensus dynamics of the General Population described in chapter §8. However, as opposed to the approached followed in §9, in this chapter we tackle this issue by means of an algebraic approach based on Singular Value Decomposition.

Singular Value Decomposition (SVD) is one of the most widely and useful techniques to reach relevant information from matrices. It allows to understand many fundamental results in matrix theory.

In order to properly introduce the SVD concept, it is convenient to recall herein some important facts about symmetric matrices. Let us consider a square matrix S. We refer to this matrix as *Hermitian* or *self-adjoint* if $S^* = S$ holds, where the * symbol denotes conjugate transpose. On the other hand matrix S is said to be *symmetric* if $S^T = S$, with T referring to the matrix transposition operation. For real matrices, both concepts are equivalent.

Spectral Theorem: Let us assume that $S \in \mathbb{C}^{n\times n}$ is Hermitian. Then there exist n (not necessarily distinct) eigenvalues $\lambda_1, \ldots, \lambda_n$ and corresponding unitary eigenvectors $\mathbf{v_1}, \ldots, \mathbf{v_n}$ such that

$$S\mathbf{v_j} = \lambda_j \mathbf{v_j} \qquad \forall j = 1, \ldots, n \tag{10.1}$$

The eigenvectors form an orthonormal basis for $\in \mathbb{C}^n$ and because S is Hermitian, they can be proven to be real. As a consequence of the spectral theorem, the matrix S can be expressed as follows:

$$S = \sum_{j=1}^{n} \lambda_j \mathbf{v_j} \mathbf{v_j}^* \tag{10.2}$$

It can be seen that this equation expresses S as the sum of the special rank-1 matrices. The singular value decomposition provides a similar way to express a rectangular matrix.

In contrast to the eigenvalue decomposition that is always applied to square matrices, the Singular Value Decomposition can be applied to a general rectangular matrix M $\in \mathbb{C}^{m \times n}$ with $m \geq n$ and rank(M) = n. We then consider the $n \times n$ matrix M^*M (which is symmetric and positive) and compute its eigenvalues λ_j and eigenvectors $\mathbf{v_j} \in \mathbb{C}^n$, $\forall j = 1, \ldots, n$ these being orthogonal to one another and with norm = 1. The eigenvalues are named so that they are decreasing in size: $\lambda_1 \geq \lambda_2 \geq \cdots \geq \lambda_n > 0$.

We can then define the *singular value*s of M as $\sigma_j = \sqrt{\lambda_j} \geq 0$. Because of the ordering of λ_j we can also state that $\sigma_1 \geq \sigma_2 \geq \cdots \geq \sigma_n > 0$

We also define $\mathbf{u_j} = M\mathbf{v_j}/\sigma_j$, $\forall j = 1, \ldots, n$. Notice that $\mathbf{u_1}, \ldots \mathbf{u_n} \in \mathbb{C}^n$, have norm equal to 1 and are orthogonal to each other.

Since we have $M\mathbf{v_j} = \sigma_j \mathbf{u_j}$, we can arrange these into a matrix form as:

$$MV = \hat{U}\hat{\Sigma} \tag{10.3}$$

where $M \in \mathbb{C}^{m \times n}$, $V \in \mathbb{C}^{n \times n}$, $\hat{U} \in \mathbb{C}^{m \times n}$ and $\hat{\Sigma} \in \mathbb{C}^{n \times n}$ and the columns of the U and V matrices are formed by the $\mathbf{u_j}$ and $\mathbf{v_j}$ vectors respectively. Furthermore, $\hat{\Sigma}$ is a diagonal matrix with its entries formed by the singular values σ_j in decreasing order.

Since the $\mathbf{v_j}$ vectors are orthonormal and V is square, V is a unitary matrix and equation 10.3 results in:

$$M = \hat{U}\hat{\Sigma}V^* \tag{10.4}$$

This expression is known as the *reduced singular value decomposition of M*.

On the other hand, since $\hat{U}$ is a $m \times n$ matrix, even if its column vectors are orthogonal, there is a non-trivial null space and the matrix is not invertible. However, this matrix can be expanded with m-n additional column vectors so that they form an orthonormal basis for $\mathbb{C}^n$. The new matrix is denoted

by U which is then unitary. Furthermore, we define the matrix $\Sigma \in \mathbb{C}^{m\times n}$ as follows:

$$\Sigma = \begin{bmatrix} \hat{\Sigma} \\ 0 \end{bmatrix}$$

The singular value decomposition (SVD) is then stated as follows: for any given $m \times n$ matrix M, it is well known (see [Horn12]) that this matrix can be expressed as:

$$M = U\Sigma V^* \tag{10.5}$$

with U being a $m \times m$ unitary matrix, Σ a $m \times n$ matrix with non-negative real values on the upper main diagonal, and V a $n\times n$ unitary matrix, and the singular values of M are defined as the elements of the upper diagonal of Σ, denoted by σ_i. The columns of U (respectively V) are the left (respectively right) singular vectors of M.

Other important properties for singular values and singular vectors are:

- The left singular vectors of M are a set of orthonormal eigenvectors of MM^*.
- The right singular vectors of M are a set of orthonormal eigenvectors of M^*M.
- The non-zero singular values of M are the square roots of the non-zero eigenvalues of both M^*M and MM^*.

The SVD can also be expressed in dyadic form as follows:

$$M = \sum_{j=1}^{n} \sigma_j \mathbf{u_j} \mathbf{v_j}^* \tag{10.6}$$

In this ordered sum, the leading terms dominate the rest of them. It can be seen the similarity with equation 10.2 which is equivalent for eigenvalues and eigenvectors.

An important concept in matrix theory is the question of how to measure the size of a matrix in terms of its entries. For this purpose, the norm of a matrix is used. One type of matrix norms are those induced by vector norms. For a p-norm of a vector (with $1 \leq\ p \leq \infty$) we define accordingly the induced p-norm of a matrix M as:

$$\|M\|_p = \sup_{\mathbf{x}\neq 0} \frac{\|M\mathbf{x}\|_p}{\|\mathbf{x}\|_p} \tag{10.7}$$

Alternatively, the norm of a matrix can be defined in terms of its entries. The most relevant one is called Frobenius norm, which is defined as follows:

$$\|M\|_F = \sqrt{\sum_{i=1}^{n}\sum_{j=1}^{n} |a_{ij}|^2} = \sqrt{tr(M^*M)} = \sqrt{\sum_{j=1}^{min(m,n)} \sigma_j^2} \tag{10.8}$$

where the trace function provides the sum of the elements of the diagonal. The last equation expresses the *Frobenius norm* in terms of the singular values of the matrix M.

A geometric interpretation of this decomposition is that the M matrix corresponds to a linear map from the unit sphere in R^n onto an ellipsoid in R^m. The axes in the canonical reference frame in R^n are rotated according to V^*, followed by a scaling of the resulting axes by means of Σ and finally with a rotation given by the matrix U. Thus, each left singular vector is rotated and scaled, with its new length given by its associated singular value. Hence, the larger the singular value, the higher the amplification in the length of the original axis in R^n by its projection onto R^m.

10.2 Optimal action based on SVD

The numerical optimization search of the action of P team (search of optimal $\mathbf{a_P}$ vector) commented in section 9.2 can also be conducted in an analytical manner by means of the SVD decomposition. The idea is that if we consider the $N \times N_P$ matrix given by:

$$M = CS_P \tag{10.9}$$

The action $\mathbf{a_P}$ multiplying this matrix (which leads to the steady state vector given by eq. 8.4) can be chosen to be the one corresponding to a right singular vector of M (in particular to V_m, associated with the highest singular vector σ_m).

As previously discussed, the norm of this vector (and that of $\mathbf{a_M}$) has to be equal to β, in order to ensure equal conditions in the competition game between both teams:

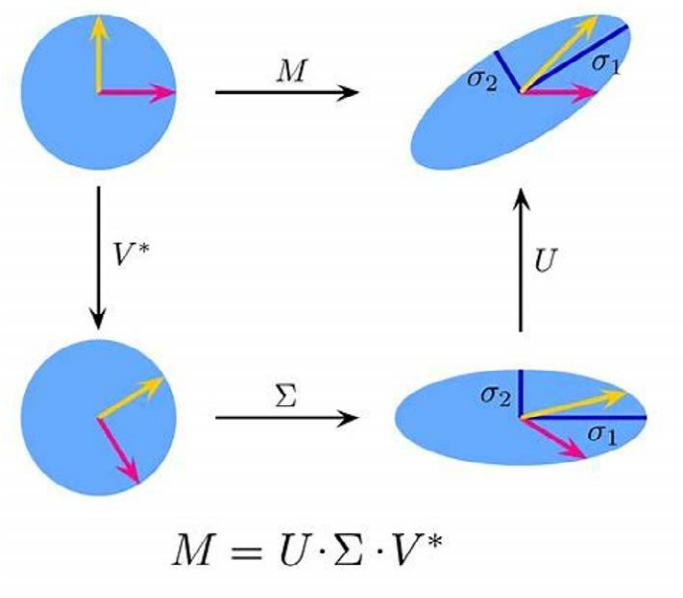

Figure 10.1: Singular Value Decomposition. Graphical interpretation (source: https://en.wikipedia.org/wiki/Singular_value_decomposition)

$$\begin{aligned} \mathbf{a_P}^{(op)} = & \quad \frac{V_m}{\|V_m\|_2}\beta \\ \sigma_m = & \quad \max \sigma_i \quad i = 1, \ldots, N \end{aligned} \tag{10.10}$$

Thus, the optimization process implies the product:

$$M\mathbf{a_P}^{(op)} = U\Sigma V^T \mathbf{a_P}^{(op)} = U_m \sigma_m \beta \tag{10.11}$$

Note that the solution obtained by this procedure entails a non-integer solution of the values selected for each agent in $\mathbf{a_P}$, as opposed to the GA search which considered only 0 or 1 as possible values. In order to properly compare both methods' payoffs, the solution obtained by SVD is rounded setting the E elements of $\mathbf{a_P}$ with higher values to 1, and the rest to zero. Figure 10.2 presents the difference between the retrieved payoff using SVD and GA. It is shown that the solution obtained by the SVD has the same or better payoff in the optimal solution search as the GA algorithm. One hundred simulations have been run for both $\mathbf{a_P}$ and $\mathbf{a_M}$ search, for random networks with parameters as in section § 9.2. It is seen that the resulting stationary value of the state vector is equal or more positive (respectively negative) for SVD than for the GA when the search for the P team (respectively M team) is conducted. Sometimes the payoff is practically the same

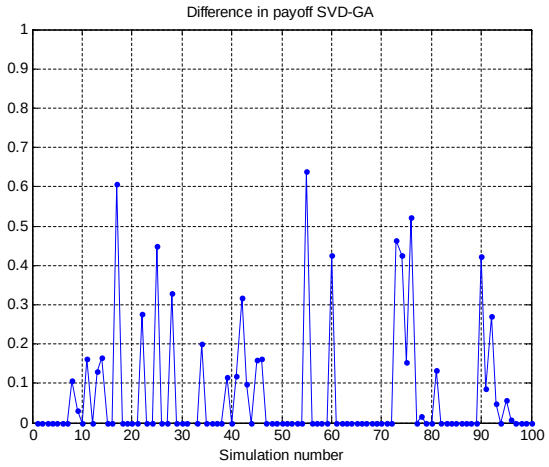

Figure 10.2: Difference between the payoffs obtained using GA and SVD in the search of optimal $\mathbf{a_P}$ and $\mathbf{a_M}$.

despite some percentage differences in the chosen agents in the action vector selected to be 1, indicating that there are agents with almost the same impact on the overall result.

Obviously, the selection of the individual actions of agents in $\mathbf{a_P}$ ($\mathbf{a_M}$) must be related to adjacency matrices S_P (S_M) and $\overline{A}$. In fact, here it is checked the relationship between the actions $\mathbf{a_P}$ ($\mathbf{a_M}$) of each element in P and M teams and their eigencentrality. For example, Figure 10.3 depicts (for one of the run cases) the vectors of actions and of eigencentralities with respect to the matrix defined in eq. 8.4.

The second vector has been rescaled to the norm of the first one. It can be observed the similarity (although not equivalence) of both values after renormalization. This fact indicates that indeed the optimal action is very close to the eigencentrality of the elements of P (or M) team in the overall network, and hence actuation proportional to this measure would lead to a nearly optimal solution.

10.3 Optimal design of team connections for the whole network

This section goes one step beyond the previous finding and look for the design of an optimal S_P (S_M) network, in order to maximize the achievable

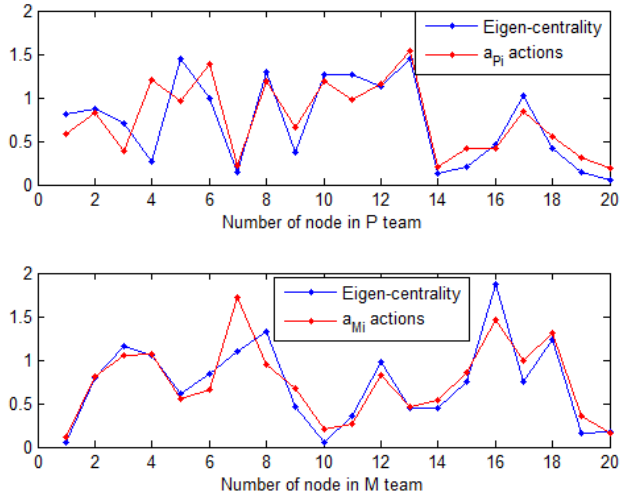

Figure 10.3: Elements of optimal action vectors $\mathbf{a_P}$ (top) and $\mathbf{a_M}$ (bottom) based on SVD, and comparison with rescaled eigencentrality of each node

payoff. The situation described in previous sections implies that the S_P and S_M adjacency matrices are given a priori and each team has to look for the optimal $\mathbf{a_P}$ and $\mathbf{a_M}$ respectively. However, we can foresee a more advanced scenario in which at least one of the teams could design the connections of each of its agents with the GP group. Such design should again follow some fairness rules related to the magnitudes of the links between agents and GP. In that sense, it is conceivable to impose that the Frobenius norm of the S_P and S_M matrix have the same value.

The network optimization process will be defined in the following for S_P, being equivalently applicable to S_M. It should be noted that the payoff of the utility function of the P team to be optimized is given by the following expression:

$$\Phi^P = \sum_{i=1}^{N} x_i(\infty) = \mathbf{u_T} C \cdot S_P \mathbf{a_P} + f(S_M, \mathbf{a_M}) \tag{10.12}$$

Here $\mathbf{u_T}$ (Target $\mathbf{u}$) is a column vector formed by N elements all equal to 1. It is worth mentioning that the second term $f(S_M, \mathbf{a_M})$ (action of M team) can be considered as a constant in the optimization process. Since this is a term with opposite sign to the first one and it is out of the control of the P team, it is taken equal to zero in the following sections without loss of generality, and it is recovered in the last section of this chapter.

Considering the SVD decomposition, it is known that the Frobenius norm

of S_P is given by the square root of the quadratic sum of its singular values [Horn12]. Hence, one could design an S_P matrix with only one nonzero singular value equal to the norm of S_M. In that case, we will have S_P as a function of its first left and right singular vectors (column vectors $\mathbf{u_1}$ and $\mathbf{v_1}$, respectively), along with σ_1:

$$S_P = \mathbf{u_1}\sigma_1{\mathbf{v_1}}^T \tag{10.13}$$

It is also observed that the first term in eq. 10.12 is given by a scalar or dot product between two vectors, $\mathbf{u_T}C$ and $S_P\mathbf{a_P}$. Such dot product is maximum if both vectors are parallel. This can be imposed by setting $\mathbf{u_1}$ as follows:

$$\mathbf{u_1} = \frac{C^T{\mathbf{u_T}}^T}{\|C^T{\mathbf{u_T}}^T\|_2} \tag{10.14}$$

and also by ensuring that $\mathbf{a_P}$ is parallel to $\mathbf{v_1}$. It should be noted that $\mathbf{v_1}$ could be chosen to be any vector, as will be discussed in the following section, allowing the most appropriate part of the P team to target $\mathbf{u_T}$. In this section, however, the whole P team is used for this goal, and thus for $\mathbf{v_1}$ we define an $N_P \times 1$ vector whose elements are all equal to 1. On the other hand, $\mathbf{a_P}$ is set parallel to this vector, imposing that its norm is equal to β (as that of $\mathbf{a_M}$) again for fairness purposes:

$$\begin{aligned} \mathbf{v_1} &= \frac{1}{\sqrt{N}}[1\ 1\ \ldots\ 1]^T \\ \mathbf{a_P} &= \frac{\beta}{\sqrt{N_P}}[1\ 1\ \ldots\ 1]^T \end{aligned} \tag{10.15}$$

Certainly, the same optimal design of S_P can equally be addressed by the M team to obtain optimal S_M.

As an example of the efficiency of optimal design of network connections, we can consider the payoff obtained by an optimal S_P designed with respect to a random general population network using the same parameters as previous sections and consensus function #1 (see table 8.1). The M team competes using a random network with S_M matrix, and it selects the optimal action $\mathbf{a_M}$ accordingly. The process is repeated for 100 cases and the average values are presented herein. It is observed that the P team significantly outperforms the M team with a sum of the state vector of 469.6. For information, we have checked the result with a random S_P competing against the same network S_M for each iteration, and the average result has been of -1.69 (close to zero as expected) when $\mathbf{a_P}$ is optimally chosen.

It should be noted that by adapting S_P and S_M, the degree matrix D affecting consensus functions #1 and #2 would be altered. Since the exercise described here results in a full S_P and S_M, in the following the equation for C in those two cases is slightly adapted, using D_m instead, which is given by:

$$D_m = D_{\overline{A}} + I \cdot (N_P + N_M) \tag{10.16}$$

with $D_{\overline{A}}$ being the degree matrix of the elements of $\overline{A}$ with the rest of this matrix (not with A in total).

10.4 Different targeted subsets

10.4.1 Single target subsets per team

The analysis considered in the previous sections assumes that the goal of both teams should be to maximize their respective influence over the whole general population GP. We can envisage, however, a different scenario in which each team is interested in the state of only a certain set or group within the GP. There are many reasons for such approach: each team might have an easier implementation on a certain part because of geographical / social constraints (e.g. a company can better influence a certain region due to the nature of its products), historical reasons (it has a more extended network within that subset of the GP), etc. This specialization is applicable to different domains such as competitions between species, electoral influence, or competition about the market share.

This new landscape can be easily adapted to the approach described in previous sections by considering that each team has a different target vector $\mathbf{u_{TP}}$ and $\mathbf{u_{TM}}$ which respectively form the basis of an associated target subspace. It is worth mentioning that the only constraint on these target vectors is that their elements are positive (leading to the addition with the desired sign for each member of the GP to be influenced) and that the overall evaluation of the team payoff is measured in unitary terms (if the sum of the elements of one target vector is higher than the other, they should be normalized to consider the level of influence per target GP member, and not over the whole targeted group).

Thus, the procedure for the computation of S_P and S_M is the one described in section 10.3, where the appropriate $\mathbf{u_T}$ is used in the computation of the associated network. The unitary payoff for P team is obtained by:

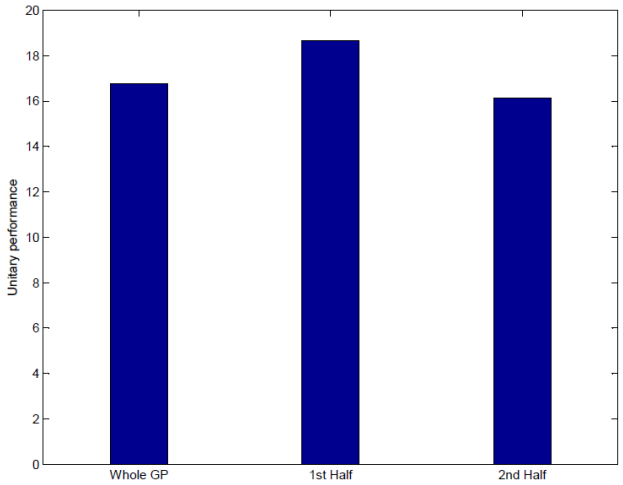

Figure 10.4: Unitary payoffs of P for different target subspaces used on the design of S_P: target subspace is either the whole GP (left bar), first half (middle bar) or second half (right bar)

$$\widetilde{\Phi} = \frac{\mathbf{u_{TP}}}{\sum_{i=1}^{N} |\mathbf{u_{TP_i}}|} C S_P \mathbf{a_P} \tag{10.17}$$

In the $\mathbf{u_{TP}}$ vector, some elements could be set to zero when not targeted by the P team. An equivalent expression is used for the M team. Figure 10.4 presents the unitary payoff for a network with the same parameters as in the previous section and with consensus function #2. A comparison is shown between the unitary payoffs of S_P for three different options: when it targets either the whole GP, the first half or the second half of GP, respectively.

It is observed that the unitary payoff for P is different even when the sum of the target vector elements is the same (as the last two cases). Certainly, the analysis shown in Figure 10.4 could have resulted in the second half of the population retrieving a higher unitary payoff than in the first half, depending on the particular GP and P team networks.

The reason for the observed difference among subspaces is related to the fact that the payoff depends on the amplitude of the $\mathbf{r_P}$ vector defined as:

$$\mathbf{r_P} = \|\mathbf{u_{TP}} C\|_2 \tag{10.18}$$

Thus, it is advisable in the selection of $\mathbf{u_{TP}}$ to take this fact into account. It can be observed that in order to maximize the associated benefit, ideally a

right singular vector of C^T (associated to a maximum singular value of this matrix) should be chosen. Nevertheless, this would most probably imply a vector with negative elements, which as previously explained would entail an addition with different signs in the influenced elements of GP, which is contrary to the definition of the problem. Hence, such optimization should be constrained to the positive orthant in the R^N space. This analysis of the best single target subspace is left as a future line of investigation.

10.4.2 Multiple target subsets per team

In order to allow for further strategy capability of each team, we can consider that they design their respective influence networks S_P and S_M by targeting at least two subspaces instead of only one (the extension to more dimensions is straightforward). For example, let us take the P team (the analysis is applicable for both teams) and consider that it targets $\mathbf{u_{TP_1}}$ ($\mathbf{u_{TP_2}}$) by means of its first (last) $N_P/2$ elements, respectively. Note that these two vectors could be set based on the needs defined by the P team as previously explained. The design of the S_P matrix can be obtained by letting:

$$S_P = \mathbf{u_1}\sigma_1{\mathbf{v_1}}^T + \mathbf{u_2}\sigma_2{\mathbf{v_2}}^T, \tag{10.19}$$

where $\mathbf{v_1}$ ($\mathbf{v_2}$) is a $N_P \times 1$ column vector with its first (second) half set to $\sqrt{2/N_P}$ and its second (first) half to zero, respectively. Obviously, $\mathbf{v_1}$ and $\mathbf{v_2}$ are orthonormal vectors as necessary for a singular value decomposition sum as in the previous equation. Regarding $\mathbf{u_1}$ and $\mathbf{u_2}$, they also have to be orthonormal. Now, for P team to target $\mathbf{u_{TP_1}}$ and $\mathbf{u_{TP_2}}$ subspaces we need to set:

$$\begin{aligned} \mathbf{u_1} &= \frac{C^T{\mathbf{u_{TP_1}}}^T}{\|C^T{\mathbf{u_{TP_1}}}^T\|_2} \\ \mathbf{u_2} &= \frac{C^T{\mathbf{u_{TP_2}}}^T}{\|C^T{\mathbf{u_{TP_2}}}^T\|_2} \end{aligned} \tag{10.20}$$

We could select $\mathbf{u_{TP_1}}$ based on the main goal of P team and look for $\mathbf{u_{TP_2}}$ so that the resulting $\mathbf{u_1}$ and $\mathbf{u_2}$ are orthonormal. Nevertheless, it should be noted that by imposing such condition, the subspace actually reached by $\mathbf{u_2}$ will have a reduced efficiency in the $\mathbf{u_{TP_2}}$ direction. The selection of $\mathbf{u_1}$ and $\mathbf{u_2}$ must therefore consider these issues.

Furthermore, it is observed in the simulations that if the first singular value has a ratio with respect to the next one significantly high (e.g. three

times higher or more) then its associated singular vector renders the best choice for $\mathbf{u_{TP_1}}$, even if the desired eigenspace is somehow different from this vector, as long as it shares part of the target elements of the GP. In such cases, the selection of $\mathbf{u_{TP_2}}$ is complementary to that of $\mathbf{u_{TP_1}}$, in order to target another subspace which is also of interest for the team's overall payoff.

Figure 10.5 presents a comparison of the ratio between the first and second singular values (SV_1/SV_2) of the consensus function C as a function of the average degree $\langle k \rangle$ and for two types of networks (random and scale-free). For each type of consensus function, 50 simulations have been run to generate on each case a random network and a free-scale network, each of them with parameters $N = 200$, $N_P = 20$ and such that the average degree $\langle k \rangle$ is either 10, 20 or 30 as shown in figure 10.5. The average value of the mentioned ratio is presented for the three consensus functions. It can be observed that the ratio is around 1 for consensus functions *Average* (#2) and $Transportandtrade$(#3), independently of $\langle k \rangle$. On the other hand, for consensus function *Damped* (#1), the singular value ratio grows with the average degree. The same effect is observed independently of the type of network that is considered (random or scale-free).

The reported results can be justified as follows. It is known [Fied75] that the first non-null eigenvalue of the Laplacian matrix of a graph (called the Fiedler value), corresponds to its algebraic connectivity, and that it is an important concept to understand the graph dynamics. The more connected a network is, the further this value is from zero. On the other hand, the consensus function C for case #1 is close to the inverse of the Laplacian associated to matrix $\overline{A}$ (being the $\overline{D}$ matrix in C the degree matrix of the whole network including the P and M team connections, and not only associated to the general population as it is $\overline{A}$). Hence, by continuity of eigenvalues, those of C should be close to the eigenvalues of the inverse of the Laplacian associated to $\overline{A}$. Thus, the second highest eigenvalue of C can be approximated to the inverse of the Fiedler value. Given the relationship between singular values and eigenvalues of a matrix, one concludes that the ratio between the first two singular values of the matrix C will be higher the more connected the network is, as it is observed in Figure 10.5.

The conclusion is that regarding case #1, for low connectivity the selection of $\mathbf{u_{TP_1}}$ can be directly based on the main desired target subspace of the team, while for higher connectivity it is rather preferable to set $\mathbf{u_{TP_1}}$ based on the singular vector associated to the first singular value, and then $\mathbf{u_{TP_2}}$ is accordingly taken for the team payoff interests. This consideration is not applicable to consensus functions #2 and #3, for which the ratio of the first

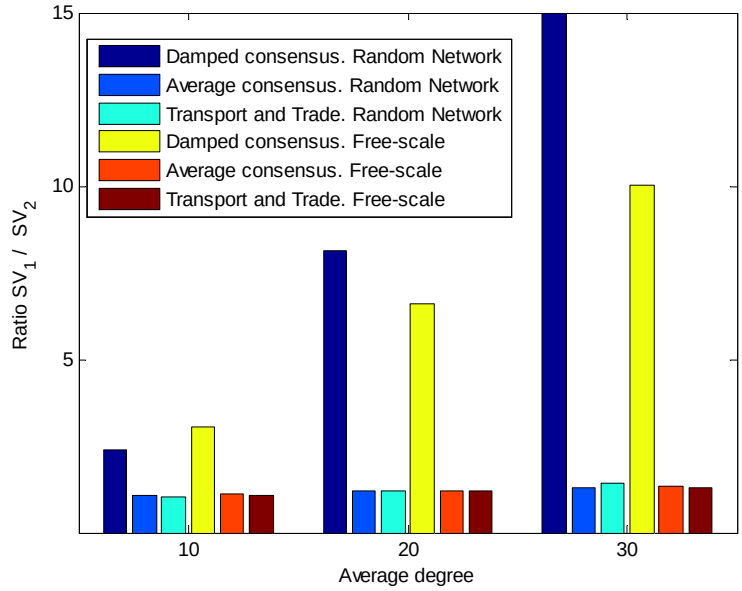

Figure 10.5: Average SV_1/SV_2 ratio between the two first singular values of the consensus function C, versus average degree for the three described consensus functions and for different GP networks topologies.

two singular values is not directly linked to the connectivity of the general population network.

10.5 Competition games on target subsets

As previously explained, the competition between P and M teams exposed in previous sections can be described in terms of two parallel optimization processes by each team, which can only select their strategy in maximizing their respective benefits regardless of the actuation of the other part of the game. This section considers the competition games in which the payoff for each team depends on the actions of both teams (in terms of designing their networks and further selection of the action vectors $\mathbf{a_P}$ and $\mathbf{a_M}$ respectively).

As an example, it is considered a game in which P and M both target the first half of GP by means of the first half of their agents, whilst they use

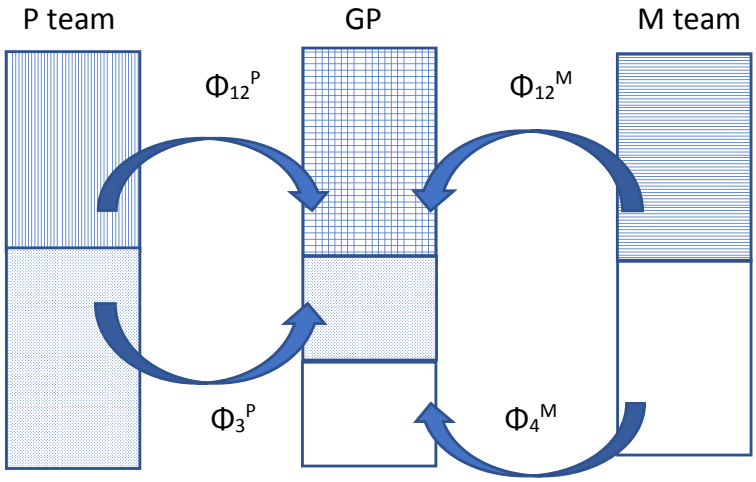

Figure 10.6: Target subspaces on GP for P and M teams.

the second half of their agents to target the third and fourth quarter of GP, respectively. The situation is depicted in Figure 10.6.

Let us denote by $\widetilde{\Phi}_{12}^{P}$ (and $\widetilde{\Phi}_{12}^{M}$) the unitary payoff function obtained by P (M) for its actuation on the first and second quarters of GP, by $\widetilde{\Phi}_{3}^{P}$ the payoff for P for its actuation on the third quarter and by $\widetilde{\Phi}_{4}^{M}$ the payoff for M for acting on the fourth quarter. Note that if both teams selected the S_P and S_M networks so that $S_P = S_M$ (by means of the optimum solution described above) then $\widetilde{\Phi}_{12}^{P} = -\widetilde{\Phi}_{12}^{M}$. The total payoff function for each team is given by:

$$\begin{array}{rcl} \widetilde{\Phi}^{P} = & \lambda_P \widetilde{\Phi}_{12}^{P} + (1-\lambda_P)\widetilde{\Phi}_{3}^{P} \\ \widetilde{\Phi}^{M} = & \lambda_M \widetilde{\Phi}_{12}^{M} + (1-\lambda_M)\widetilde{\Phi}_{4}^{M} \end{array} \tag{10.21}$$

where λ_P and λ_M represent the relative importance of the first target subspace with respect to the second one for P and M teams, respectively. These parameters can depend on the particular features of the competition (for example P team could be more interested in elements of the 1st and 2nd quarter of GP than M, and then $\lambda_P > \lambda_M$). Note that if $\lambda_P = \lambda_M = 1$ there is a zero-sum game over the first half of GP, while for $\lambda_P = \lambda_M = 0$ each

team competes for different subspaces. A similar situation occurs also for a) $\lambda_P = 1$, $\lambda_M = 0$, and b) $\lambda_P = 0$, $\lambda_M = 1$. Other scenarios consist of mixed situations between these extreme cases.

It is worth mentioning that in this case, each team targets two subspaces, the first of which is the first and second quarters of GP in both cases (with basis vector denoted as $\mathbf{u_{T_{12}}}$). The definition of the $\mathbf{u_1}$ and $\mathbf{u_2}$ vectors to obtain the S_P matrix must ensure that they are orthogonal to each other and also that each of them is computed according to eq. 10.20, with target subspaces $\mathbf{u_{T_{12}}}$ and $\mathbf{u_{T_3}}$ (for P, third quarter) or $\mathbf{u_{T_4}}$ (for M, fourth quarter). For an arbitrary C, the resulting vectors would not comply with this condition in general. Hence, $\mathbf{u_1}$ is computed based on the first subspace, while the $\mathbf{u_2}$ is computed so that it does not influence in the first one (because it could have negative elements) but rather in the second one and in the remaining quarter. Thus, for the P team we have:

$$\mathbf{u_2}^T = (\alpha_{12}\mathbf{u_{T_{12}}} + \alpha_3\mathbf{u_{T_3}} + \alpha_4\mathbf{u_{T_4}})C \tag{10.22}$$

Now, in order for $\mathbf{u_1}$ and $\mathbf{u_2}$ to be orthogonal, their dot product must be equal to zero. This results in the following condition:

$$(\alpha_{12}\mathbf{u_{T_{12}}} + \alpha_3\mathbf{u_{T_3}} + \alpha_4\mathbf{u_{T_4}})CC^T\mathbf{u_{T_{12}}}^T = 0 \tag{10.23}$$

Note that this condition is also equivalent to $C\mathbf{u_2}$ being orthogonal to $\mathbf{u_{T_{12}}}$. Similarly, it is imposed $C\mathbf{u_2}$ to be also orthogonal to $\mathbf{u_{T_4}}$. This results in the following system of equations:

$$\begin{bmatrix} \alpha_3 \\ \alpha_4 \end{bmatrix} = \begin{bmatrix} \mathbf{u_{T_3}r} & \mathbf{u_{T_4}r} \\ \mathbf{su_{T_3}}^T & \mathbf{su_{T_4}}^T \end{bmatrix}^{-1} \begin{bmatrix} -\mathbf{u_{T_{12}}r} \\ -\mathbf{su_{T_{12}}}^T \end{bmatrix} \alpha_{12} \tag{10.24}$$

with the following definition of $\mathbf{r}$ and $\mathbf{s}$ vectors:

$$\begin{aligned} \mathbf{r} = &\ CC^T u_{T_{12}}^T \\ \mathbf{s} = &\ \mathbf{u_{T_4}}CC^T \end{aligned} \tag{10.25}$$

And then, α_{12}, α_3 and α_4 are scaled to normalize $\mathbf{u_2}$. A similar approach can be defined for the M team changing subspaces accordingly. This way S_P and S_M matrices are computed.

It could be argued that a better approach for the second condition would have been to impose in the second equation that $C\mathbf{u_2}$ is directed along $\mathbf{u_{T_3}}$ (by forcing the dot product of their normalized vectors being equal to one). However, it can be checked that in general this equation cannot be solved

with real α_{12}, α_3 and α_4 and therefore it is not taken in the solution of the problem.

Additionally, it should be remarked that the solution provided above results in S_P and S_M matrices for which some of the elements are negative (particularly for the nodes linked to the fourth quarter). Certainly, this might not be physically or logically feasible for some problems, but it is still applicable to many others, and for that reason is explored here.

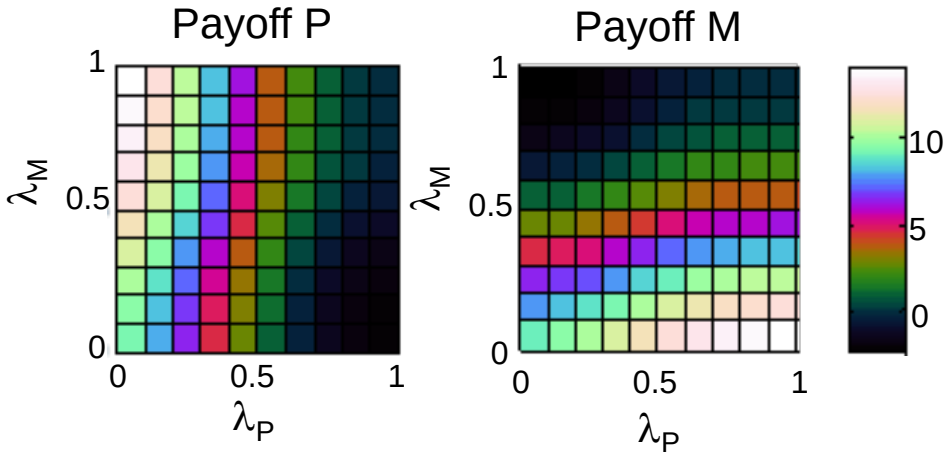

Figure 10.7: Unitary payoff (shown by a color code) as a function of λ_P, and λ_M for P and M.

Figure 10.7 represents an example of the payoff obtained by P and M in the case of a particular random GP network with steady state given by consensus function #2 and the same parameters as those used in the example for previous sections. The W matrix in C has four different sub-blocks W_{ij}, with $i, j = 1, 2$. To introduce some additional asymmetry, the upper two blocks (W_{11}, W_{12}) are randomly obtained, while all elements of W_{21} are set equal to 1 and those of W_{22} are null. The aforementioned figure depicts the unitary payoff for P and M teams as a function of λ_P and λ_M when each team uses an optimal solution for the S_P (or S_M) and its associated action. As previously commented, since the shown payoff is unitary, the total payoff for each team depends on the number of targeted elements.

For the $\lambda_P = \lambda_M = 1$ case the resulting payoff for both teams is zero since it is a zero-sum game with symmetric configuration. For the rest of values, it is no longer a pure zero-sum game and there is no symmetry.

The previous model can also introduce two additional parameters (respectively β_P and β_M, both positive) to model the effect on each team's payoff of their simultaneous activity upon a certain subspace, which could be counterproductive for the interests of both parties. For example, this would be the case if too many political statements are given by both teams to a group of voters over which they are directly competing, ultimately discouraging the associated segment of the general population to align with either of the two political options.

The following equations model the commented effect:

$$\begin{array}{rcl} \widetilde{\Phi}^P = & \lambda_P \widetilde{\Phi}^P_{12}(1+\beta_P \widetilde{\Phi}^M_{12}) + (1-\lambda_P)\widetilde{\Phi}^P_3 \\ \widetilde{\Phi}^M = & \lambda_M \widetilde{\Phi}^M_{12}(1+\beta_M \widetilde{\Phi}^P_{12}) + (1-\lambda_M)\widetilde{\Phi}^M_4 \end{array} \tag{10.26}$$

Since $\widetilde{\Phi}^P_{12}$ and $\widetilde{\Phi}^M_{12}$ have opposite signs, the resulting products implying β_P and β_M coefficients are negative as intended. These equations can be can analysed in more detail by taking into account first that:

$$\begin{array}{l} \widetilde{\Phi}^P_{12} = \mathbf{u_{T_{12}}} C\left[S_P \mathbf{a_P} - S_M \mathbf{a_M}\right] \\ \widetilde{\Phi}^M_{12} = -\widetilde{\Phi}^P_{12} \\ \widetilde{\Phi}^P_3 = \mathbf{u_{T_3}} C\left[S_P \mathbf{a_P} - S_M \mathbf{a_M}\right] \\ \widetilde{\Phi}^M_4 = \mathbf{u_{T_4}} C\left[S_M \mathbf{a_M} - S_P \mathbf{a_P}\right] \end{array} \tag{10.27}$$

Also, since $\mathbf{a_P}$ and $\mathbf{a_M}$ must be constrained to have a norm equal to a common value (denoted by β, whose square is the energy E) it can be noted that the action $\mathbf{a_P}$ (and similarly for $\mathbf{a_M}$) can be distributed between the two subspaces of action by means of the following equation:

$$\begin{array}{l} \mathbf{a_P} = f(\theta_P)[\theta_P \mathbf{v_1} + (1-\theta_P)\mathbf{v_2}] \\ f(\theta_P) = \sqrt{\dfrac{E}{\theta_P^2 + (1-\theta_P)^2}} \end{array} \tag{10.28}$$

where θ_P (resp. θ_M) is the strategy of the P team (resp. M team), and it represents the percentage of energy E being distributed among the two subspaces available to that team. Now, the following notation can be used for simplicity to define the following constant scalars, with $i = 1, 2$:

$$\begin{array}{rcl} {}^iK^P_{12} = & \mathbf{u_{T_{12}}} C S_P \mathbf{v_i} \\ {}^iK^M_{12} = & \mathbf{u_{T_{12}}} C S_M \mathbf{v_i} \\ {}^iK^P_3 = & \mathbf{u_{T_3}} C S_P \mathbf{v_i} \\ {}^iK^M_3 = & \mathbf{u_{T_3}} C S_M \mathbf{v_i} \\ {}^iK^P_4 = & \mathbf{u_{T_4}} C S_P \mathbf{v_i} \\ {}^iK^M_4 = & \mathbf{u_{T_4}} C S_M \mathbf{v_i} \end{array} \tag{10.29}$$

By analysing the equations, it can be deduced that the first, second, fourth and fifth elements in the list above are zero for $i = 2$. Also, the nonzero constants are in fact positive since they imply a bilinear form with positive matrix and with nonnegative vectors (considering the SVD decomposition of S_P and S_M). For example:

$$ {}^1K_3^P = \mathbf{u_{T_3}} C \mathbf{u_1} \sigma_1 = \mathbf{u_{T_3}} C C^T \mathbf{u_{T_{12}}} \sigma_1 > 0 \tag{10.30} $$

Considering the above definitions, we have from eq. 10.27 and eq. 10.28:

$$ \widetilde{\Phi}_{12}^P = f(\theta_P) \left[{}^1K_{12}^P \theta_P \right] - f(\theta_M) \left[{}^1K_{12}^M \theta_M +^2 K_{12}^M (1 - \theta_M) \right] \tag{10.31} $$

and similarly:

$$ \begin{aligned} \widetilde{\Phi}_3^P = & f(\theta_P) \left[{}^1K_3^P \theta_P +^2 K_3^P (1 - \theta_P) \right] \\ & - f(\theta_M) \left[{}^1K_3^M \theta_M +^2 K_3^M (1 - \theta_M) \right] \end{aligned} \tag{10.32} $$

Similar equations are applicable to the M team. This scenario can be considered as a continuous game for which a differential Nash equilibrium (NE) is to be found (see [Rat13] for details). According to proposition 2 in [Rat13], the NE of the game defined in eq. 10.26 must satisfy the following conditions (with θ_P^* and θ_M^* being the optimal strategies of P and M team, respectively):

$$ \begin{aligned} \frac{\partial \widetilde{\Phi}^P(\theta_P^*, \theta_M)}{\partial \theta_P} = 0 \quad & \frac{\partial^2 \widetilde{\Phi}^P(\theta_P^*, \theta_M)}{\partial \theta_P^2} < 0 \\ \frac{\partial \widetilde{\Phi}^M(\theta_P, \theta_M^*)}{\partial \theta_M} = 0 \quad & \frac{\partial^2 \widetilde{\Phi}^M(\theta_P, \theta_M^*)}{\partial \theta_P^2} < 0 \end{aligned} \tag{10.33} $$

Now, if β_P and β_M are equal to zero (as in the case defined in eq. 10.21) it is observed that the derivatives above render decoupled equations, so the condition to obtain θ_P^* is independent of θ_M and viceversa. This confirms the observation on the search of optimal solution given in eq. 10.12, for which the optimal solution is taken as a separate optimization exercise for each team. However, in the general case where β_P and β_M are nonzero, the resulting equations are indeed coupled and the optimal solution must be found solving the system of equations.

It should be noted that in eq. 10.26 λ_P and λ_M could vary in the long term depending on external conditions (changes in market tendencies, etc.). The NE would vary accordingly. This is observed in the following numerical example.

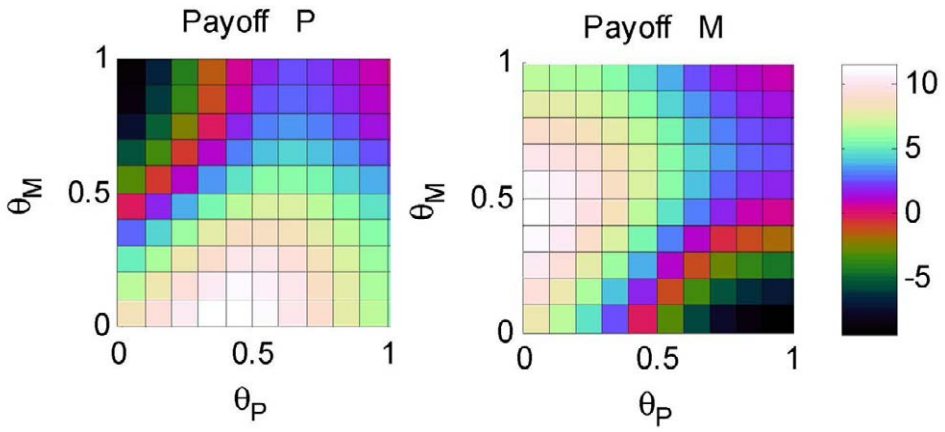

Figure 10.8: Unitary payoff for P and M teams as a function of the control variables θ_P, θ_M (with $\lambda_P = 0.1$ and $\lambda_M = 0.1$)

The exercise is continued with the same GP network used for Figure 10.7. Nevertheless, it should be noticed that the game considered here is different since now the governing equations given by eq. 10.27 are coupled, with $\beta_P = \beta_M = 0.1$. Out of the possible values of λ_P and λ_M we take 0.1 and 0.1, respectively, for the first phase of the analysis, and then their values are changed to $\lambda_P = 0.8$ and $\lambda_M = 0.9$, associated to a change in environmental conditions of the game. For information, Figure 10.8 presents the payoff for each team for the first set of λ_P and λ_M, as a function of the control variables θ_P and θ_M.

The NE can be computed by means of the conditions given in eq. 10.33, for which the actual derivation of the gradient is given in the Appendix (see equation A.2). The obtained pair of values corresponding to the first phase is $NE_1 = [0.583, 0.586]$. The second NE is found at $NE_2 = [0.883, 0.935]$. Furthermore, the second derivative of the payoff function is negative for both NE, as required also in eq. 10.33.

Now it can be envisaged an iterative process in which each team tries to optimize its payoff based on the observed status at each step and the local derivative of its payoff function. The way that the NE is dynamically reached by both teams is based on a *steepest ascent* algorithm, as opposed to *descent* described in [Rat13] since here it is considered a payoff function

(instead of a cost) to be maximized. The dynamic equation is given by:

$$\begin{bmatrix} \theta_P^{n+1} \\ \theta_M^{n+1} \end{bmatrix} = \begin{bmatrix} \theta_P^{n} \\ \theta_M^{n} \end{bmatrix} + h \begin{bmatrix} \dfrac{\partial \widetilde{\Phi}^P(\theta_P^n, \theta_M^n)}{\partial \theta_P} \\ \dfrac{\partial \widetilde{\Phi}^M(\theta_M^n, \theta_M^n)}{\partial \theta_M} \end{bmatrix} \tag{10.34}$$

The results of the implementation of this algorithm for $h = 10^{-4}$ is shown in the blue thick curve in Figure 10.9, where the aforementioned value NE_1 is reached, after starting from an arbitrary value at $[0.1, 0.6]$. Similarly, the red thick curve depicts the evolution of both P and M strategies, reaching a NE which is also coherent with the NE_2 value referred above. The same figure depicts also the level lines of the payoff curves shown in Figure 10.8 (with dashed lines corresponding to P payoff, and solid lines to M payoff). Thus, they correspond only to the first referred phase represented by the thick blue line. It is observed that the trajectory evolves considering the simultaneous ascent related to both payoff surfaces, until a zero derivative is reached as previously explained.

It should be remarked that indeed the reached NE is not Pareto optimum, since both teams could have benefited from a better payoff (for example with $\theta_P = \theta_M = 0$). This should come as no surprise since the teams choose their strategies according to the local information at each step, reacting only to the observed reality, which is a function of the iterative action of the opponent team, but collaboration for Pareto optima is not involved in the definition of the game.

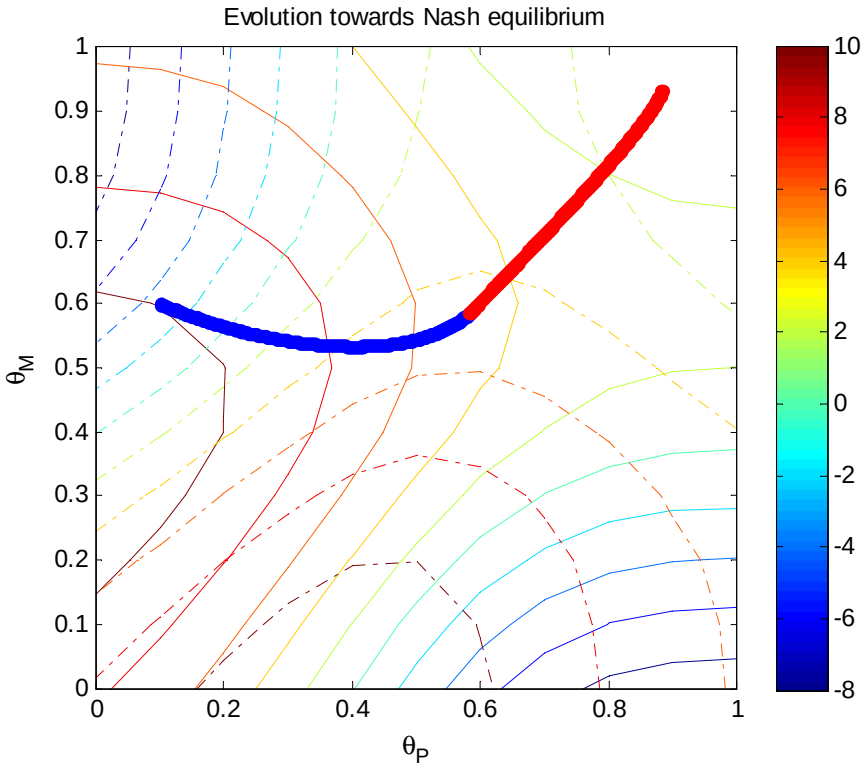

Figure 10.9: Dynamics to reach NE for first (blue) and second (red) phases. Contour lines for P (dashed) and M (solid) payoff corresponding to the first phase.

Part IV

Conclusions

Chapter 11

Conclusions and future work

Conclusions

This thesis has addressed the application of control to the dynamical behaviour of complex systems, in the framework of vibrational dynamics and of games on complex networks. Relevant conclusions have been obtained in both cases in terms of the control strategies to be followed.

In the case of laser control of HCN vibrational dynamics, the results have shed very important insights in terms of controlling the dynamic regime by means of the frequency of the applied laser to the molecule, and also on the related dissociation behaviour. A frequency analysis has been conducted of the laser driven nonlinear dynamics of HCN described with a widespread 2D vibrational model including the HC and CN stretchings. The dependence of the dynamics with the laser frequency has been thoroughly studied, this representing an extension of previous studies [Set12]. A SALI map has been used to characterize the level of ergodicity of the system across the phase space, and the structural dependency on the laser frequency has been studied. Relevant information has been retrieved on the dependency on the laser frequency, by putting forward its relationship with the fundamental frequencies of the system tori to characterize the molecule behavior in terms of chaoticity and dissociation observed in the phase space. As a result of the analysis of the system in the time and frequency domains, the dependence of the dynamics on the driving field indicates that this is a plausible parameter to be used for control purposes.

Regarding complex networks, we have addressed the competition between two teams that are connected to a network of elements, each of them retrieving a certain payoff as a result of the steady state reached by the nodes in the general network GP. These nodes follow certain consensus dynamics and the

analysis presented here is applicable independently of the chosen consensus function. Each team competes with the same energy available for the set of agents, while the adjacency matrices S_P and S_M defining the connection of each team with the general network have the same norm.

The following list summarizes the most relevant particular conclusions reached during the research presented here:

1. We have confirmed that in the HCN vibrational dynamics there is a very robust 1:1 resonance between the HC and CN stretchings which represents the strongest bottleneck for IVR in the molecule.

2. This fact explains that when the laser is on the ratio $\omega_F/\omega_{1,2}^{[1:1]}$ appears as the most significant one from the dynamical point of view[Kol54a, Arn61, Mos68, Ber78, Chi79].

3. Similarly to Ref. [Set12], we find the existence of two regions in phase (or frequency) space, namely the dissociation hub (DH) and the noble hub (NH), which depend on the value of ω_F and are most relevant for the laser/molecule interaction. Since the energies considered in this work are substantially higher than that of the molecular minimum, the frequencies of the system cannot be approximated to the harmonic ones that can be derived from the potential Morse functions, and should be accurately computed in order to correctly explain the laser/molecule interaction.

4. The destruction of tori in phase space is to be regarded in terms of the relation of the laser frequency with frequencies $\omega_F = \omega_{1,2}^{[1:1]}$ and $\omega_F = \omega_2^{[3:2]}$ associated with resonance regions 1:1 and 3:2, respectively. A rational resonance with either these frequencies lead to the destruction of tori in the dynamics in the corresponding region, whilst a proportional relation with the golden mean lead to a high level of regularity in that area of the phase space.

5. The frequency map clearly shows that the resonance (1, -1, 0) constitutes a robust bottleneck dividing the frequency space of the HCN in the presence of a laser into two different regions, the NH and DH.

6. Dissociation phenomena are also observed in the frequency domain when the laser frequency is increased. A high degree of chaoticity is present in those trajectories. The obtained results are in good relation with those observed in phase space. In all cases dissociating trajectories

depart from the DH. Conversely, trajectories with initial conditions in the NH and in the 1:1 resonance region do not lead to dissociation.

7. A figure in the format as Fig. 6.8 can be used summarize how the molecular tori destruction depends on the $\omega_F/\omega 1, 2^{[1:1]}$ ratio, and how this affects the dynamics of the system.

8. On games over complex networks, this research has analysed the optimal actuation of each agent within one team (forming an optimal action vector), first from a numerical perspective based either on exhaustive search for solutions or by means of genetic algorithms, and then by an analytical solution based on singular value decomposition of a suitably chosen matrix. By comparing both results, it has been verified the optimality of the technique based on singular values.

9. This approach has been further explored to obtain the optimal design of the matrices S_P and S_M that brings a maximum achievable payoff when selecting the optimal action vector. It has been shown that singular value decomposition renders the optimal solution in the design of the network connecting one team to the GP.

10. The validity of the results in games on networks is independent on the consensus function, which provides a high flexibility in the applicability of the results.

11. It is observed that the average ratio between the first two singular values of the consensus function increases with average degree in the case of damped consensus, while it is close to 1 for the other two types of consensus function. The theoretical justification is provided, based on the Laplacian matrix.

12. The scope of the game can be further generalized by considering the possibility of each team targeting a different subgroup within GP, and also of aiming towards more than one subgroup. In the second case, each team can play with the distribution of its optimal actuation on each subspace considering also the equivalent strategy followed by the opposing team.

13. It is observed that games over subspaces of the target population allow the numerical computation of a Nash equilibrium based on steepest ascent, by simulating the trajectory of each team. It is verified that the retrieved outcome matches the analytically computed result.

Future work

The development of control algorithms to bring the system to target regions of phase space and frequency map (based on the presented concepts of fundamental frequencies and relation with the laser frequency) will be the subject of further research. The results in Fig. 6.8 should play a crucial role in making these algorithms precise. Furthermore, the conclusions reached for the HCN molecule can also be analyzed for other type of molecules. A step beyond should also take into account the effect of energy as an additional degree of freedom (along with laser frequency) in the molecular vibrational dynamics control problem.

On the other hand, the analysis on games on complex networks could also be generalized to the problem of more than two teams. This extended setup could be addressed by introducing complex numbers in the analysis presented here, where each team is assigned a certain desired phase in the complex plane, aiming to lead the population close to that value. Furthermore, the idea of competing dynamics in a network attending to opposite interests has been explored here for consensus dynamics, but these type of games could similarly be extended to synchronization phenomena, as a set of Kuramoto oscillators. The analysis on conformist and contrarians addressed in [Jad04, Hong11b] can be a starting point for the application of the theoretical framework established in this thesis to games over oscillator networks between two external teams. Additionally, the present investigation in games on networks opens the door to future steps such as proper characterization of interactions within the GP network, or robustness of the optimal strategies to uncertainties (both in the GP topology and in the consensus dynamics). Also, the analysis could be extended to different dynamics not necessarily subject to a steady state solution but where the subspace division and the strategy based on singular values can still be valid. Furthermore, the flexibility of the described game setup and optimal strategies for a team brings an opportunity to apply this approach to a variety of scenarios such as competition within a market, strategies for influencing public opinion, or biological games on networks. On the latter case, it is worth commenting that, as opposed to other studies such as in [Kar11], the present study assumes elements outside the general population that indirectly affect the state of the population's elements, along with a certain intelligence in the coordination of agents within a team. This can be a particular advantage in situations where such central intelligence is not present on the opposing side, such as combating an illness within an individual or a community (both of them associated to a network where the game is established).

Appendix A

Numerical methods

A.1 Numerical methods for HCN dynamics analysis

A.1.1 Symplectic Hamilton equations propagation

In this thesis, the propagation of the Hamilton equations for the analysis of the HCN molecule is conducted following the sympletic method known as Störmer-Verlet[Hai03]. The generic equations are as follows:

$$\left.\begin{aligned}
\mathbf{p}[n+\frac{1}{2}] &= \mathbf{p}[n] - \frac{h}{2}\nabla_{\mathbf{q}} H(\mathbf{p}[n+\frac{1}{2}], \mathbf{q}[n]), \\
\mathbf{q}[n+1] &= \mathbf{q}[n] + \frac{h}{2}(\nabla_{\mathbf{p}} H(\mathbf{p}_{n+\frac{1}{2}}, \mathbf{q}_n) + \nabla_{\mathbf{p}} H(\mathbf{p}[n+\frac{1}{2}], \mathbf{q}[n+1])), \\
\mathbf{p}[n+1] &= \mathbf{p}[n+\frac{1}{2}] - \frac{h}{2}\nabla_{\mathbf{q}} H(\mathbf{p}[n+\frac{1}{2}], \mathbf{q}[n+1]),
\end{aligned}\right\} \tag{A.1}$$

where h is the integration step, H is the Hamiltonian, and $\nabla_{\mathbf{p}} H, \nabla_{\mathbf{q}} H$ are the partial derivatives of H with respect to $\mathbf{p}$ and $\mathbf{q}$, which are to be evaluated at the points given in the equations. Since $\mathbf{p}$ and $\mathbf{q}$ are vectors, such partial derivatives are indeed gradients of H in the associated directions. Although these equations are implicit, for separable Hamiltonian as in the HCN case, they render explicit equations. In the case of the HCN and considering the Hamiltonian with the laser, we have:

$$\left.\begin{aligned}
p_1[n+\frac{1}{2}] =& p_1[n] - hD_1\alpha_1\left(1-e^{-\alpha_1 q_1[n]}\right)e^{-\alpha_1 q_1[n]} - \\
&- \frac{h}{2}\lambda_F \cos\omega_F t[e^{-\eta(q_1[n]+r^e_{\mathrm{CH}})}(-\eta\Sigma + d\Sigma)], \\
p_2[n+\frac{1}{2}] =& p_2[n] - hD_2\alpha_2\left(1-e^{-\alpha_2 q_2[n]}\right)e^{-\alpha_2 q_2[n]}, \\
q_1[n+1] =& q_1[n] + h(\frac{p_1[n+\frac{1}{2}]}{M_{CH}} - \frac{p_2[n+\frac{1}{2}]}{M_C}), \\
q_2[n+1] =& q_2[n] + h(\frac{p_2[n+\frac{1}{2}]}{M_{CN}} - \frac{p_1[n+\frac{1}{2}]}{M_C}), \\
p_1[n+1] =& p_1[n+\frac{1}{2}] - hD_1\alpha_1\left(1-e^{-\alpha_1 q_1[n+1]}\right)e^{-\alpha_1 q_1[n+1]} - \\
&- \frac{h}{2}\lambda_F \cos\omega_F t[e^{-\eta(q_1[n+1]+r^e_{\mathrm{CH}})}(-\eta\Sigma + d\Sigma)], \\
p_2[n+1] =& p_2[n+\frac{1}{2}] - hD_2\alpha_2\left(1-e^{-\alpha_2 q_2[n+1]}\right)e^{-\alpha_2 q_2[n+1]},
\end{aligned}\right\} \tag{A.2}$$

with:

$$\left.\begin{aligned}
\Sigma &= \sum_{j=1}^{4} A_j (q_1 + r^e_{\mathrm{CH}})^j, \\
d\Sigma &= \sum_{j=1}^{4} j A_j (q_1 + r^e_{\mathrm{CH}})^{j-1}, \\
d^2\Sigma &= \sum_{j=2}^{4} j(j-1) A_j (q_1 + r^e_{\mathrm{CH}})^{j-2},
\end{aligned}\right\} \tag{A.3}$$

and the last equation $d^2\Sigma$ is used in the computation of the SALI coefficient as shown in the next epigraph.

A.1.2 SALI coefficient computation for HCN molecule

Equation 2.59 shows how to propagate vector v_i to compute the SALI coefficient. For this purpose the Hessian of the Hamiltonian is to be computed. In the case of the HCN dynamics, the Hessian is given as:

$$\nabla^2 = \begin{bmatrix} \nabla_a & 0 \\ 0 & \nabla_b \end{bmatrix}, \tag{A.4}$$

where the 0's denote a 2x2 zero matrices, and ∇_a, ∇_b are given as follows:

$$\nabla_a = \begin{bmatrix} \nabla_{a11} & 0 \\ 0 & \nabla_{a22} \end{bmatrix}, \tag{A.5}$$

and

$$\nabla_b = \begin{bmatrix} \frac{1}{M_{CH}} & -\frac{1}{M_C} \\ -\frac{1}{M_C} & \frac{1}{M_{CN}} \end{bmatrix}, \tag{A.6}$$

with

$$\left.\begin{aligned} \nabla_{a11} =& 2D_1\alpha_1^2(2e^{-2\alpha_2 q_1[n]} - e^{-\alpha_2 q_1[n]}) - \\ & - \lambda_F cos(\omega_F t)e^{-\eta(q_1 + r^e_{\mathrm{CH}})})(\Sigma\eta^2 - 2\eta d\Sigma + d^2\Sigma), \\ \nabla_{a22} =& 2D_2\alpha_2^2(2e^{-2\alpha_2 q_2[n]} - e^{-\alpha_2 q_2[n]}), \end{aligned}\right\} \tag{A.7}$$

A.2 Numerical methods for game dynamics towards Nash equilibrium

The evaluation of the eq. 10.33 implies a gradient, whose expression is detailed herein (with the definition of the variables and functions as given in that section):

$$\begin{aligned} &\frac{\partial\widetilde{\Phi}^P(\theta_P^n, \theta_M^n)}{\partial\theta_P} = \\ &\lambda_P({}^1K_{12}^P f(\theta_P) - \frac{(EK_{12}^P\theta_P^n(4\theta_P^n - 2))}{(2((\theta_P^n - 1)^2 + (\theta_P^n)^2)^2 f(\theta_P))})(\beta_P({}^1K_{12}^M\theta_M^n f(\theta_N) - {}^1\ K_{12}^P\theta_P^n f(\theta_P)) + 1) - \\ &- (({}^1K_3^P - {}^2\ K_3^P)f(\theta_P) - \frac{(E({}^1K_3^P\theta_P^n - {}^2\ K_3^P(\theta_P^n - 1))(4\theta_P^n - 2))}{(2((\theta_P^n - 1)^2 + (\theta_P^n)^2)^2 * f(\theta_P))})(\lambda_P - 1) + \\ &+ \beta_P\lambda_P({}^1K_{12}^P f(\theta_P) - \frac{(E{}^1K_{12}^P\theta_P^n(4\theta_P^n - 2))}{(2((\theta_P^n - 1)^2 + (\theta_P^n)^2)^2 f(\theta_P))})({}^1K_{12}^P\theta_M^n f(\theta_N) - {}^1\ K_{12}^P\theta_P^n f(\theta_P)) \end{aligned} \tag{A.8}$$

$$\frac{\partial\widetilde{\Phi}^M(\theta_M^n,\theta_M^n)}{\partial\theta_M} =$$
$$-((^1K_4^M -^2 K_4^M)f(\theta_M^n) - \frac{(E(^1K_4^M\theta_M^n -^2 K_4^M(\theta_M^n-1))(4\theta_M^n-2))}{(2((\theta_M^n-1)^2+(\theta_M^n)^2)^2 f(\theta_M^n))})(\lambda_M-1)-$$
$$-\lambda_M(^1K_{12}^M f(\theta_M^n) - \frac{(E^1K_{12}^M\theta_M^n(4\theta_M^n-2))}{(2((\theta_M^n-1)^2+(\theta_M^n)^2)^2 f(\theta_M^n))})(\beta_M(^1K_{12}^M\theta_M^n f(\theta_M^n) -^1 K_{12}^P\theta_P^n f(\theta_P^n))-1)$$
$$-\beta_M\lambda_M(^1K_{12}^M f(\theta_M^n) - \frac{(E^1K_{12}^M\theta_M^n(4\theta_M^n-2))}{(2((\theta_M^n-1)^2+(\theta_M^n)^2)^2 * f(\theta_M^n))})(^1K_{12}^M\theta_M^n f(\theta_M^n) -^1 K_{12}^P\theta_P^n f(\theta_P^n)) \tag{A.9}$$

Bibliography

[Are08] A. Arenas, A. Díaz-Guilera, J Kurths, Y Moreno, C Zhou. *Synchronization in complex networks*. Physics reports 469 (3) 93-153 (2008).

[Arn61] V.I. Arnold. *Small denominators. I. Mapping the circle onto itself*. Izv. Aka. Nauk. SSSR, Ser. Math. 25 (1) 21-86 (1961) and correction Izv. Akad. Nauk SSSR Ser. Mat., 28 (2) 479480 (1964)

[Arr10] F. J. Arranz, L. Seidel, C. G. Giralda, R. M. Benito, and F. Borondo. *Scars at the edge of the transition from order to chaos in the isomerizing molecular systems LiNC-LiCN and HCN-HNC, and* HO_2. Phys.Rev. E 82, 026201 (2010).

[Atk06] P. W. Atkins, J. de Paula (2006). Physical Chemistry. W.H. Freeman and Company ed. (2006).

[BaAl99] A-L. Barabási, R. Albert. *Emergence of Scaling in Random Networks*. Science Vol. 286 (5439) 509-512 (1999).

[Ball06] C. Ballester, A. Calvo-Armengol, Y. Zenou. *Whos Who in Networks. Wanted: The Key Player*. Econometrica 74 (5) 1403-1417 (2006).

[Ban02] A. D. Bandrauk, Y. Fujimura, and R. J. Gordon. Laser Control and Manipulation of Molecules. ACS Symposium Series, 821. American Chemical Society Ed., Washington DC, (2002)

[Bar08] A. Barrat, M. Bhartélemy, A. Vespignani. Dynamical Processes on Complex Networks. Cambridge University Press (2008).

[Bay99] J.S. Bay. Fundamental of Linear State Space Systems. McGraw Hill Ed. (1999).

[Beni15] P. Benitez, J. C. Losada, R. M. Benito, and F. Borondo. *Using the small alignment index chaos indicator to characterize the vibrational dynamics of a molecular system: LiNC-LiCN*. Phys. Rev. E, 92 042918 (2015).

[Ber78] M. V. Berry. *Regular and irregular motion*. AIP Conf. Proc. 46 (1), 16 (1978).

[Blo84] N. Bloembergen, A. H. Zewail. *Energy Redistribution In Isolated Molecules and the Question of Mode-Selective Laser Chemistry Revisited*. J. Phys. Chem. 88 (23) 5459-5465 (1984).

[Boc00] S. Boccaletti, C. Grebogi,Y. Lai, H. Mancini, D. Maza. *The control of chaos: theory and applications*. Physics Reports 329 (3) 103-197 (2000).

[Boc02] S. Boccaletti, J. Kurths, G.Osipov, D.L.Valladares, C.S.Zhou. *The synchronization of chaotic systems*. Physics Reports 366 (1-2) 1-101 (2002) .

[Boc06] S. Boccaletti, V. Latora, Y. Moreno, M.Chavez, D.-U. Hwang. *Complex networks: Structure and dynamics*. Physics Reports (45) 175-308 (2006).

[Boc08] S. Boccaletti. The synchronized dynamics of complex systems. Monograph Series on Nonlinear Science and Complexity (6). A. Luo, G. Zaslavsky ed. (2008).

[Bot95] J. Botina, H. Rabitz, and N. Rahman. *A new approach to molecular classical optimal control: Application to the reaction HCN→HC+N*. J. Chem. Phys. 102, 226 (1995).

[Bram14] Y. Bramoullé, R. Kranton, M. DAmours. *Strategic Interaction and Networks*. American Economic Review 104 (3) 898930 (2014).

[Bre10] A. Bressan. Noncooperative Differential Games. A tutorial. Penn State University Ed. (2010).

[Bre11] A. Bressan. *Non-cooperative Differential Games*. Milan Journal of Mathematics 79 (2) 357-427 (2011).

[Brez04] R. Brezina and W.K. Liu. *Control of Bond Excitation and Dissociation in HCN Using Laser Pulses*. J. Phys. Chem. A 108 (41), 8852-8859 (2004).

[Bro10] H. Broer, F. Takens. Dynamical Systems and Chaos. Applied Mathematical Sciences 172. Springer-Verlag (2010)

[Bry75] A. E. Bryson Jr. and Y.C. Ho. Applied Optimal Control. Optimization, Estimation and Control. Hemisphere Publ. Corp. Halsted Press. (1975).

[Che91] S. Chelkowski and A. D. Bandrauk. *Control of vibrational excitation and dissociation of small molecules by chirped intense inflared laser pulses.* Chem. Phys. Lett. 186 (2-3) 264-269 (1991)

[Che96] C. M. Dion, S. Chelkowski, A. D. Bandrauk, H. Umeda, and Y. Fujimura. *Numerical simulation of the isomerization of HCN by two perpendicular intense IR laser pulses.* J. Chem. Phys. 105, 9083 (1996).

[Chi79] B. V. Chirikov. *A universal instability of many-dimensional oscillator systems.* Phys. Rep. 52(5) 263-379 (1979).

[Dav81] M. J. Davis and E. J. Heller. *Quantum dynamical tunneling in bound states.* J. Chem. Phys. 75 (1) 246 (1981).

[Del15] J.C Delvenne, R. Lambiotte, L. E.C. Rocha. *Diffusion on networked systems is a question of time or structure.* Nature Communications 6, 7366 (2015).

[Dia08] B. C. Dian, G. G. Brown, K. O. Douglass, F. S. Rees, J. E. Hohns, P. Nair, R. D. Suenram, and B. H. Pate. *Conformational isomerization kinetics of pent-1-en-4-yne with 3,330 cm*^{1} *of internal energy measured by dynamic rotational spectroscopy.* Proc. Natl. Acad. Sci. 105 (35) 12696-12700 (2008).

[Dum93] H. S. Dumas and J. Laskar. *Global dynamics and long-time stability in Hamiltonian systems via numerical frequency analysis* Phys. Rev. Lett. 70, 2975 (1993).

[Eas10] D. Easly, J. Kleinberg. Networks, Crowds, and Markets: Reasoning about a Highly Connected World. Cambridge University Press (2010).

[Ege02] M. Egerstedt and X. Hu, Formation control with virtual leaders and reduced communications. 15th IFAC World Congress (2002)

[Ell18] M. Elliot, B. Golub. *A network approach to public goods.* Journal of Political Economy, 0 (2018). DOI: 10.1086/701032.

[Ess04] J. Essinger. Jacquard's Web. Oxford University Press (2004).

[Est15] E. Estrada. Introduction to Complex Networks: Structure and Dynamics. Banasiak J., Mokhtar-Kharroubi M. (eds) Evolutionary Equations with Applications in Natural Sciences. Lecture Notes in Mathematics, vol 2126, 93-131.(2015).

[Far09] S. C. Farantos, R. Schinke, H. Guo, and M. Joyeux. *Energy Localization in Molecules, Bifurcation Phenomena, and Their Spectroscopic Signatures: The Global View*. Chem. Rev. 109 (9) 4248-4271 (2009).

[Far12] M. Fardad, X. Zhang, F. Lin, and M. R. Jovanovic. *On the Optimal Dissemination of Information in Social Networks*. 51st IEEE Conference on Decision and Control, 2539-2544 (2012).

[Fet80] A.L. Fetter, J.D. Walecka. Theoretical mechanics of particles and continua. McGraw Hill (1980).

[Fied75] M. Fiedler. *A property of eigenvectors of nonnegative symmetric matrices and its application to graph theory.* Czechoslovak Math Journal 25 (4) 619-633 (1975).

[Fri16] T.L. Friesz, D. Bernstein. Foundations of network optimization and games. Springer (2016).

[Gal10] A. Galeotti, S. Goyal, M.O. Jackson, F. Vega-Redondo. *Network games.* Review of Economic Studies 77 (1) 218244 (2010).

[Gao14] J. Gao, Y.Y. Liu, R. M. DSouza, A.L. Barabasi. *Target control of complex networks*. Nature communications 5, 5415 (2014).

[Gol80] H. Goldstein. Classical Mechanics, 2nd Ed. Addison-Wensley publishing company (1980).

[Gong05a] J. Gong, A. Ma, and S. A. Rice. *Isomerization and dissociation dynamics of HCN in a picosecond infrared laser field: A full-dimensional classical study*. J. Chem. Phys. 122 (14) 144311 (2005).

[Gong05b] J. Gong, A. Ma, and S. A. Rice. *ibid. Controlled subnanosecond isomerization of HCN to CNH in solution*. J. Chem. Phys. 122 (20) 204505 (2005).

[Goy07] S. Goyal. Connections - An introduction to the Economics of Networks. Princeton University Press (2007).

[Grew10] M. S. Grewal, A. P. Andrews. *Applications of Kalman filtering in aerospace 1960 to the present (historical perspectives).* IEEE Control Systems 30 (3) 69-78 (2010).

[Gri10] C. Griffin. Game Theory: Math 486 Lecture Notes. Penn State University (2010).

[Gros11] C. Gros. Complex and Adaptive Dynamics Systems. Springer-Verlag (2011).

[Gru00] M. Gruebele. *Molecular vibrational energyflow: A state space approach.* Adv. Chem. Phys. 114, 193 (2000).

[Gru04] M. Gruebele and P. G. Wolynes. *Vibrational Energy Flow and Chemical Reactions.* Acc. Chem. Res. 37 (4) 261-267 (2004).

[Guc83] J. Guckenheimer, P. Holmes. Nonlinear Oscillations, Dynamical Systems and Bifurcations of Vector fields. Applied Mathematical Sciences 42. Springer-Verlag (1983)

[Hai03] E. Hairer, C. Lubich, and G. Wanner. *Geometric numerical integration illustrated by the StrmerVerlet method.* Acta Numerica 12, 399-450 (2003).

[Hale91] J. Hale, H. Koçak. Dynamics and bifurcations. Springer-Verlag (1991).

[Har94] T. Harju. Lecture Notes on Graph Theory. Department of Mathematics, University of Turku, Finland (1994-2011).

[Has02] R. Hasbani, B. Ostojic, P. R. Bunker, and M.-Yu. Ivanov. S*elective dissociation of the stronger bond in HCN using an optical centrifuge.* J. Chem. Phys, 116 (24) 10636 (2002).

[Hav10] S. Havlin, R. Cohen. Complex Networks. Structure, Robustness and function. Cambridge University Press (2010).

[Hea94] J.F. Heagy, T.L. Carrol, L.M. Pecora. *Synchronous chaos in coupled oscillator systems.* Physical Review E 50 (3) 1874-1886 (1994).

[Hong11a] H. Hong, S. Strogatz. *Kuramoto model of coupled oscillators with positive and negative coupling parameters: An example of conformist and contrarian oscillators.* Phys. Rev. Lett. 106 (5), 054102 (2011).

[Hong11b] H. Hong, S. Strogatz. *Conformists and contrarians in a kuramoto model with identical natural frequencies.* Phys. Rev. E 84 (4) 046202 (2011).

[Horn12] R.A. Horn, C.R. Johnson. Matrix Analysis, Cambridge University Press (2012).

[Jack10] M.O. Jackson. Social and economic networks. Princeton University Press (2010).

[Jack14] M.O. Jackson, Y. Zenou. Games on Networks. Handbook of Game Theory, Vol. 4, Peyton Young and Shmuel Zamir, eds., Elsevier Science (2014).

[Jad04] A. Jadbabaie, N. Motee, M. Barahona. *On the Stability of the Kuramoto Model of Coupled Nonlinear Oscillators.* Proceeding of the 2004 American Control Conference 4296-4301 (2004).

[Jaf80] C. Jaffe and P. L. Brumer. *Local and normal modes: A classical perspective.* J. Chem. Phys. 73 (11) 5646 (1980).

[Kal60] R.E. Kalman. *A New Approach to Linear Filtering and Prediction Problems.* Transactions of the ASMEJournal of Basic Engineering, 82 (1) 35-45 (1960).

[Kang16] Chul-Goo Kang. *Origin of Stability Analysis: "On Governors" by J.C. Maxwell [Historical Perspectives].* IEEE Control Systems 36.5, pp. 77-88 (2016)

[Kar11] B Karrer and M.E.J. Newman. *Competing epidemics on complex networks.* Physical Review E 84, 036106 (2011).

[Kat95] A. Katok, B. Hasselblatt. Introduction to the modern theory of dynamical systems. Cambridge University Press (1995).

[Kha01] Hassan K. Khalil. Nonlinear Systems. Prentice Hall (2001).

[Kol54a] A. N. Kolmogorov. *On the Conservation of Conditionally Periodic Motions under Small Perturbation of the Hamiltonian.* Dokl. Akad. Nauk SSSR 98, 527-530 (1954) (Engl. transl.: Stochastic Behavior in Classical and Quantum Hamiltonian Systems, Volta Memorial conference, Como, 1977, Lecture Notes in Physics, vol. 93, Springer, 1979, pp. 5156)

[Kol54b] A.N. Kolmogorov. *The general theory of dynamical systems and classical mechanics* (Russian). Proceedings of the International Congress of Mathematicians (Amsterdam, 1954), Vol. 1, pp. 315333 (1954).

[Kur84] Y. Kuramoto. Chemical Oscillators, Waves, and Turbulence. Springer-Verlag (1984).

[Las92] J. Laskar, C. Froeschlé, and A. Celletti. *The measure of chaos by the numerical analysis of the fundamental frequencies. Application to the standard mapping.* Physica D 56 (2-3) 253-269 (1992).

[Las93a] J. Laskar. *Frequency analysis for multi-dimensional systems. Global dynamics and diffusion.* Physica D 67 (1-3) 257-281 (1993).

[Las93b] J. Laskar, F. Joutel, and P. Robutel. *Stabilization of the Earth's obliquity by the Moon.* Nature 361, 615-617 (1993).

[LeC10] P. Le Calvez, J. Wang. *Some remarks on the Poincaré-Birkhoff theorem.* Proc. Amer. Math. Soc. 138, 703 (2010).

[Lei05] D. M. Leitner. *Heat transport in molecules and reaction kinetics: the role of quantum energy flow and localization.* Adv. Chem. Phys. 130B, 205 (2005).

[Lich92] A. J. Lichtenberg and M. A. Lieberman. Regular and Chaotic Dynamics. Springer, New York. (1992).

[Liu11] Y.Y. Liu, J.J. Slotine, A.L. Barabasi. *Controllability of complex networks.* Nature 473, 167173 (2011).

[Liu16] Y.Y. Liu, A.L. Barabasi. *Control Principles of Complex Networks.* Reviews of Modern Physics 88 (3) 035006 (2016).

[Lop16] A. López-Pina, J. C. Losada, R. M. Benito, and F. Borondo. *Frequency analysis of the laser driven nonlinear dynamics of HCN.* J. Chem. Phys. 145 (24) 244309 (2016).

[Lor93] Lorenz, E. N. The Essence of Chaos. University of Washington Press (1993).

[Los08] J. C. Losada, R. M. Benito, and F. Borondo. *Frequency map analysis of the 3D vibrational dynamics of the LiCN/LiNC molecular system.* Eur. Phys. J. Special Topics 165, 183-193 (2008).

[Los98] J. C. Losada, J. M. Estebaranz, R. M. Benito, and F. Borondo. *Local frequency analysis and the structure of classical phase space of the LiNC/LiCN molecular system*. J. Chem. Phys. 108 (1) 63 (1998).

[Losk07] A Loskutov. *Dynamical chaos: systems of classical mechanics*. Physics Uspekhi 50 (9) 939 - 964 (2007).

[Lou09] U. Lourderaj and W. L. Hase. *Theoretical and Computational Studies of Non-RRKM Unimolecular Dynamics*. J. Phys. Chem. A 113 (11) 2236-2253 (2009).

[Louz12] V. H. P. Louzada, N. A. M. Araujo, J. S. Andrade, Jr, H. J. Herrmann. *How to suppress undesired synchronization*. Scientific Reports 2, 658 (2012).

[Mar18] J.R. Marden and J.S. Shamma. *Game Theory and Control*. Annu. Rev. Control Robot. Auton. Syst. 1, 10534 (2018).

[Mil67] S. Milgram. *The Small World Problem*. Psychology Today 1 (1) 61-67 (1967).

[Mitc96] M. Mitchell. An introduction to genetic algorithms. MIT Press (1996).

[Mos68] J. Moser. *Lectures on Hamiltonian Systems*. Am. Math. Soc. Mem. 81, 1-60 (1968).

[Mye91] R. Myerson. Game Theory: Analysis of Conflict. Harvard University Press (1991).

[New03] M.E.J. Newman. *The Structure and Function of Complex Networks*. SIAM review 45 (2) 167-256 (2003).

[New10] M.E.J. Newman. Networks. An introduction. Oxford University Press (2010).

[Nis07] N. Nissam, T. Roughgarden, E. Tardos, V. V. Vazirany. Algorithmic Game Theory. Cambridge University Press (2007).

[Noe1918] E. Noether, *Invariante Variationsprobleme*. Nachr. König. Gesell. Wissen. Göttingen, Math.Phys. Kl. 235257 (1918). English translation in: Transport Theory and Statistical Physics, 1 (3), 183207 (1971).

[Oga10] K. Ogata. Modern Control Engineering. Prentice Hall (2010).

[Olf06] R. Olfati-Saber. *Flocking for multi-agent dynamic systems: Algorithms and theory.* , IEEE Trans. Autom. Control 51 (3) 401-420 (2006).

[Olf07] R. Olfati-Saber, A. Fax, R.M. Murray. *Consensus and Cooperation in Networked Multi-Agent Systems.* Proceedings of the IEEE 95 (1) 215-233 (2007)

[Ott90] E. Ott, C. Grebogi, J.A. Yorke. *Controlling chaos.* Phys. Rev. Lett. 64 1196 (1990).

[Poi1890] J.H. Poincaré. Sur le problème des trois corps et les équations de la dynamique (French) (On the three body problem and the equations of dynamics), Acta Math. 13, 1270(1890).

[Por18] *Porter centrifugal governor on a Corliss steam engine.* https://en.wikipedia.org/wiki/Centrifugal_governor (2018)

[Rab03, Sha03] H. Rabitz. *Chemistry. Shaped laser pulses as reagents.* Science 299 (5606), 525-7 (2003)

[Rad88] G. Radons, T. Geisel, and J. Rubner. *Classical chaos versus quantum dynamics: KAM -tori and cantori as dynamical barriers.* Adv. Chem. Phys. 73, 891 (1988).

[Rat13] L.J. Ratliff, S.A. Burden, S. Shankdar Sastry. Characterization and Computation of Local Nash Equilibria in Continuous Games. 51st Annual Allerton Conference on Communication, Control and Computing, Oct 2013. 917-924 (2013).

[Rav13] A. Raval, A. Ray. Introduction to biological networks. CRC Press (2013).

[Ric00] S. A. Rice and M. Zhao. Optical Control of Molecular Dynamics. John Wiley Ed., New York, (2000)

[Sant08] A. Santiago, R. M. Benito. A*n extended formalism for preferential attachment in heterogeneous complex networks.* EPL 82, 58004 (2008).

[Sat02] Y. Sato, E. Akiyama, and J.D. Farmer. *Chaos in learning a simple two-person game.* Proceedings of the National Academy of Sciences 99 (7) 4748-4751 (2002).

[Sha03] M. Shapiro and P. Brumer. Principles of the Quantum Control of Molecular Processes. Wiley Ed., New York (2003).

[Sco14] H. Scott Dumas. The KAM story. World Scientific Publishing (2014).

[Ser18] S. Serrano. http://www.ootroestudio.com/portfolio_page/arbor-ludi. Visited Dec-2018 (2018).

[Set12] A. Sethi and S. Keshavamurthy. *Driven coupled Morse oscillators: visualizing the phase space and characterizing the transport*. Mol. Phys. 110 (9-10) 717-727 (2012).

[Sib82] E. L. Sibert III, W. P. Reinhardt, and J. T. Hynes. *Classical dynamics of energy transfer between bonds in ABA triatomics*. J. Chem. Phys. 77 (7) 3583 (1982).

[Silv08] S. de Silvestri, G. Cerullo, G. Lanzani. Coherent Vibrational Dynamics. CRC Press (2008).

[Simo99] C. Simó (ed.). Hamiltonian Systems with three or more degrees of freedom. NATO ASI Series C 533. Kluwer Ed. New York (1999).

[Sko07] Ch. Skokos, T. C. Bountis, and Ch. Antonopoulos. *Geometrical properties of local dynamics in Hamiltonian systems: The Generalized Alignment Index (GALI) method*. Physica D 231 (1) 30-54 (2007).

[Sli01] M. Slikker, A. van den Nouweland. Social and Economic Networks in Cooperative Game Theory. Kluwer Academic Publisher (2001).

[Stro03] S. Strogatz. Sync: The emerging science of spontaneous order. Penguin Books (2003).

[Tar01] A. M. Tarquis, J. C. Losada, R. M. Benito, and F. Borondo. *Multifractal analysis of tori destruction in a molecular Hamiltonian system*. Phys. Rev. E 65, 016213 (2001).

[Tesf06] L. Tesfatsion, K.L. Judd (Eds.). Agent-based computational economics: A constructive approach to economic theory. Handbook of Computational Economics Volume 2. Elsevier Science (2006).

[Tra69] J. Travers and S. Milgram. *An experimental study of the small world problem*. Sociometry 32, 425443 (1969).

[Var06] A. J. C. Varandas and S. P. J. Rodrigues. *New Double Many-Body Expansion Potential Energy Surface for Ground-State HCN from a Multiproperty Fit to Accurate ab Initio Energies and Rovibrational Calculations*. J. Phys. Chem. A 110 (2) 485-493 (2006).

[Vel01] L. V. Vela-Arevalo and S. Wiggins. *Time-frequency analysis of classical trajectories of polyatomic molecules*. Int. J. Bifurc. Chaos 11 (5) 1359-1380 (2001).

[Ver17] M. Vernon. *Tapestry weaving and the Jacquard loom*. https://www.thetapestryhouse.com/blog/tapestry-weaving-and-the-jacquard-loom/ (2017).

[Wat98] D.J. Watts, S.H. Strogatz. *Collective dynamics of 'small-world' networks*. Nature 393, 440442 (1998).

[Wig03] S. Wiggins. Introduction to Applied Nonlinear Dynamical Systems and Chaos. Springer-Verlag (2003).

[Wil98] E. O. Wilson. Consilience. Knopf, New York (1998).

[Win67] A. T. Winfree. *Biological rhythms and the behavior of populations of coupled oscillators* J. Theor. Biol. 16, 15-42 (1967).

[Xia04] L. Xiao and S. Boyd. *Fast linear iterations for distributed averaging.* Systems and Control Letters 53, 65-78 (2004).

[Xia05] L. Xiao, S. Boyd and S. Lall. *A scheme for asynchronous distributed sensor fusion based on average consensus.* Proc. 4th Int. Symp. Information Processing in Sensor Networks 63-70 (2005).

[Za77] W. Zachary. *An information flow model for conflict and fission in small groups.* Journal of Anthropological Research, 33 (4) 452-473 (1977).

[Zha14] J. Zhao, O. Liu & X. Wang. *Competitive Dynamics on Complex Networks*. Scientific Reports 4, 5858 (2014).

[Zha15] J. Zhao, O. Liu, L. Wang, and X. Wang. *Relative Influence Maximization in Competitive Dynamics on Complex Networks*. IEEE 54th Annual Conference on Decision and Control (CDC), 6583-6588 (2015).

[Zho98] K. Zhou, J. Doyle. Essentials of Robust Control. Prentice Hall Ed. (1998).